SMALL DISPLACEMENT MEASUREMENT IN ULTRASOUND: QUANTITATIVE OPTICAL NONCONTACTING DETECTION METHODS

by

Adel Sarrafzadeh-Khoee

Dissertation submitted to the Faculty of the
Virginia Polytechnic Institute and State University
in partial fulfillment of the requirements for the degree of
Doctor of Philosophy
in
Engineering Mechanics

APPROVED:

John C. Duke, Jr., Chairman

Richard O. Claus

Mark S. Cramer

Edmund G. Henneke II

Daniel Post

March, 1986

Blacksburg, Virginia

SMALL DISPLACEMENT MEASUREMENT IN ULTRASOUND: QUANTITATIVE OPTICAL NONCONTACTING DETECTION METHODS

by

Adel Sarrafzadeh-Khoee

John C. Duke, Jr., Chairman

Engineering Mechanics

(ABSTRACT)

In this study the description and development of intensity-based laser interferometric techniques for the detection and measurement of ultrasonic stress waves and their small displacement amplitudes is presented. The dynamic displacement sensitive interferometers described in the following chapters allow the quantitative point-by-point measurement of both in-plane and out-of-plane components of surface displacement motion.

These uniquely developed interferometric sensors are:

1) an optical system design for the detection of the surface acoustic wave (Rayleigh wave). The technique is based on the Fourier analysis of coherent light and diffraction imaging properties of an illuminated grating;

2) the design and construction of a two-beam unequal-path laser interferometer for the measurement of out-of-plane surface displacement of ultrasonic waves;

3) extension of a flexible fiber optic probing device which is optically coupled to the test arm of the above two-beam

interferometer. This permits scanning of the test surface which may be at some distance from the main optical system components;

4) the design and construction of a laser speckle interferometer for retro-reflective diffusing surfaces in which the in-plane displacements of the ultrasonic wave are interrogated.

The inherent advantages of these newly designed optical configurations in terms of their greater simplicity, feasibility, and sensitivity over the conventional counterparts (classical/speckle laser interferometers) are explained. The function-response limitations of these interferometric sensors on lateral displacement resolution, on upper and lower-bound displacement sensitivity (dynamic range), on high-frequency bandwidth probing capability, on low-frequency environmentally associated noise disturbance, and on specularly reflective or diffusively retro-reflective specimen surface preparation are also mentioned.

Finally, in a series of experimental observations, the application of a couple of these acoustic sensors in pulsed-excitation ultrasonic testing methods is cited. Specifically, the optically detected ultrasonic signals revealing the true nature of the various surface displacement modes of vibration are presented.

ACKNOWLEDGEMENTS

The author wishes to thank Dr. John C. Duke, Jr. for his encouragement and intellectual support during the research for and preparation of this dissertation. Gratitude is also extended to the author's committee members, Drs. Richard O. Claus, Mark S. Cramer, Daniel Post, and Edmund G. Henneke II, whose valuable input helped improve this effort. Lastly, the author extends sincere appreciation to his wife, , for her love and support, and accordingly dedicates this dissertation to her.

TABLE OF CONTENTS

I. INTRODUCTION 1

II. REVIEW OF PREVIOUS WORK 7

III. METHOD OF ANALYSIS 19

3.1 Optical Phase Displacement 19

3.2 Basic Interferometer 20

3.3 Two-Beam Interference 22

3.4 Intensity Versus Small Transient Displacement . 24

3.5 Sensitivity And Theoretical Minimum Detectable Displacement 27

3.6 Resolution 28

3.7 Summary 29

IV. OPTICAL SYSTEMS FOR SMALL DYNAMIC DISPLACEMENT MEASUREMENTS 31

4.1 DIFFRACTION GRATING IMAGING TECHNIQUE 31

4.1.1 Grating Image Formation 32

4.1.2 Diffraction Imaging Interferometer 33

4.1.3 Image Processing (Optical Convolution) 36

4.1.4 Surface Acoustic Wave Amplitude Versus Optical Intensity 39

4.1.5 Calibration 47

4.1.6 Resolution 49
4.1.7 Sensitivity And Theoretical Minimum Detectable Disturbance 49
4.1.8 Comparison With Other Optical SAW Detectors . 50
4.2 TWO-BEAM UNEQUAL-PATH INTERFEROMETER USING BLAZED GRATING 51
4.2.1 Reflection Blazed Diffraction Grating 52
4.2.2 Principles of Blazed Grating Interferometer . 54
4.2.3 Acoustic Wave Amplitude vs Optical Intensity . 63
4.2.4 Calibration & Large Phase Shift 65
4.2.5 Comparison with Two-Beam Michelson-type Interferometers 67
4.3 FLEXIBLE FIBER OPTIC PROBING INTERFEROMETER . . 68
4.4 LASER SPECKLE INTERFEROMETER FOR RETRO-REFLECTIVE DIFFUSING SURFACES 71
4.4.1 Laser Speckle 71
4.4.2 System Configuration 75
4.4.3 Resolution 77
4.4.4 Special Speckle Interferometric Arrangements . 77
4.4.5 In-Plane/Out-Of-Plane Displacement Sensitivity 79

V. APPLICATIONS 86
5.1 Light Scattering Surface Preparation 89
5.2 Lateral Resolution 99
5.3 Directivity Measurement 116

5.4 Excitation Characteristics of Piezoelectric Transducers 124

VI. SUMMARY AND REMARKS 137

APPENDIX A. FIBER-END PREPARATION 141

APPENDIX B. DIFFUSIVE RETRO-REFLECTION 145

REFERENCES 148

VITA 151

LIST OF ILLUSTRATIONS

Figure 1. Components of particle displacement (u,v,w) 5

Figure 2. Two-beam laser displacement interferometer. 21

Figure 3. Interferometric intensity vs relative phase shift between the two beams. 23

Figure 4. Two-beam interferometric fringes. 25

Figure 5. Diffraction imaging properties of a Fourier transform lens. 34

Figure 6. Diffraction grating imaging optical setup for the measurement of SAW 35

Figure 7. Position of imaged grating lines relative to a fixed grating 38

Figure 8. Optimum operating condition for the spacing between diffracted orders 41

Figure 9. Diffraction action of a single-order blazed reflection grating. 53

Figure 10. Diffracted first-order beam in the direction normal to the grating plane 55

Figure 11. Diffracted first-order beam in the direction normal to the grating plane 56

Figure 12. Diffraction action of a fine reflection blazed grating: 57

Figure 13. Schematic diagram of a two-beam unequal-path interferometric system 60

Figure 14. Diffraction action of a fine reflection blazed grating: 61

Figure 15. Unchanged optical path differences for the movement of the blazed grating 62

Figure 16. Schematic diagram of a flexible single-mode fiber optic interferometric system. 70

Figure 17. Schematic diagram of the double-beam speckle interferometric arrangement 72

Figure 18. Laser speckle image of a small interrogating area of a retro-reflective 73

Figure 19. Schematic diagram of a laser speckle interferometric system 76

Figure 20. Double-beam illumination of a specularly diffusing surface 80

Figure 21. Double-beam illumination of a retro-reflective diffusing surface 81

Figure 22. Single-beam illumination of a specularly diffusing surface 82

Figure 23. Single-beam illumination of a retro-reflective diffusing surface 83

Figure 24. Block diagram of a generalized ultrasonic NDT system. 87

Figure 25. Schematic diagram of an optical sensor viz. the ultrasonic signal 88

Figure 26. An optical response to the transverse surface displacement of a PZT 91

Figure 27. An optical response to the transverse surface displacement of a PZT 92

Figure 28. An optical response to the normal surface displacement of a PZT 93

Figure 29. An optical response to the normal surface displacement of a PZT 94

Figure 30. An optical response to the transverse surface displacement along the width 95

Figure 31. An optical response to the transverse surface displacement along the width 96

Figure 32. An optical response to the transverse surface displacement along the length 97

Figure 33. An optical response to the transverse surface displacement along the length 98

Figure 34. An optical response to the transverse surface displacement of a PZT driven 100

Figure 35. An optical response to the transverse surface displacement of a PZT driven 101

Figure 36. An optical response to the transverse surface displacement of a PZT driven 102

Figure 37. An optical response to the transverse surface displacement of a PZT driven 103

Figure 38. Two sandwiched plates containing a couplant area to simulate "delamination". 105

Figure 39. Positions of an epicentered fiber optic probing beam 106

Figure 40. An optically detected ultrasonic signal amplitude for the position (a) 107

Figure 41. An optically detected ultrasonic signal amplitude for the position (b) 108

Figure 42. An optically detected ultrasonic signal amplitude for the position (c) 109

Figure 43. The near-field (Fresnel) and the far-field (Fraunhofer) beam profiles 111

Figure 44. Schematic diagram of a transducer/aluminum block assembly 114

Figure 45. Optically recorded transient signal of an undamped transducer element 115

Figure 46. Far-field amplitude diffraction curves. . 117

Figure 47. Optically recorded signal for the transducer axis along the fiber 119

Figure 48. Optically recorded signal for the transducer axis along the off-axis 120

Figure 49. Optically recorded signal for the transducer axis perpendicular to fiber 121

Figure 50. The three positions of the sending ultrasonic transducer around the point of 122

Figure 51. Experimentally observed acoustic displacement amplitudes 123

Figure 52. Optical response of an unwanted radial excitation for a 125

Figure 53. Optical response of a normal excitation for a thickness-expander 126

Figure 54. The same as Fig. 53, using the fiber optic interferometer. 127

Figure 55. Optical response of a normal excitation for a thickness-shear 128

Figure 56. Optical response of a transverse excitation for a thickness-shear 129

Figure 57. Optical response of a transverse excitation along the length 131

Figure 58. Optical response of a transverse excitation along the width 132

Figure 59. Optical response of a normal excitation for a thickness-shear 133

Figure 60. Optical sensor response of an ultrasonically excited specimen. 135

Figure 61. Piezoelectric transducer response of an ultrasonically excited specimen. 136

Figure 62. Optical fiber end conditions: (a)rough; (b)tilted; (c)good. 142

Figure 63. Typical examples of fiber end preparations. 143

Figure 64. Schematic ray diagram of retro-reflector material: 146

Figure 65. Magnified (100X) top view of retro-reflective spheres on tape surface. 147

I. INTRODUCTION

The use of a piezoelectric or electromagnetic transducer (EMAT) as an ultrasonic probing mechanism is common in ultrasonic measurements. But piezoelectric ceramics (e.g. PZT) cannot recognize the nature of stress waves caused by acoustic emissions or externally stimulated ultrasonic signals. In other words, the excitation detected by the ultrasonic surface displacement transducer at the points of contact with the specimen cannot be identified as a true out-of-plane or in-plane disturbance; most likely the detected signal will represent a combination of these two types of motions. Consequently, when using ultrasound the nature of and the complete surface displacement analysis of the source/specimen interface is not well characterized. Moreover, for the nondestructive testing of materials using low-power ultrasound, the quantitative evaluation (e.g., the interrelations between mechanical properties and ultrasonic measurements) needs to be obtained. To bridge these two sets of physical parameters, optical techniques can be utilized to gain well characterized and quantitative information (e.g. displacements) about a body under static or dynamic loadings. The advent of the laser and the development of laser interferometry enabled investigators to achieve greater precision and accuracy. The long temporal coherence length

and the intensity of laser radiation make possible the measurement of very small changes of metrological parameters over large distances.

In ultrasonic applications, the advantages of using optical displacement sensors as opposed to any of the other conventional transducers can be summarized as follows:

a) Optical displacement sensors do not require any direct contact with the sample. As a result, there are no acoustic parameter changes or shape changes of the stress waves associated with the interface constraints that piezoelectric crystals/ceramics or polymer transducers usually exert.

b) Optical transducers, due to their inherent broad-band sensitivity, will respond to a wide range of ultrasonic stress wave frequencies.

c) A noisy response is inherent in piezoelectric transducers due to multiple reflections ("ringing") from the back face of the element when they are used in the wide frequency-bandwidth applications. However, optical detectors do not possess such limitations.

d) The ultimate sensitivity of the optical displacement interferometers is in terms of the optical path length

differences which may be tens of thousands of times smaller than the optical wavelength.

e) Optical systems can usually be calibrated, so that the actual displacement amplitudes of the acoustic signals can be obtained.

f) Since the focused spot diameter of the illumination laser beam can be reduced to several microns, examination of very small regions of interest (point-by-point interrogation) can be achieved.

g) Optical sensors can operate at high or low temperatures , in hostile radioactive or corrosive environments, and in geometrically complex locations where smooth surface mounting of bulky mechanical transducers is not possible.

h) Unlike the piezoelectric transducers, in which the efficient transfer of ultrasonic energy to or from the sample is done through the use of the proper acoustic matching medium, optical transducers are free from such a coupling problem. Thus, the variability due to the couplant response, which complicates the long-time and repeating measurements, is not present in the non-contacting sensors.

i) Laser interferometric detectors can be used in conjunction with a contactless method (e.g., laser-generated stress pulses) for a more refined ultrasonic characterization of materials.

The ever-increasing ultrasonic applications in nondestructive testing and materials evaluation has given rise, not surprisingly, to the development of acousto-optical techniques which combine the physics of acoustics and optics. The acoustic energies under investigation may be propagating due to different types of elastic waves---surface acoustic waves (SAW) and bulk waves (e.g. longitudinal or shear waves)---which are all different in nature. Figure 1 shows a particle excitation for an ultrasonic wave which, in general, can have three displacement components. For example, the particle disturbances in an isotropic medium which is excited ultrasonically can be either parallel to the direction of wave propagation, u, or perpendicular to it, v, and w. Here, u and v are the two components of the in-plane and w is the out-of-plane displacement.

As was mentioned earlier, stress wave propagation in a solid material may occur in different modes of vibration. An example of these types of waves are: body waves; surface waves; and in the case of plates and thin-walled bars, Lamb waves, flexural waves, and head waves can propagate. Thus, the complete identification of the components in an acoustic disturbance can help to understand the stress wave processes

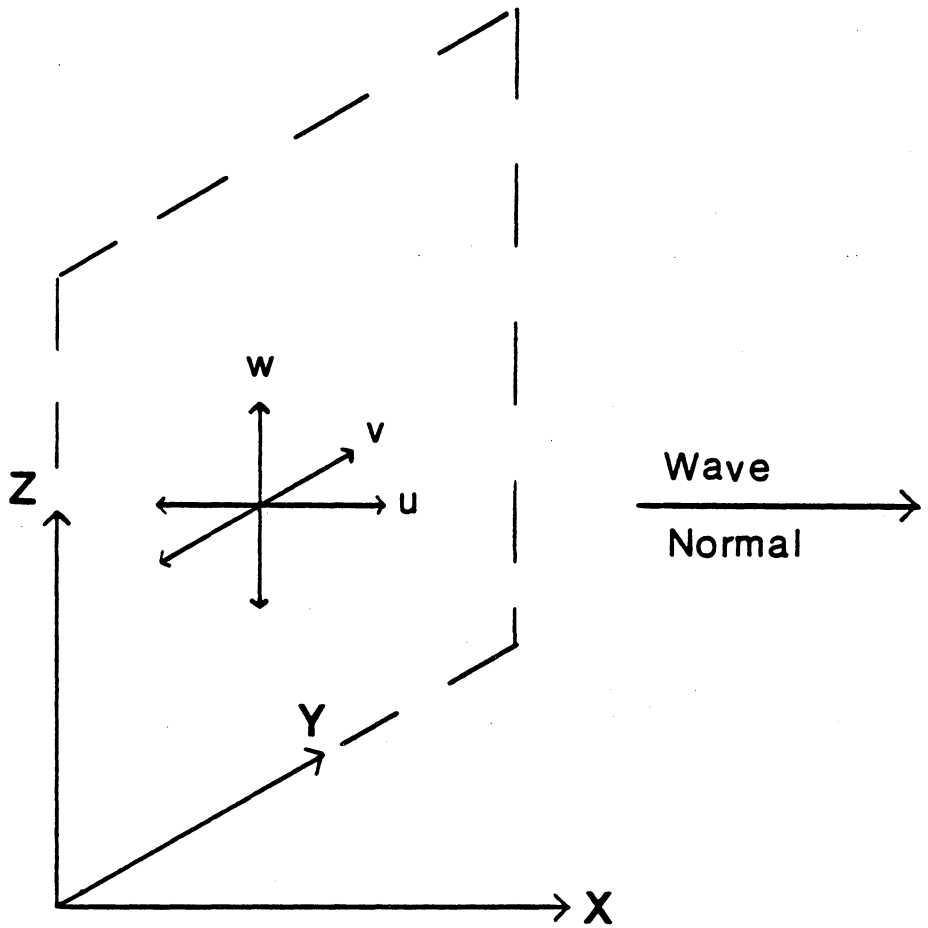

Figure 1. Components of particle displacement (u,v,w): in 3-D Cartesian coordinate system (x,y,z).

in the final ultrasonic investigation. It follows that different optical sensors may be needed which can be tuned for looking at a particular particle surface disturbance (out-of-plane/in-plane displacement) of the material under study.

In general, the optical sensing of ultrasonic signals is done by a variety of different interferometers. The classical interferometers (an example of which is the Michelson interferometer that will be described in the following chapters) are used for specularly reflective surfaces. The laser speckle interferometer is used for diffusing reflective surfaces. There are shortcomings in the system design of these conventional laser and laser speckle interferometers that have been used so far. For that reason, several unique optical systems have been designed here which have some advantages over their conventional counterparts. In this investigation of the quantitative evaluation of propagating stress waves in materials by optical means, the primary objective has been the development of laser interferometric techniques for measuring both out-of-plane and in-plane surface displacements of ultrasonic and surface acoustic waves. These unique optical systems are the outgrowth of that objective.

II. REVIEW OF PREVIOUS WORK

The basic feature of an optical sensor is its response to the optical phase change which it encounters. When unmodulated light is used to interrogate the points in motion on the reflective surface of an object, the reflected light is phase modulated (due to the fluctuation in the optical path length traveled) by the spatial disturbances of the moving particles. Since the speed of light is high (3×10^8 m/s in free space), the frequency of the oscillation of such a visible electromagnetic wave (e.g., 630 nm for the red line of wavelength) is extremely high ($\simeq 5 \times 10^{14}$ cycles/s). Therefore, photodetectors with very fast response characteristics are needed to observe the phase changes of such high frequency signals. Practically, however, the fastest available photodetectors (with very short rise-time responses) are still not fast enough for such an application. To overcome this problem, other means of detection have been sought. By bringing together the two optical waves (modulated and unmodulated) and time-averaging the resultant optical wave amplitude, the intensity distribution can be used to monitor the corresponding phase displacement changes. The variability in the intensity using coherent light is caused by the phenomenon called interference. This entire method of observation is called two-beam interferometry.

There are two basic classes of interferometers: ones made by the division of wavefront or by the division of amplitude. In the division of wavefront kind of interferometer, the wavefront of a monochromatic optical source is spatially split. This may be accomplished by placing a large stop with small openings (pinholes) in front of the optical source. The waves diffracted due to the openings emerge as a new set of wavelets which interact in space to form the interference distribution. With the division of amplitude, some type of beam-splitting device is used to divide the source intensity. The main subject of discussion here is interferometry of the latter kind which has already been given considerable attention by the investigators in this field. The optical interference by reflection from specular surfaces (the classical interferometer) and from diffused surfaces (the speckle interferometer) are two examples based on the division of amplitude. The new design, development, and application of these two types of interferometers is the goal of this research into the complete displacement analysis of ultrasonic stress waves in solid materials.

The classification of systems in the quantitative optical detection of acoustic waves is incomplete if the following two interferometers are not mentioned. Another kind of classical interferometer, the multi-beam interferometer (which employs the interference of a number

of superimposing beams), has been used to measure very small displacements. The increase in the sensitivity of this system compared to simple two-beam interferometry (which is also used to measure small displacements) is due to the sharpness of the fringe distribution. Optical heterodyning (heterodyne interferometry) is another very sensitive method which can be used for measuring both the amplitude and the phase of the acoustic wave. The heterodyne system is based on the superimposition of two waves of different frequencies. In the two-frequency interferometer using a coherent wave, the Doppler effect (which is a shift in the wavelength) is used to measure the consequent shift in velocity of the wave. Since heterodyne interferometry is performed at a shifted frequency of high cycles per second (several tens of MHz), the system response will remain insensitive to much lower frequency environmental noise signals. In short, the phase-modulated optical wave can be monitored using the amplitude-modulation (AM) method (classical interferometry) or the frequency-modulation (FM) method (heterodyne interferometry).

An extensive review of methods for optically probing ultrasonic waves, in particular surface acoustic waves (SAW), was presented by Stegeman [1]. Stegeman discussed the diffraction phenomenon caused by the interaction of light with matter (which is acoustically perturbed) and classified the methods of optical detection into three separate

categories: simple probing, Fabry-Perot interferometry, and the heterodyne method. Laser interferometric detection of ultrasonic waves is not just confined to nondestructive inspection using surface acoustic waves. Numerous other specialized optical sensors have been designed for the noncontacting investigation of acoustic emission and transient ultrasonic stress waves. In the paragraphs that follow, the principal optical systems for measuring small surface displacements in a variety of problems---both out-of-plane and in-plane disturbance of continuously propagating waves (e.g. SAW) and transient stress waves on specularly and diffusely reflective surfaces---are illustrated. In the review of the literature, only the work pertinent to ultrasonic detection is presented.

One of the early methods of optically probing ultrasonic waves, the diffraction technique [2], was designed based on the fundamental principle of the interaction of light with sound, the periodic distortion of the surface with a propagating surface wave. Specifically, the moving phase grating causes diffraction and modulation of the light. The diffraction pattern, produced as a consequence of the interaction of the two waves on the surface under study, can be used as a basis for the optical detection of surface acoustic waves (Rayleigh wave). The intensity and the direction of the scattered light can be used to determine the wavelength, velocity, amplitude, and propagating direction

of the surface waves. In order for the various diffracted orders to be clearly resolved, the propagating ultrasonic surface wave must have a relatively long wave train compared to the diameter of the monochromatic light beam incident on the workpiece; furthermore, it must also have a single frequency. Therefore, this technique cannot be used for the study of transient waves, like acoustic emission waves, which may comprise a wide range of frequencies.

The knife-edge technique of Whitman and Korpel [3] was applied in a simple way to detect and observe the propagating ultrasonic surface wave. The basic principle of the technique is based on the heterodyne interference of two slightly different frequencies corresponding to two optical fields superimposed upon a square-law detector. A collimated laser beam is focused on a surface which is excited with a surface acoustic wave transducer. The beam reflected under undisturbed conditions (in which no wave is propagating on the surface) subsequently deviates because of surface corrugation. The reflected laser beam is then recollimated and a knife-edge interrogates the light beam by blocking just half of the reflected beams. This method can also be adapted for the study of any transient acoustic wave (e.g. AE) having a broad range of frequencies. But a reduction in sensitivity to lower acoustic wave frequencies and an insensitivity to the direction of the propagating ultrasonic wave, when it is

parallel to the knife-edge, restricts the applicability of such a system.

The Fourier transform technique using coherent light was utilized by Haskell [4] to obtain the optical convolution (i.e., auto-correlation or cross-correlation functions) of two spatial signals. In such a case, the optically transmitted/reflected amplitude signal (i.e. object) can be Fourier-transformed by using a simple lens so that the spatial time-domain signal is transformed into a spatial frequency-domain signal on which the optical signal is spectrally distributed in proportion to the Fourier transform of the signal. Based on these principles, the Fourier analysis of coherent light and the imaging of the periodic object (e.g. grating) through diffraction properties of the illuminated grating has been found to have a potential application in the detection of surface acoustic waves.

Moreover, in the early research carried out as part of the author's investigative objectives, a new approach similar to that of Jablonowski [5] to the detection and the analysis of SAW has been conceived as follows: If the frequency of the grating and the focal length of the transform lens is properly chosen such that the two principal diffracted orders (resulting from the coherent illumination of the grating) interrogate the crest and the trough of a single-frequency surface acoustic wave (in this case, the spacing between the two diffracted orders is one-half the wavelength of SAW), the

phase-modulated grating image will be constructed. The formation of the grating image is a direct result of the image-forming property of simple lenses. The grating image is produced by the interference of the spectral orders (which is a consequence of the grating property and not the lens itself) of the grating. The image formed in this manner is called the "diffraction image". In such an optical arrangement, however, the time-dependent amplitude of SAW imposes a fluctuating shift of the grating image position. Finally, the superposition of this grating image on a similar fixed grating will result in an optical convolution process. The deviation in transmitted light intensity through the fixed grating can be photoelectrically observed. The output signal is found to be proportional to the small displacement amplitude of surface acoustic waves.

Ultrasonic stress wave detection by interferometric techniques has been another application which employs the principle of two-beam interferometry. Optical systems of this kind have successfully been used to detect ultrasonic stress waves (both SAW and bulk waves) and acoustic emission waves. Optical interferometers measure the optical path length differences of two coherent beams of light. In some applications, this path length sensitivity can be used to measure the instantaneous surface displacements as a function of time. The prime example of a system based on the aforementioned principle is the Michelson interferometer.

Therein, the interest is in detection of very small-amplitude high-frequency disturbances. The same feature that makes the technique so useful, i.e., path length sensitivity, also limits the system's sensitivity. In the case of the Michelson interferometer the path length difference caused by an unwanted vibration of the reference mirror will affect overall output of the detection system. Ideally, one wants the large amplitude and low frequency of such a disturbance, predominantly existing in the laboratory and testing environment, to have no effect on the detection apparatus. By large displacement amplitude, one usually means disturbances larger than the amplitudes in the range of several hundred angstroms which are produced on the workpiece by stimulated acoustic emission, the ultrasonic transducer, or the breaking of a pencil lead or a glass capillary against the surface of the workpiece. A number of different techniques have been employed to compensate for interferometer path length sensitivity to unwanted noise vibration; tuning of the interferometer to the proper operating point for maximum sensitivity was sought by Mezrich and co-workers [6,7]. For example, the basic arrangement of the Michelson interferometer with the addition of the path length stabilizer for low frequency reference mirror fluctuation was used [8,9] for the detection of transient acoustic emission signals. The results were compared with the response of an acoustic emission transducer, and not

surprisingly it was proven that an optical transducer is superior to a piezoelectric transducer in many respects.

An alternative method to free the optical interferometer from the aforementioned problems is the use of the differential interferometer as designed by Palmer [10]. Palmer used two spatially interfering laser beams produced by an optical beam-dividing mechanism and directed both beams onto the surface of the specimen under study. Since two beams now travel close together and follow the same path, neither a sudden movement of the workpiece nor atmospheric pressure change along the trajectory of the two beams will affect the path length difference. The detection mechanism in this kind of system usually consists of a fixed (stationary) Ronchi grating. In order to achieve maximum sensitivity, this grating should be properly positioned with respect to the fringe pattern produced by the two beams. When the system is used for detection of ultrasonic SAW, the displacement amplitude (which is the measure of the optical path difference of two beams) depends on the separation of the two focused beams on the surface. And when the separation is exactly half the wavelength of the propagating SAW, system sensitivity will be optimized. A number of two-beam differential interferometers were designed by Palmer and co-workers, as well as by other investigators, for the measurement of surface (Rayleigh) waves [11,12]. Although evidence exists to indicate that the optical differential

interferometer can be successfully employed to detect surface acoustic waves, the system's inability to remain as sensitive to other types of stress waves (e.g., transient acoustic emissions and bulk waves incident on the surface) makes it less useful than the Michelson-type interferometers.

The interferometers described in the previous paragraphs are only sensitive to the out-of-plane displacement of the motion of the test surface under strain. In order to be able to measure the in-plane displacements on the test surface, a laser speckle interferometer based on the double illumination arrangement of Leendertz [13] can be utilized. The speckle effect is produced when a diffusing surface is illuminated in coherent light. The intensity of the speckle pattern is a random distribution caused by interference of the light amplitudes from all of the contributing points on the diffusing illuminated area. The speckle grains are considered to be attached to the diffusing object surface so that if the object surface is disturbed, the speckle patterns are disturbed too. Consequently, the motion of the points on the illuminated area causes a variation in the detailed distribution of the correlation speckle pattern. By detecting this speckle pattern deformation (twinkling of the combined speckle patterns), the information about the surface displacement amplitudes of the stress wave exciting the illuminated object surface can be obtained.

The application of laser speckle systems for measuring small dynamic in-plane (transverse) displacements or vibrations has been reported by a number of authors. Joyeux and Lowenthal [14] discussed a generalized Moire' method in which a randomly scattering surface as opposed to a linear specimen grating (used in the classical Moire' method) is illuminated by a fine virtual grating. Based on the same theory, they also designed a separate system in which a single coherent laser beam illuminates a diffusing test surface. Two diffusely scattered beams were selected to combine and form the speckle interference. The detection of rather higher frequency (e.g. 24.4 KHz) signals of in-plane vibration was reported by Ueha, Shiota, Okada, and Tsujiuchi [15]. Their laser speckle interferometer was based on the optical heterodyne technique in which the two illuminating beams on the diffusing surface were frequency-shifted through an acousto-optic modulator. Using the speckle method in the frequencies of the ultrasonic regime, small in-plane displacements were obtained by Iijima and co-workers [16]; the displacement amplitude of a piezoelectric crystal resonating in the thickness-shear mode was determined. Dandliker and Willemin [17] designed a heterodyne speckle interferometer which was only sensitive to the actual high-frequency small-amplitude signals of ultrasonic excitations. Their unique optical system was arranged such that the complete mechanical movement (in-plane and

out-of-plane displacements) could be measured without changing the location of the diffusely reflecting object surface.

III. METHOD OF ANALYSIS

The subject that will be dealt with in detail in this chapter is the theory behind optical techniques for acoustic sensing; the method of analysis will also be developed.

3.1 Optical Phase Displacement

Optical phase sensing as a linear detector is potentially useful for the noncontacting monitoring of ultrasonic waves. Optical phase (σ) is linearly related to optical path length (OPL) which in turn is related to acoustic amplitude, i.e.,

$$\sigma = (k)\ (OPL)\ ,$$

where $k = 2\pi/\lambda$ is the optical wave propagational constant and λ is the wavelength. The change in the optical path length will introduce a shift in the optical phase which will be the direct indication of the acoustic displacements. In general, a change in the optical phase can occur due to the variation in the refractive index of the medium and the optical path difference of the wave. That is,

$$\Delta\sigma = (\Delta k)\ (OPL) + (k)\ \Delta(OPL).$$

If the contribution of the first term on the right hand side of the above expression is small compared to the second term, the phase shift (ϕ) can simply be represented as

$$\phi = \Delta\sigma \simeq (k)\ (OPD)$$

where the optical path difference (OPD)=Δ(OPL). Since the optical frequencies are extremely high ($\simeq 10^{15}$ Hz), the direct monitoring of optical phase changes, even with the fastest available photodetectors, will not be possible. So phase sensing must be converted into amplitude or intensity sensing by means of optical interferometers.

3.2 Basic Interferometer

A basic interferometric system is the Michelson interferometer, shown schematically in Figure 2. The laser beam (LS) is divided into two beams by a beamsplitter (BS) of about a 50% transmittance/reflectance coefficient. The reference beam (b) is directed toward a stationary mirror (RM). The test beam (a) interrogates the specularly reflective surface of the specimen (S) undergoing a normal mechanical vibration (d) due to ultrasonic excitation.
The two orthogonal reflected beams become colinear after the second encounter with the beamsplitter and coherently

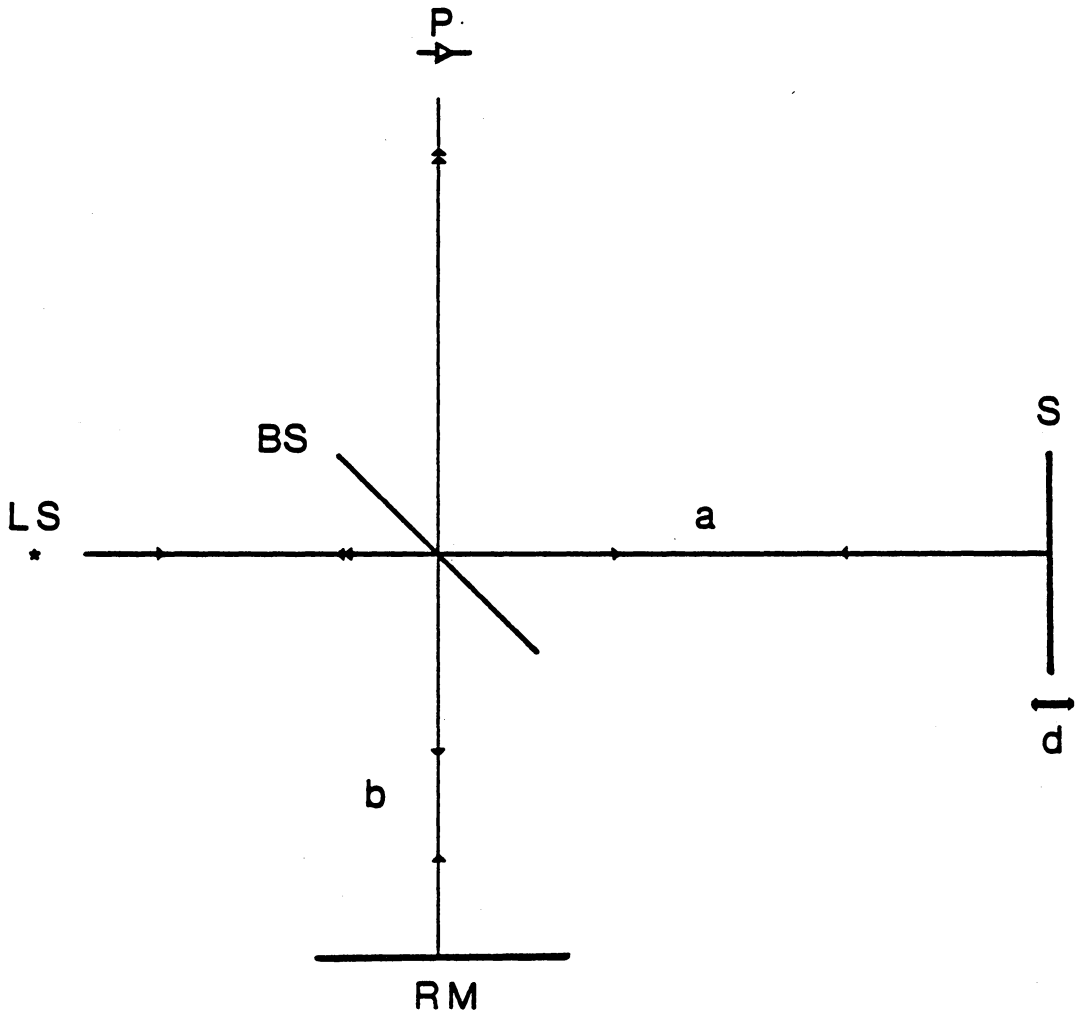

Figure 2. Two-beam laser displacement interferometer.

interfere to produce the optical intensity which can be monitored by a photodetector (P).

3.3 Two-Beam Interference

The superposition of two coherent optical beams of uniform or non-uniform wavefronts is called two-beam intensity interference. The coherent properties of the laser and the technique for utilizing the above phenomenon in order to gain useful information about a body under mechanical/thermal excitation is concisely described by Post [18].

Using a slightly different formulation but basically following the same straightforward derivation of the coherent superposition carried out in the above reference, the following formula can be obtained:

$$P = C(1 + \cos \phi) = 2C \cos^2 \phi/2 \quad .$$

This states that the intensity of the two-beam interferometric pattern (P) is a function of the cosine squared of the relative phase differences between the two beams. In this expression, the coefficient C is a function of laser beam power and fringe visibility (contrast).
The curve in Figure 3 represents the variation in optical intensity versus the relative phase shift and the photograph

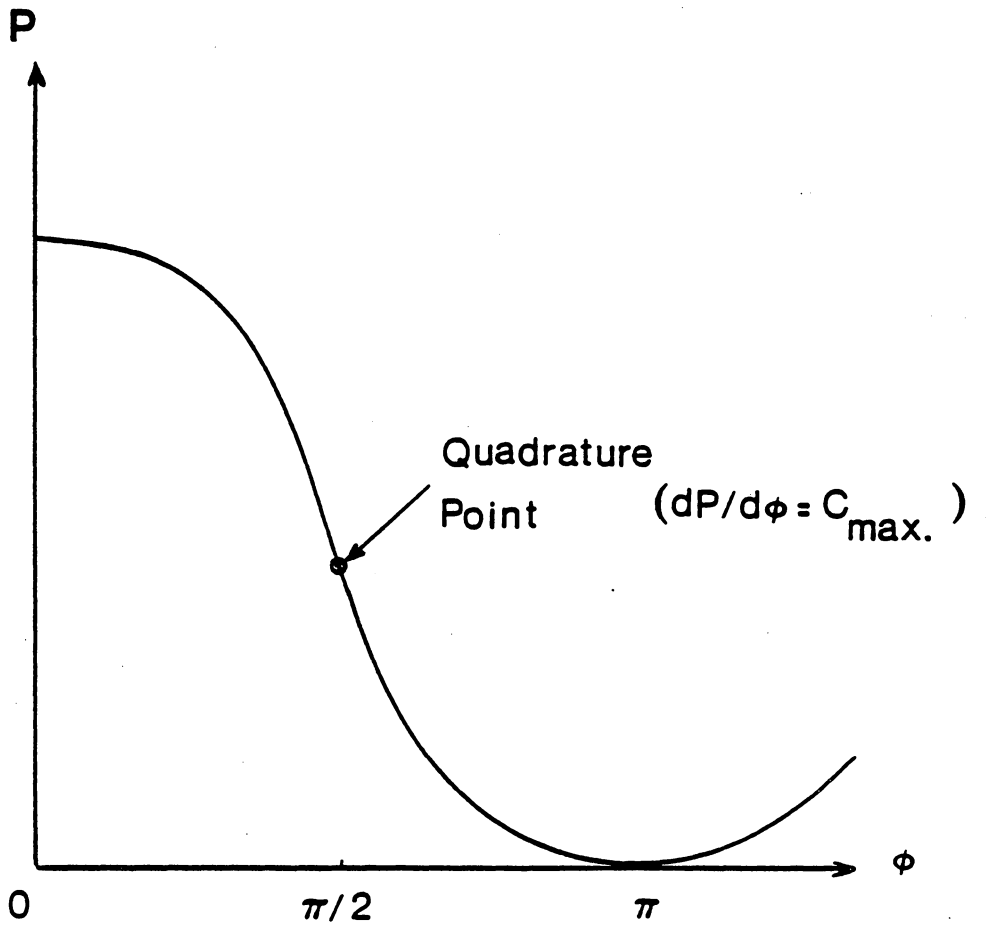

Figure 3. Interferometric intensity vs relative phase shift between the two beams.

(Figure 4) shows a typical fringe pattern in which at least one beam has a spherical wavefront.

The rate at which the intensity varies with respect to the optical phase change is determined by:

$$dP/d\phi = C \sin \phi \ .$$

In order to operate at the maximum detection sensitivity, i.e., the smallest change in phase resulting in the largest variation in intensity, the interferometer must be tuned at its quadrature point at all times. In that case,

$$dP/d\phi = C(\text{maximum}).$$

3.4 Intensity Versus Small Transient Displacement

The relation for optical intensity in an expanded form can be rewritten as

$$P = C + C \cos \phi \ ,$$

in which the first term on the right hand side of the equation is the DC component and the second term is the interferometric intensity.

Figure 4. Two-beam interferometric fringes.

The substitution of the optical path difference caused by surface mechanical excitation in terms of the relative phase change, i.e.,

$$\phi = 2\pi/\lambda\ [(a - b) \pm 2d],$$

modifies the interferometric term as:

$$I = C \cos[2\pi/\lambda\ (a - b) \pm 4\pi d/\lambda].$$

If the relative spacing between the reference mirror and the specimen surface from the beamsplitter is such that

$$2\pi(a - b)/\lambda = n\pi/2 \qquad (n = \text{odd integer}),$$

then

$$I = C \sin(4\pi d/\lambda).$$

For small disturbances compared to the wavelength of light used ($d << \lambda$), the sine of the argument becomes almost equal to the argument itself. Therefore,

$$I = C\ 4\pi d/\lambda,$$

and the output photodetector signal current along with the above optical intensity become linearly proportional to the small displacement. The variation in the light intensity due to surface disturbance of the test sample can be photoelectrically observed. The photodetector converts the optical power into an electrical current. For a photodetector with a quantum efficiency of α, the RF signal current produced by the incident optical intensity is

$$i(\text{signal}) = \alpha I.$$

3.5 Sensitivity And Theoretical Minimum Detectable Displacement

The sensitivity of the detected signal is limited by the presence of the noise inherent in the detecting system. This would include: laser noise (optical) caused by fluctuation of laser power output; Johnson noise (thermal) caused by the load resistor of the photodetector; the electronic noise in the electronic signal processing components; and shot noise (photon) of the square-law detector, which is considered to be the most limiting factor in sensitivity. Other sources of noise, which will be taken into consideration in a later section, are low-frequency environmental noises (mechanical and thermal).

The DC optical power, C, incident on the photodetector, gives rise to the rms shot noise current. That is,

$$i(\text{noise}) = (2eCB)^{0.5} \ ,$$

where

C = averaged optical intensity on photodiode

B = detection bandwidth

e = electron charge (1.6×10^{-19} colm).

The minimum detectable displacement amplitude is obtained when noise current and signal current are equal (S/N=1), i.e., i(noise) = i(signal). Thus, in terms of output laser power, P_0, the minimum detectable displacement is written as

$$d(\text{minimum}) = (2eB/\alpha\eta P_0)^{0.5} \ \lambda/4\pi,$$

where η = optical system efficiency and $P_0 = C$. For example, the theoretical minimum detectable displacement for a He-Ne laser, P_0 = 10 mW, α = 0.35 A/W, B = 1 MHz, and $\eta \approx 20\%$ is calculated to be about 3×10^{-4} A° .

3.6 Resolution

The lateral resolution is limited by the diameter of the focused laser beam on the surface under study. The focused

laser beam size should be small compared to the shortest acoustic wavelength. Since the phase displacement is averaged under the finite region of the focused light spot, the system response for the acoustic wavelength comparable to the diameter of the focused area goes to zero. A spot size diameter of less than one-half of the acoustic wavelength is acceptable, but for practical purposes, the spot size is set not to exceed one-tenth of the acoustic wavelength. The absolute limit of spot size diameter is governed by the collimating property of the laser beam and the focusing power of the imaging lens. That is, the finite size of the interrogating focused laser beam is linearly proportional to the focal length and is inversely porportional to the diameter of the collimated beam incident on a lens.

3.7 Summary

Let us recap a few of the advantages of using laser displacement interferometers in conjunction with high-speed opto-electronic sensors for the detection of ultrasonic waves: they are both noncontacting and quantitative; they have both high spatial resolution and high displacement sensitivity; they are able to achieve wide-band frequency probing with a short response time; and they are extremely flexible. However, compared to off-the-shelf transducers, these sensors have less displacement sensitivity due to the

inherent noisy fluctuation in laser power output and to photosensor shot-noise signal current.

IV. OPTICAL SYSTEMS FOR SMALL DYNAMIC DISPLACEMENT MEASUREMENTS

In this chapter the design, construction, and development of several unique laser interferometric systems for acoustic sensing will be presented. For each system, the principles of operation, the inherent capability of the interferometer for absolute calibration, its maximum sensitivity adjustment, the simplicity of the optical configuration, and its advantages over the conventional interferometers are explained.

4.1 DIFFRACTION GRATING IMAGING TECHNIQUE

This system is based on diffraction grating imaging using coherent optical illumination. The instantaneous surface displacement magnitude of surface acoustic waves imposes a fluctuating shift in the grating image with respect to the fixed grating. The coherent Fourier analysis and optical convolution processing of two spatially superimposed gratings can be used for the detection of the surface acoustic wave (Rayleigh wave) and its displacement amplitude.

4.1.1 Grating Image Formation

Diffraction grating imaging and its application in displacement measurements encompass two of the unique properties of the laser beam, namely, spatial coherence and collimation. A spatially coherent and collimated laser light is passed through a transmission linear diffraction grating. An example of such a grating is the Ronchi ruling, a square-wave grating which has equal spacing of clear and opaque lines. The collimated beam illumination of the grating produces the strong undiffracted order and the odd diffracted orders, which are the unique diffraction properties of such a linear grating. The diffraction pattern far from the grating is the far-field (Fraunhofer) diffraction. Simple lenses under coherent illumination can also be used to form the far-field diffraction pattern of the grating. In that case, the diffraction pattern at one focal plane of a lens is the Fourier transform of the grating at the other focal plane of the lens. The intensity of the diffraction orders (Fourier transforms) in the focal plane of the lens is proportional to the far-field diffraction pattern of the grating. The brightest order is the undiffracted (DC) order and the spatial frequencies corresponding to different odd diffracted orders are formed in both directions away from the central order. Of course,

the lens aperture and the object distance (spacing between the grating and lens) determine the highest diffraction order which can be gathered and transformed by the lens. Figure 5 shows a diffraction grating imaging representation using a double convex lens. A grating located at twice the focal length from the transform lens is Fourier-transformed in the transform plane on the opposite side of the lens. The transform lens used in such an application is actually used to invert the spatial Fourier-transformed orders and reconstruct (image) the grating onto the transform plane.

4.1.2 Diffraction Imaging Interferometer

The simple arrangement shown in Figure 6 is designed to detect and measure the surface acoustic wave displacement amplitude. An expanded/collimated laser beam illuminates a transmission linear diffraction grating (e.g., the Ronchi ruling). The undiffracted (zero) order and odd diffracted orders resulting from the action of such a square-wave grating is collected and focused by a lens onto the specularly reflective surface of the specimen. The reflecting diffracted orders from the surface are then spatially interfered and the resultant grating image is placed at some distance away from the surface.

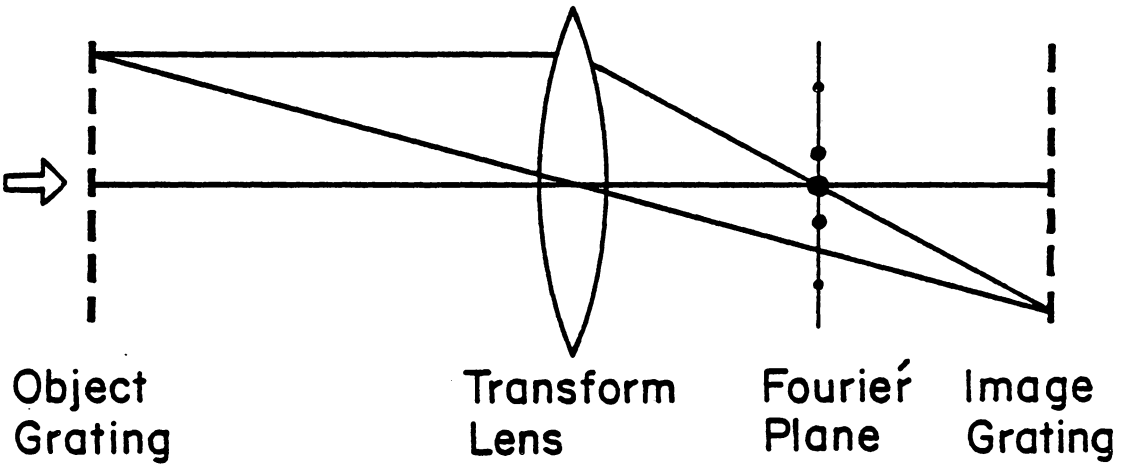

Figure 5. Diffraction imaging properties of a Fourier transform lens.

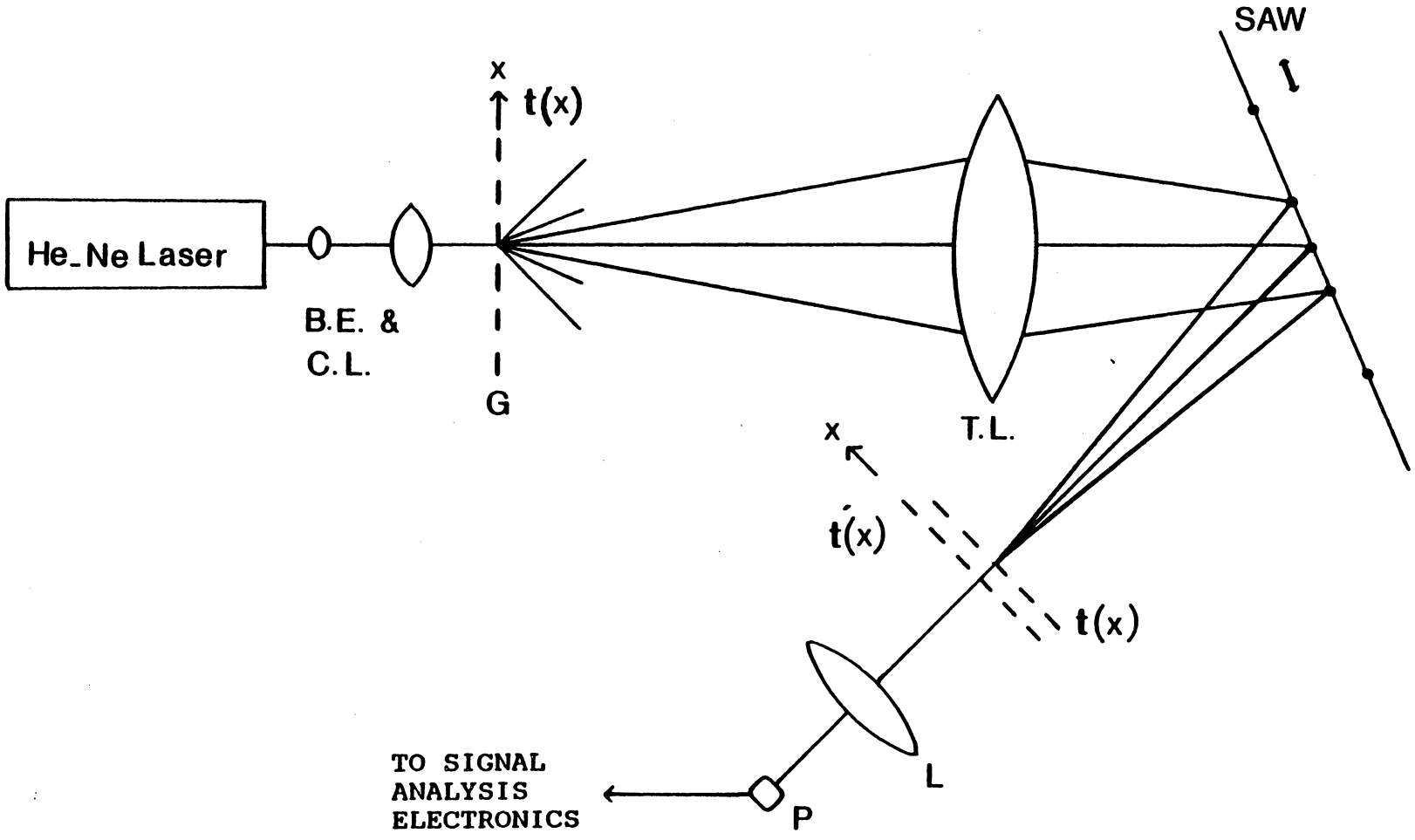

Figure 6. Diffraction grating imaging optical setup for the measurement of SAW displacement amplitudes.

If the surface under study is supporting a surface acoustic wave, the relative optical phase change among the diffracted orders, due to differing optical path lengths traveled by these orders, will phase-modulate the grating image. The grating image shift in the direction perpendicular to the grating image lines is even more pronounced when the neighboring diffracted orders are focused at convex and concave points of the surface acoustic wave. The fluctuation in grating image shift, which is a function of instantaneous surface wave displacements, is used as a tool to measure the surface acoustic displacement amplitude.

4.1.3 Image Processing (Optical Convolution)

For the measurement of optical intensity modulation, a second Ronchi grating with the same line spacing as the grating image periodicity is placed in a stationary position at the grating image location. The sweeping of the grating image over the fixed grating results in an optical convolution process of the two spatial grating lines. As was mentioned earlier, the grating image fluctuates back and forth on the image plane under the action of surface wave displacement. Note that the magnitude of the grating image shift will be optimum (therefore, the detection will be at its maximum sensitivity) when the neighboring orders are

interrogating the crests and troughs of the surface acoustic wave. For such an arrangement, the spacing between the neighboring odd orders are exactly one-half the wavelength of the surface acoustic wave. The shift in the grating image can be measured using the method of optical convolution of two spatial signals [19]. In the optical arrangement of Figure 6, the convolution will be performed on the two gratings. That is, when the grating image is swept across the fixed grating due to acousto-mechanical displacement of the surface, the amplitude transmittance of light, which is just the convolution integral, will vary. The resultant modulated intensity can then be gathered and focused on an optical square-law detector by a lens. Consequently, the optical transfer function of the two gratings, which is the measure of surface wave displacement amplitude, can be monitored following the photodetector's output.

The response of the optical system is optimized when the position of the fixed grating lines is carefully adjusted with respect to the grating image lines. Maximum sensitivity is achieved for the two gratings configuration shown in Figure 7. Therein, only one-quarter of the grating pitch (one-half the width of each transparent line of the transmission grating) is set open to the light transmission. At this operating point, the change in transmitted optical power is maximum with respect to the grating shift. The

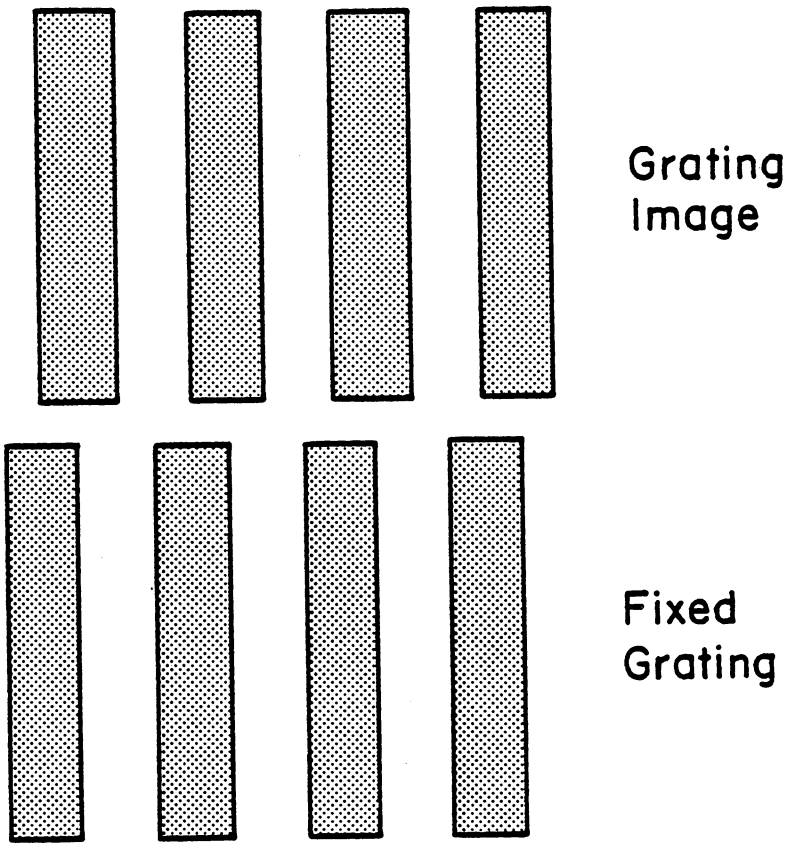

Figure 7. Position of imaged grating lines relative to a fixed grating for maximum sensitivity.

optical intensity will repeat itself for every one-half period grating image shift.

4.1.4 Surface Acoustic Wave Amplitude Versus Optical Intensity

The decomposition of a continuous square-wave into its pure sinusoidal components is called a Fourier analysis or a spectral decomposition of the square wave. The amplitude transmittance for a square-wave type grating (e.g., the Ronchi ruling) of amplitude T and pitch g, can be written in a Fourier series after Reference [20]:

$$t(x)= -T/2 + T \Sigma\{[\sin(n\pi/2)/(n\pi/2)]\cos[n\pi x/(g/2)]\},$$

where x is the position in the direction perpendicular to the grating lines. The grating image, which is an inverted Fourier transform of the object grating, is reflected from a specular specimen surface. The reflected amplitude representation of the grating image is

$$t(-x)=-T/2+T\Sigma[\sin(n\pi/2)/(n\pi/2)]\cos[-n\pi x/(g/2)-\delta-\psi],$$

where δ is the phase constant representing an arbitrary grating placement with respect to the optical axis and ψ is

the additional phase term representing an orientation of the reflective surface with respect to the optical axis. Furthermore, any disturbance on the surface such as Rayleigh wave surface displacement will phase-modulate the diffracted orders upon reflection. In order to make the analysis easier, only the main contributing orders (0, ± 1) will be considered here.

The surface deformations introduced at focused first order positions (see schematic diagram of Figure 8) can be represented as

$$u_{-1} = U \cos(2\pi ft)$$
$$u_{+1} = U \cos[2\pi(ft - d/\Lambda)],$$

where f and Λ are the frequency and the wavelength of the surface acoustic wave, and d is the spacing between the two first diffraction orders.
Thus, the peak-to-peak displacement of the surface acoustic wave is

$$u = u_{-1} - u_{+1} = U\{\cos(2\pi ft) - \cos[2\pi(ft - d/\Lambda)]\},$$

where U is the displacement amplitude of SAW. In a special case, where the spacing between the two first diffraction orders is one-half the surface acoustic wavelength (i.e., d

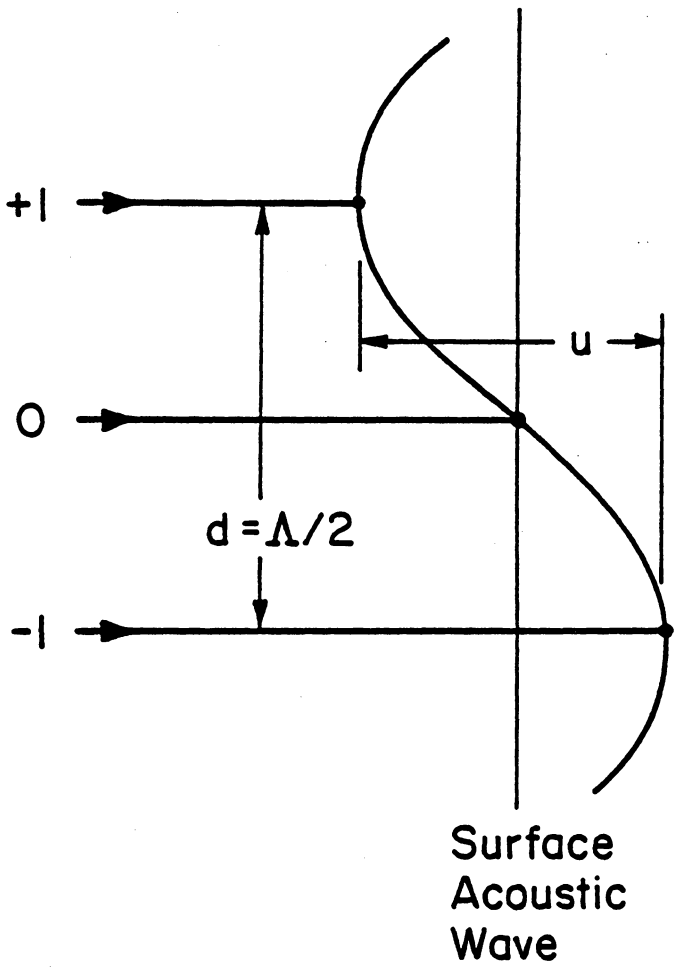

Figure 8. Optimum operating condition for the spacing between diffracted orders and SAW wavelength.

= $\Lambda/2$), the relative displacement of the points supporting these two orders with respect to the zero order will accurately correspond to the displacement amplitude of the surface acoustic wave. Then,

$$u = 2U \cos(2\pi ft).$$

The presence of a surface acoustic wave introduces a fluctuation in the phase displacement of the grating image. This variable phase change which is linearly proportional to u can be written as

$$\beta = 2ku = 4\pi u/\lambda \ .$$

Consequently, the grating image oscillates back and forth along the x-direction at the frequency, f. Note that the appearance of the factor two (2) in the above expression is due to the light traveling twice through the surface acoustic wave displacement amplitude. The small displacements of the surface waves introduce grating image shifts of small magnitudes compared to the grating pitch. Although such fast and small fluctuations of the grating image can hardly be seen or photographed, they can easily be detected photoelectrically.

Considering the zero order and the two first orders, the amplitude transmittance of the grating image can be represented as:

$$t(x) = T\{1/2 + 2/\pi \cos[-\pi x/(g/2) - \delta - \psi]\}.$$

Representing the amplitude transmittance of the fixed grating in a similar fashion, one can also write:

$$t'(x) = T\{1/2 + 2/\pi \cos[\pi x/(g/2) + \delta']\},$$

where δ' is the phase constant representing the arbitrary grating placement with respect to the optical axis.

Since the transform lens inverts the image, the grating image $t(-x)$ is formed at the image plane. Thus, the resultant light transmittance through the stationary grating is the product of $t(-x)$ and $t'(x)$. This product is the optical transfer function of the two gratings. The second lens in the system configuration of Figure 6 transforms the above function into spatial spectral orders (Fourier transforms) which are focused onto the transform plane. The intensity of these spectral orders can be obtained using the diffraction integrals. For example, if a pinhole is placed on the optical axis in the transform plane (spatially filtering the higher orders), the amplitude of the light

focused on the photodetector will be proportional to the diffraction integral

$$\int t'(x)\, t(-x)\, dx.$$

The presence of the surface acoustic wave which brings about the fluctuating phase term, β , causes the grating image to be wiped across the fixed grating. If the image is shifted by an amount, x', corresponding to a phase change of β , i.e.,

$$x' = \beta/k = 2u ,$$

then the transmitted light amplitude incident on the photodetector is just the convolution integral

$$\int t'(x)\, t(x' - x)\, dx.$$

To perform the above integral, the relative phase terms, δ', δ, and ψ can be adjusted so that only one-quarter of the fixed grating period would be transparent to the light. This particular setting, in which the change in transmitted light amplitude is maximum with respect to the shift in the grating image, enhances the sensitivity. The convolution integral (also written as t'(x')*t(x')) is the amplitude of light reaching the photosensor. The photodiode is a square-law

detector which responds to the intensity of the received light. Hence, the light intensity is derived by

$$| t'(x')*t(x')|^{2} .$$

The above optical power incident on the photodetector contains two contributing terms (see Chapter III). That is,

$$P(\text{total}) = C(\text{steady}) + I(\text{interferometric}).$$

The first term on the right hand side of the total optical intensity is the DC component which represents the main contribution to the shot noise in the photodetector. The second term, the interferometric term, describes the optical signal power corresponding to the instantaneous surface acoustic wave displacement. That is, the variable transmitted optical intensity (excluding the DC term) with respect to the relative phase shift between the gratings can be written as

$$I = P_0/4 \sin(4\pi u/\lambda),$$

where P_0 is the laser output power and the gratings have 50% reflectance/transmittance coefficients. For a small surface acoustic displacement amplitude, i.e., $u << \lambda$, the variable

light power on the photodetector will be linearly proportional to the instantaneous surface displacement. This insures the desirable linear response to the measured displacements. Thus,

$$I = (P_0/4)(4\pi u/\lambda) \ .$$

In general, the surface of the specimen is not 100% reflective and not all the diffracted orders are efficiently gathered by the lenses. Thus, for the system efficiency of η (excluding the 50% losses of the gratings, the above expression can be rewritten as

$$I = \eta P_0 \pi u/\lambda \ .$$

The photodetector converts the absorbed optical power into an electrical signal current such that

$$i(\text{signal}) = \alpha \ I \ ,$$

where α is the photodetector quantum efficiency. Obviously, the photodetector's RF output current is also directly proportional to the displacement amplitude of the surface acoustic wave. This current can be electronically filtered,

amplified, and displayed on an oscilloscope. The corresponding amplifier output voltage can be written as

$$V = (4\pi u/\lambda)\, A\ ,$$

where A is a function of system efficiency, photodetector responsivity, laser power, and amplifier gain. Therefore, the instantaneous surface displacement corresponding to the observed output voltage can be obtained once the system calibration voltage, A, is determined.

4.1.5 Calibration

The absolute calibration of the system is necessary in order to obtain the exact measurement of the surface acoustic wave displacement amplitude. In general, the amplifier output voltage is expressed as

$$V = A \sin(4\pi u/\lambda),$$

where u is not small enough compared to λ so that the sine function cannot be approximated with its argument. The system calibration is accomplished if the maximum amplifier output voltage, A, is known. This condition is satisfied for large displacement amplitudes in which

$$\sin(4\pi u/\lambda) = 1.$$

That is,

$$4\pi u/\lambda = n\pi/2 , \qquad n = 1, 3, 5, \ldots$$

The smallest displacement amplitude necessary to exhibit the required voltage, A, is

$$u = \lambda/8.$$

For example, a calibrating displacement of 791 A^0 (peak-to-peak) is needed when a He-Ne laser beam of 6328 A^0 wavelength is used. Once the calibration voltage is obtained, the absolute instantaneous displacement, u, can be derived from the expression relating the amplifier output voltage to u.

It is important to realize that the experimentally determined calibration voltage requires an ultrasonic generation of a surface acoustic wave with a relatively large displacement amplitude and a single frequency. The excitation of SAW can usually be accomplished using either a wedge or interdigital transducer (IDT). The operating condition of the system can also be achieved using a verifocal imaging lens in order to optimally adjust the

spacing of the diffracted orders to comply with the one-half SAW wavelength. Obviously, the challenge for an experimentalist is to try to actually implement the system.

4.1.6 Resolution

The lateral resolution of the system is limited by the diameter and the spacing of the focused diffracted orders on the surface under study. The light spots corresponding to focused zero and odd diffracted orders should be small compared to the shortest surface acoustic wavelength. The ultimate spot size diameter tolerated, without the zero order and the first order beams actually overlapping, is about one-quarter of a SAW wavelength. For example, a very conservative estimate for the highest detectable frequency of SAW is about 1 MHz when the focused laser beam diameters of 1 mm are used.

4.1.7 Sensitivity And Theoretical Minimum Detectable Disturbance

The ultimate sensitivity of the optical system is related not only to the operating condition (optimum positioning of fixed grating with respect to grating image), but also to the signal-to-noise ratio of the electrical

signal current of the photodetector. The total optical intensity reaching the photodetector is the sum of the DC and the RF optical power. The signal-to-noise ratio is just a small fraction of the ratio of RF to DC optical signal. The incident steady (DC) optical intensity on the photodetector corresponds to the main source of optical noise (shot noise) which limits the sensitivity. The rms signal photocurrent corresponding to the sinusoidal variation of SAW is given as

$$i(\text{rms}) = i(\text{peak})/\sqrt{2}.$$

Thus, the theoretical minimum detectable surface wave displacement amplitude (for S/N = 1, i.e., i(rms) = i(noise)) can be calculated as

$$u(\text{minimum}) = (eB/\eta\alpha P_0)^{0.5}\ 2\lambda/\pi\ ,$$

where i(noise) is the rms shot-noise current described in Chapter III. An estimated value for λ = 6328 A^0 , P_0 = 10 mW, α = 0.35 A/W, η = 80%, and B = 1 MHz is around 10^{-3} A^0 .

4.1.8 Comparison With Other Optical SAW Detectors

The optical system configuration of this uniquely designed SAW sensor is very simple. Basically it consists

of two Ronchi rulings, an imaging lens, and a laser source. The sensitivity to the measured SAW displacement amplitude of this optical sensor (like Palmer's differential interferometer or Jablonowski's grating interferometer) is twice that of a Michelson-type interferometer. Since all diffractions are reflected by the same surface, the thermal fluctuation of the environment and rigid body movement of the surface will equally affect all of the orders but will not change the optical path differences. Thus, the advantage of this optical sensor (unlike the Michelson interferometer) is that it remains insensitive to those low-frequency noise disturbances.

4.2 TWO-BEAM UNEQUAL-PATH INTERFEROMETER USING BLAZED GRATING

This system is based on two-beam unequal-path interferometry using a single-order blazed diffraction grating. Just like the Michelson-type interferometer, this interferometer is used for the out-of-plane (normal) surface displacement (e.g., compressional wave) measurement of any ultrasonic or transient acoustic emission signals.

4.2.1 Reflection Blazed Diffraction Grating

A plane reflection blazed grating is shown in Figure 9. The grating is constructed by a number of densely packed right angle prisms grooved on the surface of a plane glass block on which a thin layer of aluminum has been deposited for increased reflectivity. In contrast to ordinary (amplitude or phase) diffraction gratings where the undiffracted (zero) order has the stronger intensity, in a blazed diffraction grating the stronger intensity is shifted to some higher order. This happens when the mirror reflection of the incident beam from the prism's facets coincides with any particular set of diffracted orders. Consequently, the blazed grating has a higher diffraction efficiency compared to the ordinary grating. For a given optical wavelength, the intensity of the diffracted beams, in general, is a function of the shape, angle, and depth of the grooved surfaces and of the grating surface reflectivity. The angle of the principal diffraction order is solely determined by the proper choice of the wavelength used and by grating spacing (pitch). The simple relations governing such a grating's diffraction properties, grating equation and blazed angle, can be written as

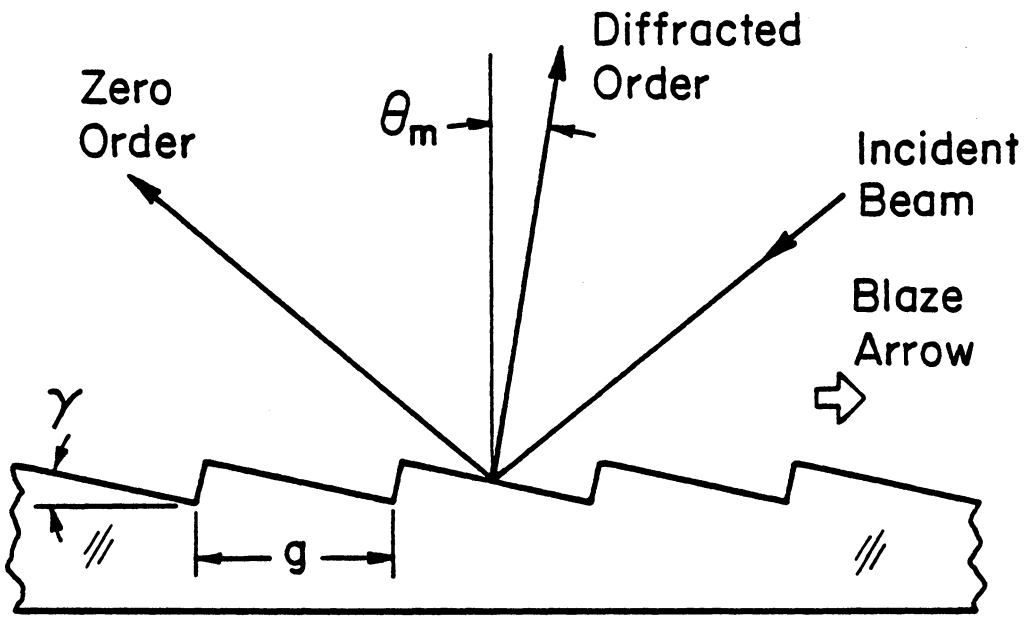

Figure 9. Diffraction action of a single-order blazed reflection grating.

$$\sin \theta = m\lambda/g + \sin \alpha$$

$$\gamma = (\alpha + \theta)/2 \ ,$$

where g = grating pitch, m = diffraction order, θ = diffracted angle, α = angle of incidence, and γ = blaze angle. For a more detailed analysis of diffraction blazed grating and its properties, see Reference [21].

As was mentioned previously, when the correct light wavelength is used, when the spacing of linearly grooved surfaces is proper, and when the selection of the blaze angle is correct, the grating behaves such that an incident coherent beam of the laser emerges in two dominant diffracted orders, e.g., the zero and the first order. As shown in Figures 10 and 11, the angle of incidence and its direction with respect to the blazed arrow can also be chosen so that the dominant diffracted order beam from the fine blaze grating bisects the angle between the dominant zero order beam and the incident beam. Such an arrangement will provide a single-order blazed diffraction grating with two dominant orders of near equal intensity.

4.2.2 Principles of Blazed Grating Interferometer

Referring to Figure 12, consider the conditions where: a) the incident laser source (LS) is in a direction normal

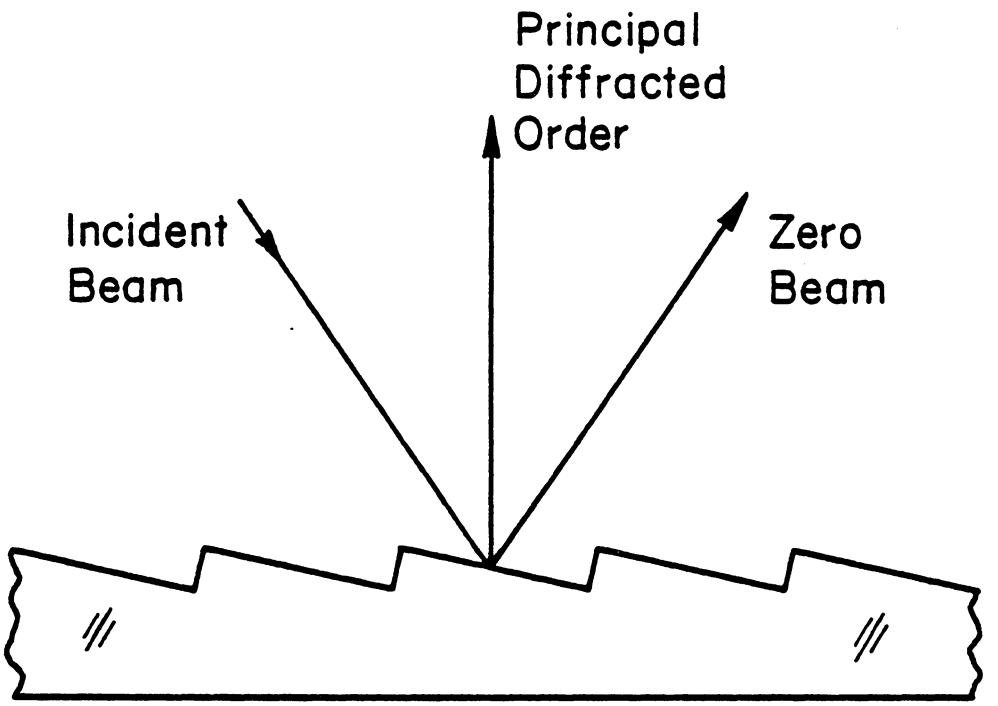

Figure 10. Diffracted first-order beam in the direction normal to the grating plane for the incident beam along the blaze arrow direction.

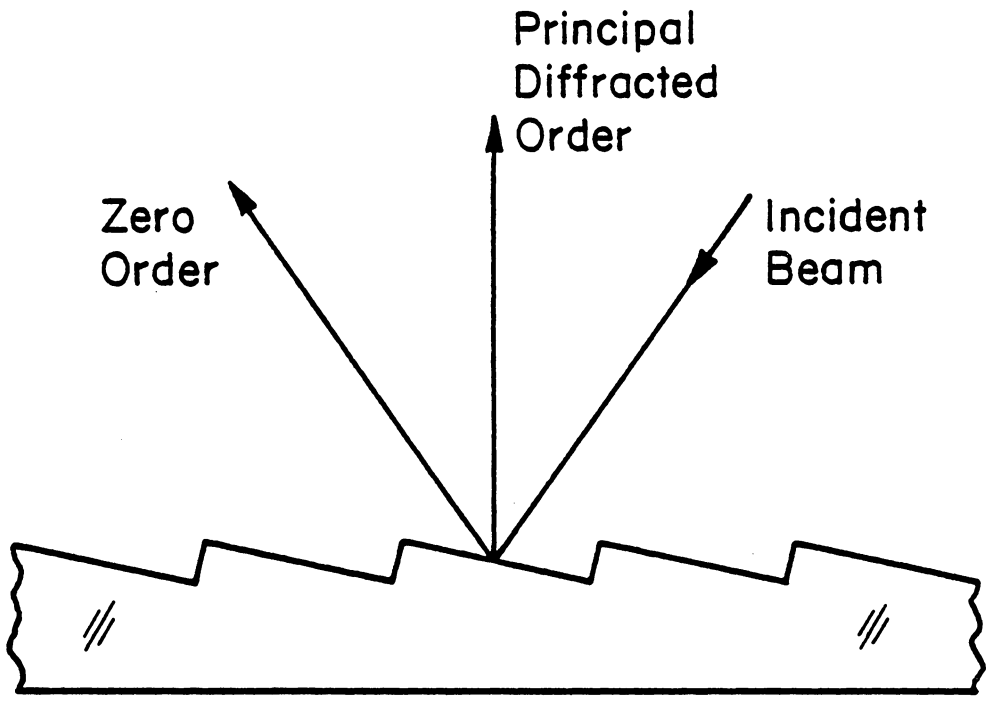

Figure 11. Diffracted first-order beam in the direction normal to the grating plane for the incident beam opposite the blaze arrow direction.

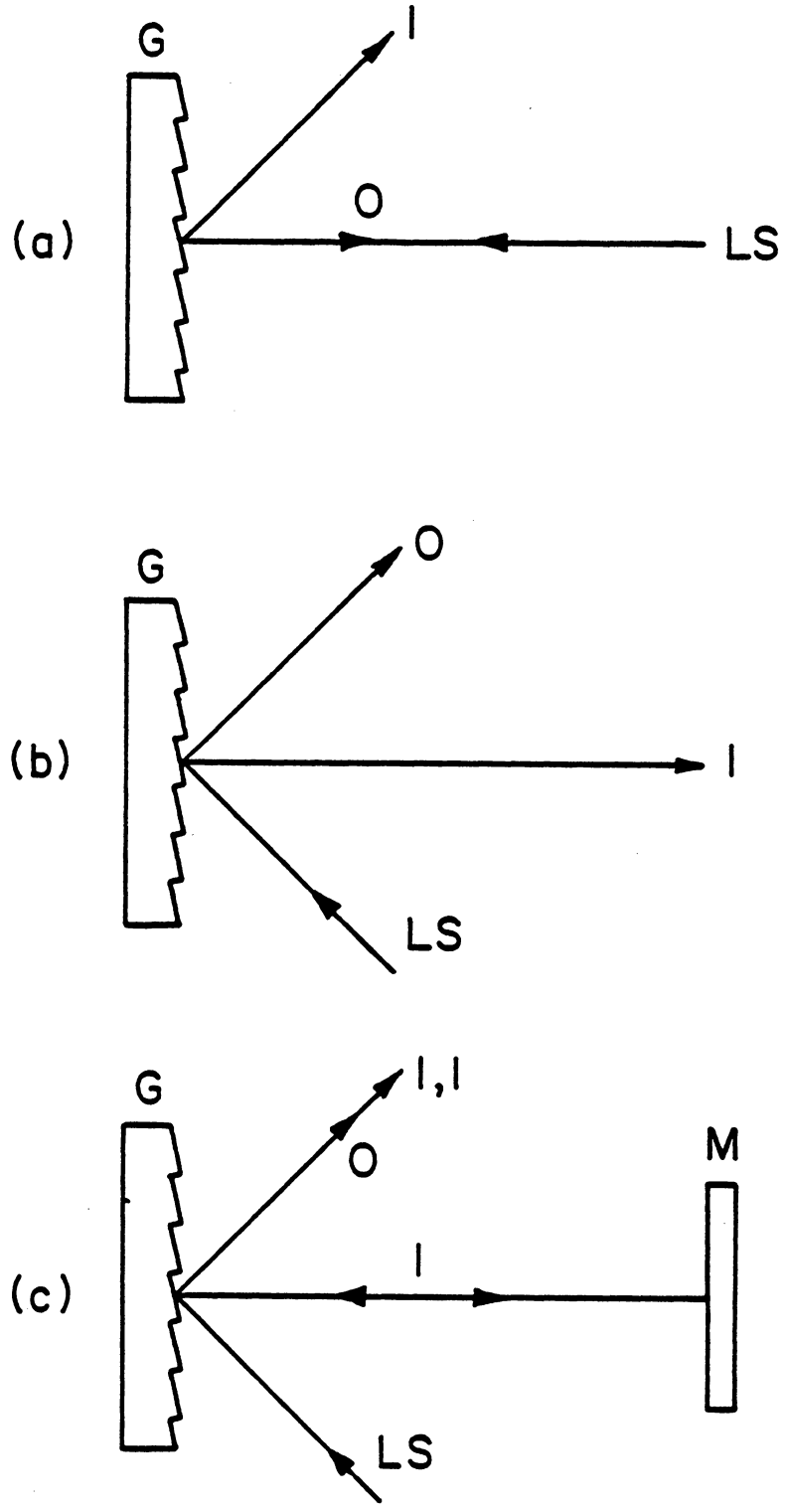

Figure 12. Diffraction action of a fine reflection blazed grating: (a)normal incidence; (b)twice the blaze angle incident in blaze arrow direction; (c)two-beam interference from simultaneous action of (a) and (b).

to the grating plane. In this case the undiffracted beam (0) also emerges in the direction normal to the grating (G) and the principal diffracted beam (1) emerges at twice the blaze angle with respect to normal incident direction. The latter is the natural direction of reflection from grooved surfaces; b) The incident angle is twice the blaze angle with respect to grating normal and oriented toward the blaze arrow. In this case the first order beam bisects the angle between the zero order and the incident direction. Interestingly enough, this diffracted beam is along the direction normal to the grating plane; c) in arrangement (b) if a mirror (M) is placed perpendicular to the first order direction so that the action of arrangement (a) is added, a two-beam interferometric system is developed. The reference arm of the interferometer is the zero order---the natural reflection of the incident beam from the grating plane---and the sensing arm is the first order diffraction. The sensing arm after reflection from the test surface is diffracted again by the action of the grating. Consequently, the resulting first order diffraction of the original first order (1,1) is superimposed upon the original zero order diffraction (0) and produces an interference pattern. The unequal-path interference of these two beams is the basic optical component of the main sensor. The system represented in

Figure 13 is the complete interferometric sensor used for the measurement of dynamically perturbed surface displacement.

This particular two-beam unequal-path interferometer, like the Michelson interferometer which is sensitive to the unwanted vibration of the reference mirror, suffers from the low-frequency movement of the grating. In order to compensate for this undesirable optical path difference, a totally different configuration can also be arranged. As shown in Figure 14, consider the conditions where: a) the angle of incidence in the direction opposite to the blaze arrow is adjusted such that the first order again bisects the angle between the zero order and the incidence; b) case (b) of Figure 12 is again reproduced; c) in arrangement (a) if a reflective surface (S) is positioned perpendicular to the undiffracted zero order so that the action of arrangement (b) is added, a two-beam interferometric system is again developed. This time the interferometric pattern produced by the two interfering beams (i.e., 1 and 0,1 orders) will be viewed from the normal direction to the grating plane. As was previously mentioned, the advantage of this particular configuration is that it is insensitive to the movement of the grating. To illustrate that, the optical ray analysis shown in Figure 15 will be useful. The dotted lines represent the slightly moved (exaggerated in this figure) grating, G', and its corresponding interferometric arms. For

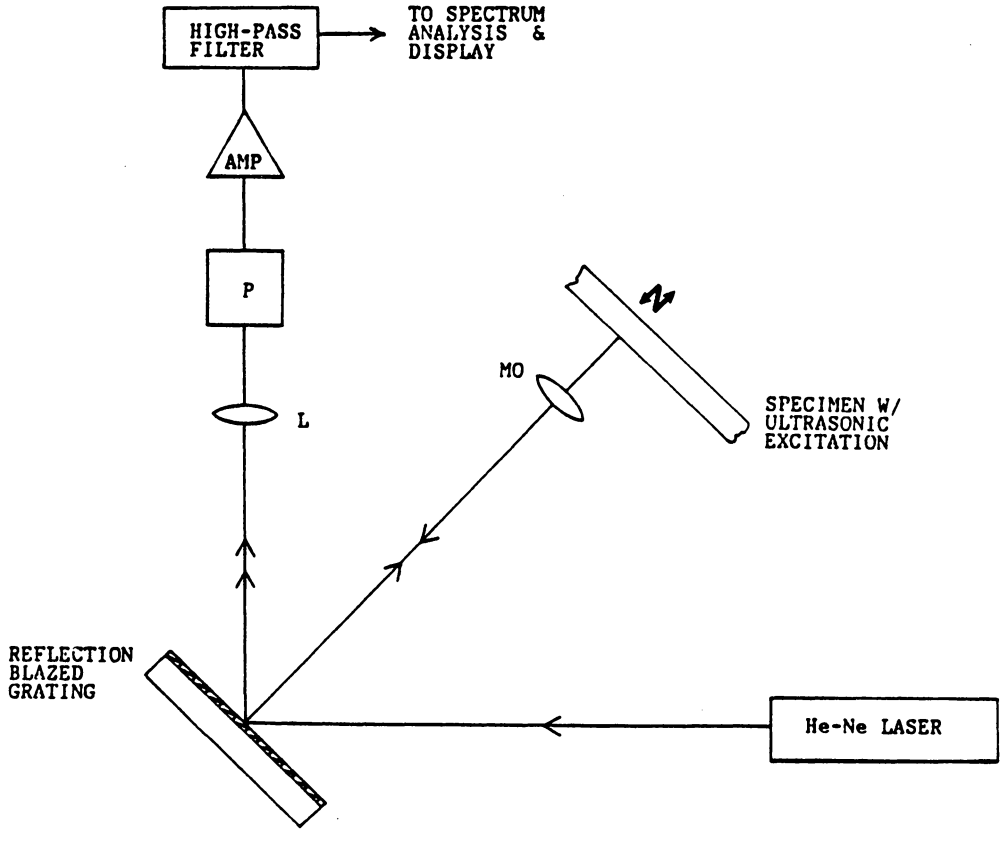

Figure 13. Schematic diagram of a two-beam unequal-path interferometric system for measuring the small out-of-plane displacement of an ultrasonically excited reflective surface.

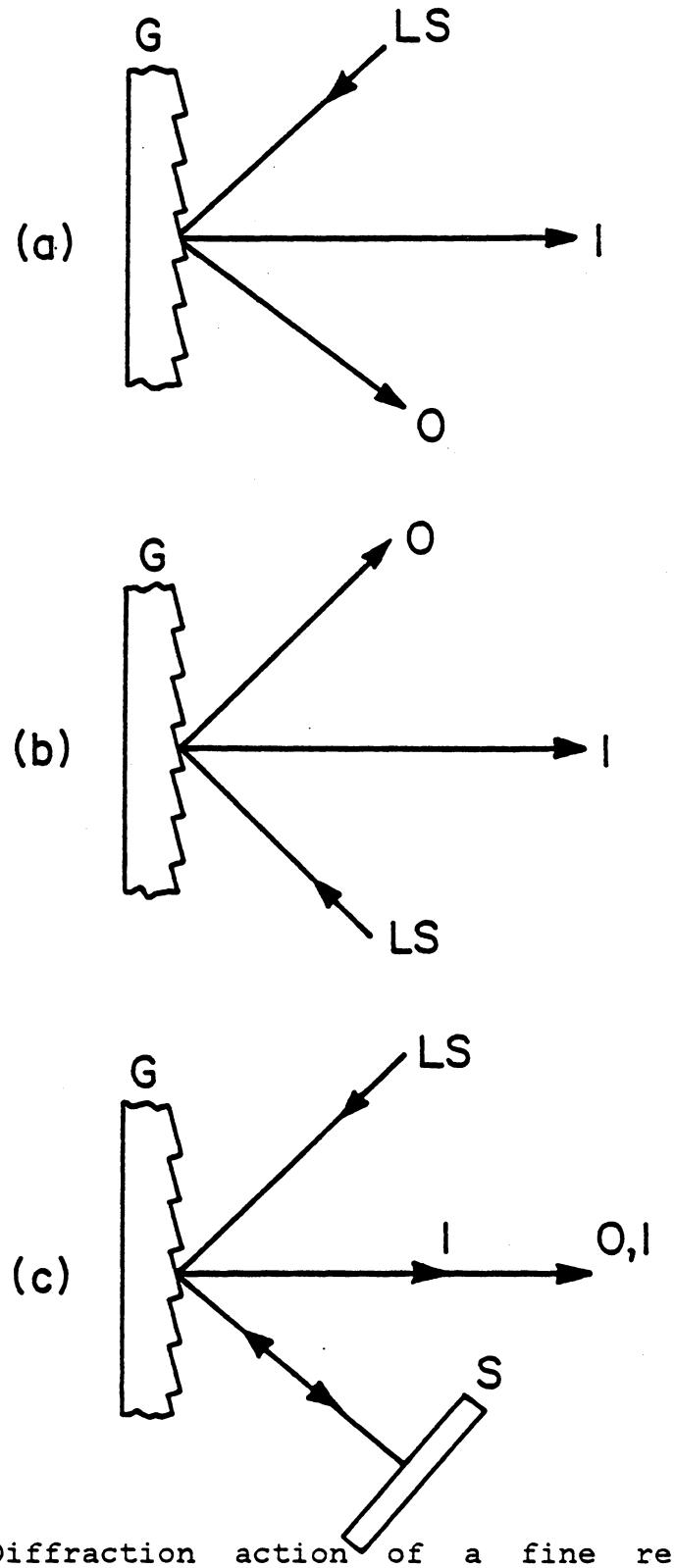

Figure 14. Diffraction action of a fine reflection blazed grating: (a)twice the blaze angle incident opposite the blaze arrow direction; (b) and (c) are the same as Figures 12b and 12c, respectively.

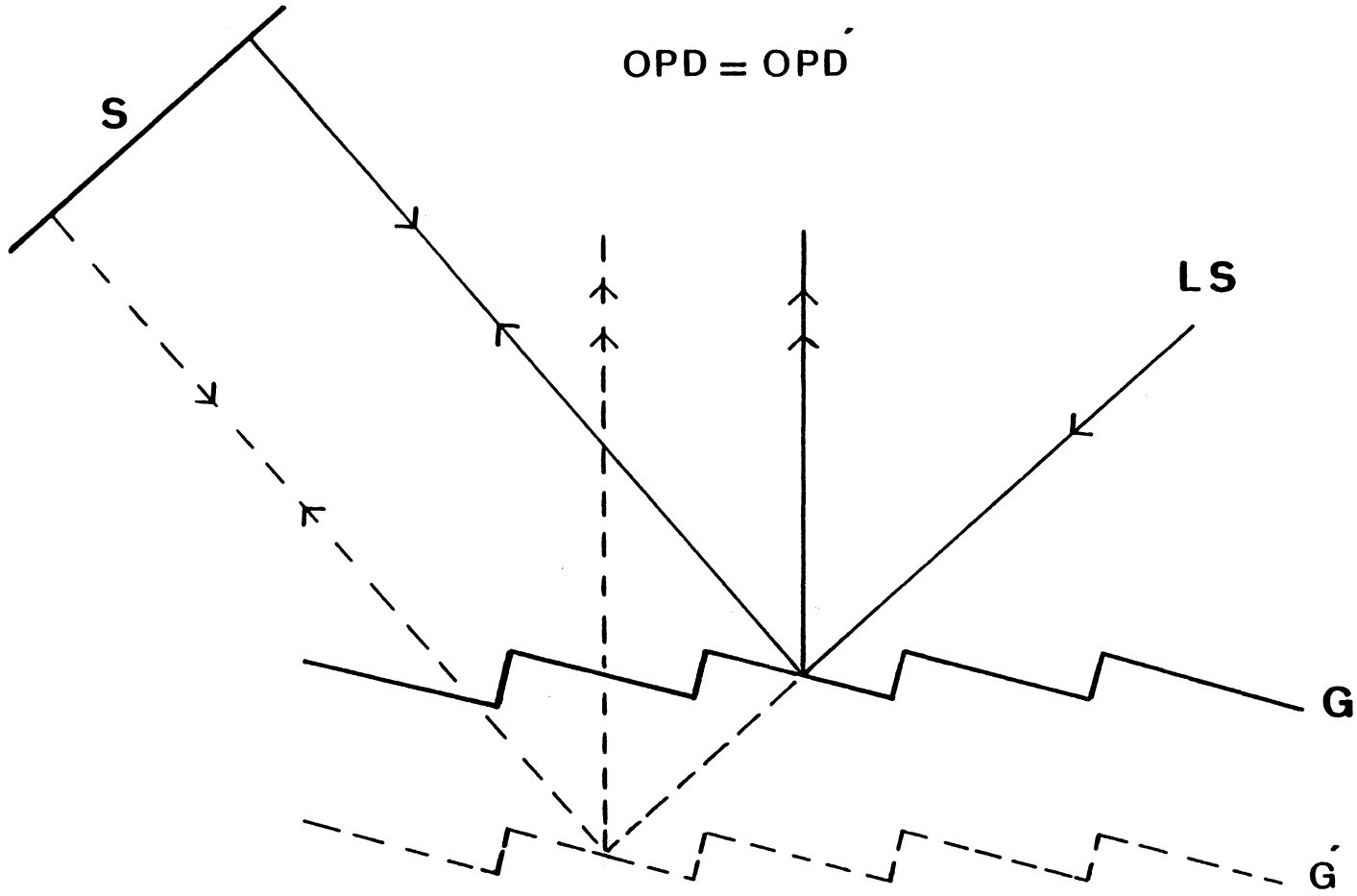

Figure 15. Unchanged optical path differences for the movement of the blazed grating with respect to a fixed position.

a 45-degree incident angle, the optical path difference for two grating positions will be the same at all times (i.e., OPD = OPD').

4.2.3 Acoustic Wave Amplitude vs Optical Intensity

The test arm and the reference arm are the two interfering coherent beams of the optical system. The phase change in the test arm with respect to the reference arm is introduced due to the distance between the grating and the surface under study. This distance will change due to surface displacement fluctuation caused by the presence of ultrasonic stress waves. In that case, the phase displacement is written as

$$\phi = 2kl + 2ku \ ,$$

where

l = optical distance between grating and the test surface
$k = 2\pi/\lambda$, optical wave number
$u = U \cos \omega t$, ultrasonic surface displacement
$\omega = 2\pi f$, angular frequency of the ultrasonic oscillation.

The factor of two in the expression for the phase displacement denotes the fact that light travels twice through the optical path between the grating and the test surface. If both superposing beams of the interferometer have the same optical intensity (this is a reasonable assumption since both zero order and first order diffractions of the blazed grating have relatively close intensities), upon superposition the resultant optical intensity deviates from a minimum of zero to a maximum of four times the intensity of each beam, depending on the phase difference between the two beams. Using the expression already stated in Chapter III, the intensity of the two-beam interference is written as

$$P = C[1 + \cos(2kl+2kU \cos \omega t)].$$

If the spacing between the grating and the test surface is such that it introduces a phase of $n\pi/2$ radians(n is an odd integer), then

$$P = C[1 + \cos(\pi/2+2kU \cos \omega t)].$$

Therefore, the interferometric term is simply rewritten as

$$I = C \sin(2kU \cos \omega t).$$

If the amplitude of the surface displacement is much smaller than the optical wavelength, $u << \lambda$, the sine can be approximated to be equal to its argument. Thus,

$$I = 2CkU \cos \omega t.$$

This linear relationship between the instantaneous surface displacement, $u = U \cos \omega t$, and the optical intensity (time-averaged of the optical field) is the prime factor in the use of such a two-beam interferometer for quantitative detection.

4.2.4 Calibration & Large Phase Shift

The optical interferometer described earlier has the same sensitivity as any of the Michelson-type interferometers. The output of the interferometer can be calibrated so that the absolute magnitude of the surface displacement can be determined. If the surface under study is subjected to large displacement excitations ($u > \lambda/4$) and the peak-to-peak signal output is noted, then the magnitude of the smaller displacements ($u < \lambda/4$) can be obtained from its peak-to-peak signal output.

As was mentioned earlier, the interference of two equal-intensity beams has a magnitude which varies between

two extreme opposite values depending on the relative phase difference (ϕ) between the test and reference beams. For the interferometer to operate at the point of maximum sensitivity (i.e., smallest phase shift giving rise to largest change in intensity), the relative phase must be kept constant halfway between the two limiting phases throughout the operation. Unfortunately, the presence of low-frequency mechanical and thermal fluctuations existing in the testing environment alters the proper tuning. To solve this problem, a slight modification to the optical system of Figure 13 may suffice--- the blazed diffraction grating can be driven by a low-frequency piezoelectric crystal at a large displacement amplitude so that the face of the grating translates at least an amount $\lambda/4$. This causes the passage of phase difference through the optimum point of sensitivity at the instant of high-frequency transient surface fluctuations. The frequency of the phase shifter should be low enough to allow the entire signal to be detected at the maximum operating condition (quadrature point). Through the use of this large phase shifter the interferometer can also be calibrated.

4.2.5 Comparison with Two-Beam Michelson-type Interferometers

The above system is simpler than the Michelson interferometer; the reflection blazed diffraction grating is the primary component of the interferometer. Through a simple rearrangement of the grating, e.g., by selecting the zero order as the sensing arm a two-beam interferometer is formed in which the mechanical movement of the grating does not introduce any optical path difference between the first and the zero order beams of the interferometer. Therefore, unlike the Michelson interferometer, this arrangement is not sensitive to the low-frequency noise associated with the unwanted mechanical vibration of the reflection grating. Moreover, in the ordinary Michelson interferometer only half of the laser power is utilized and the other half is fed back into the laser. The optical intensity returning into the laser might alter the laser power output which in turn might cause an increase in the signal noise level and reduce the sensitivity. The feedback problem is usually solved by using optical or acousto-optical isolators [22] which effectively prevent any light from entering the laser. In another treatment of the problem, a dual-quadrature Michelson interferometer [7] was constructed basically to take advantage of the complementary optical intensity pattern

which was fed back to the laser. For the two-beam unequal-path interferometer, which utilizes a single-order blazed diffraction grating, most of the energy of the incident laser beam is distributed into the zero and the first order so that very little light corresponding to the second order diffraction is returned to the laser. it does not have the problem of one-half the laser output being fed back to the laser and causing the introduction of optical noise into the detected signal. Also, the possible vibration of the blazed grating component will not introduce the unwanted low-frequency noise signal which exists due to the movement of the reference mirror in Michelson-type interferometers.

4.3 FLEXIBLE FIBER OPTIC PROBING INTERFEROMETER

The use of optical fibers as a light guiding medium can be a great advantage in optical probing flexibility [23]. In this regard, an attempt has been made to utilize single-mode-step-index fiber optic interferometry. There are special kinds of single-mode optical fibers that preserve the state of linearly polarized light, which must be maintained in the interferometric application. These types of birefringent fibers have geometric flexibility and allow the test arm of the interferometer to be isolated from the bulky

optical table. There are two classes of fiber optic sensors. In one application the fiber itself is used as a sensing device (intrinsic sensor [24]). In another application it is used to simply guide the optical wave through its medium (extrinsic sensor). The latter has been incorporated into the two-beam unequal-path interferometric system. The optical system shown in Figure 16 is the optical fiber link extension of the probing arm of the previously discussed interferometer (see section 4.2.2 in this chapter).

The test arm of the interferometer in the air medium has been coupled into the fiber medium (≈ 8-meter-long) using a microscope objective (5X) to focus the beam on the carefully prepared front flat surface of the stripped fiber (see Appendix A). The highly birefringent, polarization preserving single-mode optical fiber is used to operate at an optical wavelength of 630 nm. The second microscope objective provides the beam illumination and reception from the reflective surface under study. The use of an interferometric fiber optic sensor in this fashion allows the ultrasonic scanning of the reflective surface of a stationary object which is located away from the bulky optical bench.

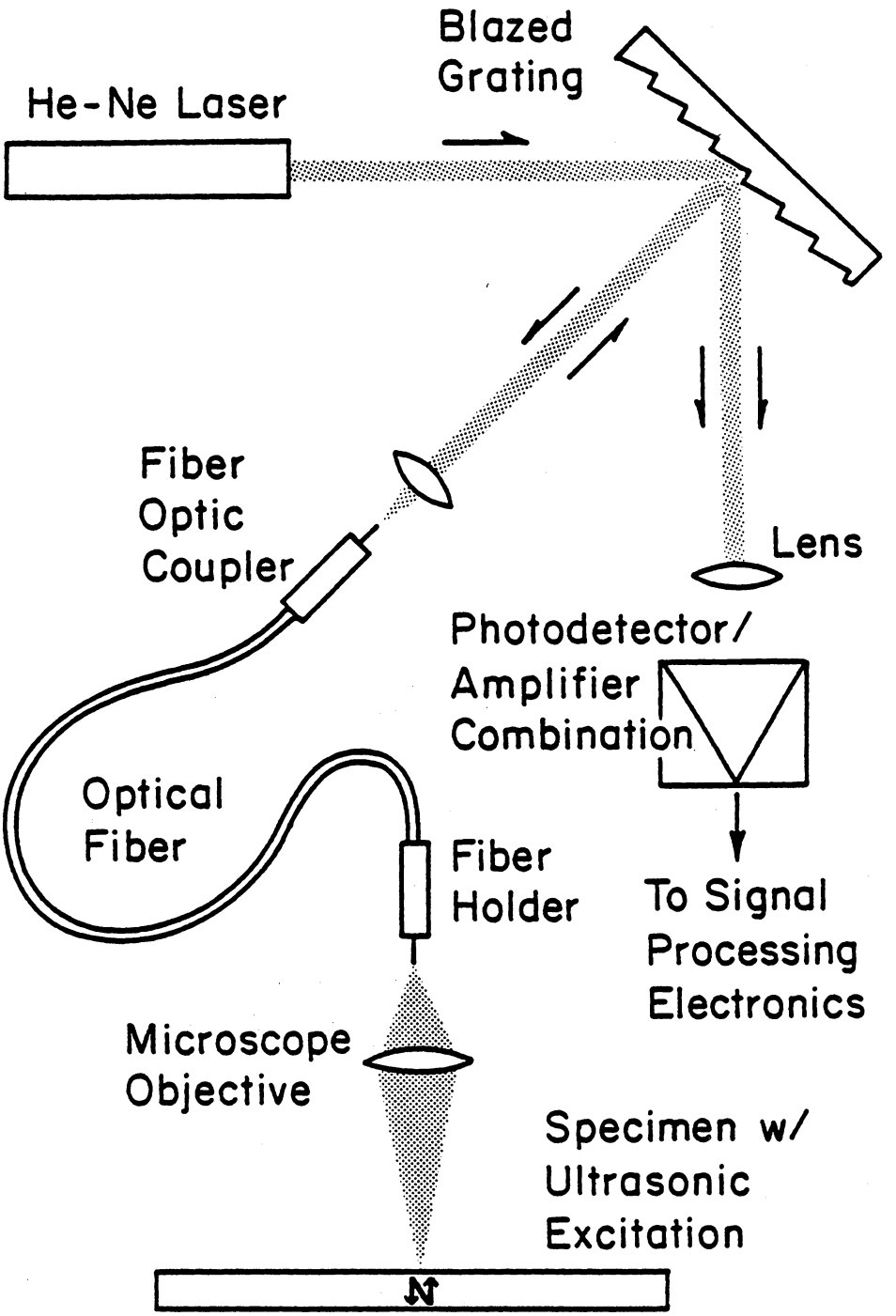

Figure 16. Schematic diagram of a flexible single-mode fiber optic interferometric system.

4.4 LASER SPECKLE INTERFEROMETER FOR RETRO-REFLECTIVE DIFFUSING SURFACES

The interferometers described so far, as well as any of the Michelson-type interferometers are only sensitive to the out-of-plane displacement of the motion of the test surface under strain. In order to measure the in-plane displacements on the test surface, a new speckle interferometer has been designed. The speckle effect is produced when a diffusing surface is illuminated in coherent light. The intensity of the speckle pattern is a random distribution caused by interference of the light amplitudes from all of the contributing points on the diffusing illuminated area [25].

4.4.1 Laser Speckle

For the in-plane surface displacement measurement of a diffusing reflective surface, laser speckle interferometry based on the double-beam illumination arrangement of Leendertz [13] can be used. Figure 17 shows the optical ray analysis for a " subjective " speckle pattern imaged by a lens.

A specularly diffusive object is interrogated by two symmetrically illuminating beams of laser light. The portion of the scattered laser beams (the speckle pattern) formed by

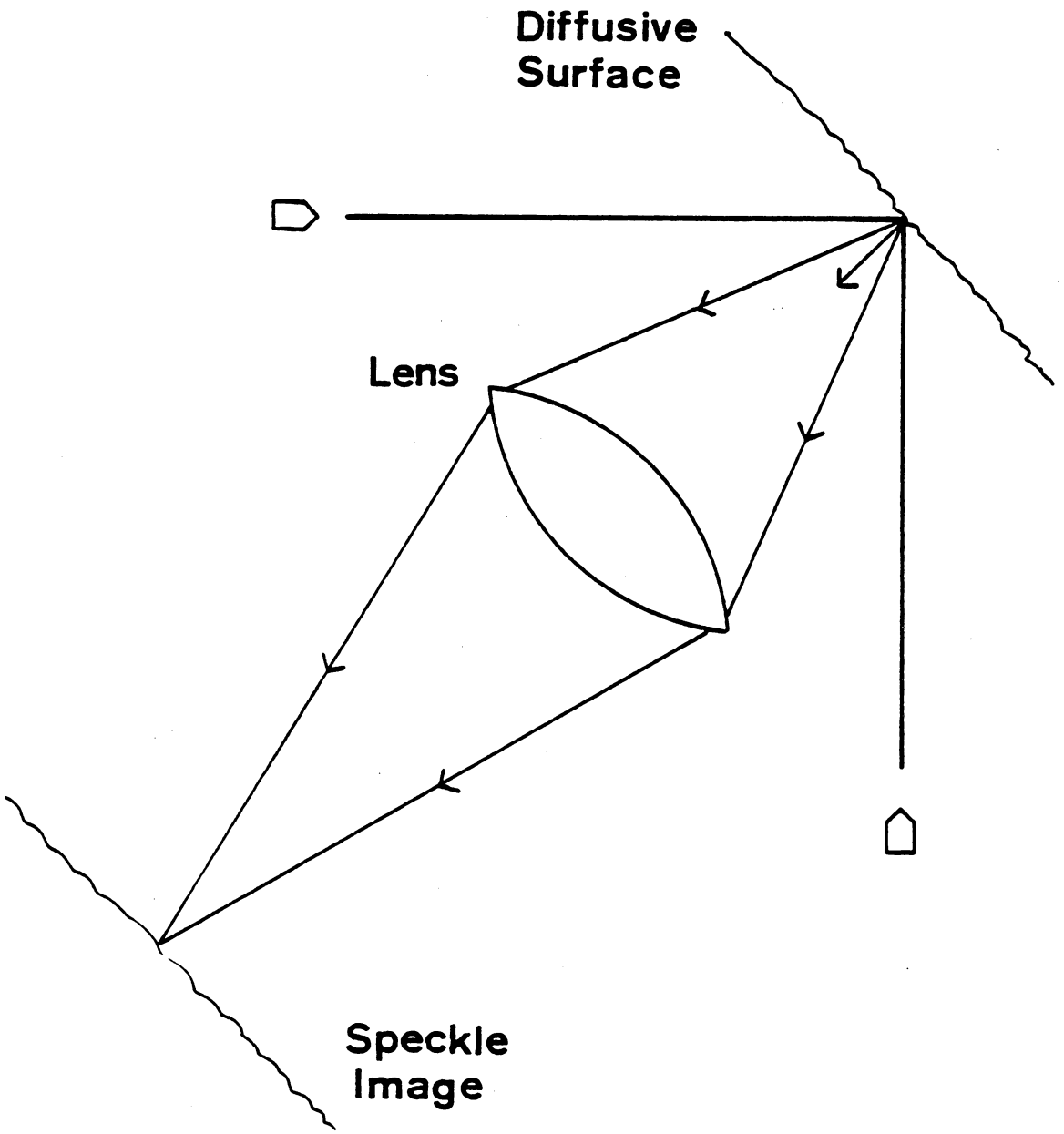

Figure 17. Schematic diagram of the double-beam speckle interferometric arrangement and an imaging lens.

each beam is gathered by an imaging lens. The two spatially superimposed speckle images then coherently interfere to produce the combined (correlated/uncorrelated) speckle patterns. This effect can also be accomplished by the scattering of light on a retro-reflective diffusing surface area under interrogation. Figure 18 is a photograph of such a speckle pattern. The bright and dark cells in the speckle pattern are formed due to multiple interference of all contributing points (diffusive reflectors) on the illuminated area. The diffusing surface is made with stick-on sheeting of a high grain retro-reflective material (see Appendix B). Spherical scattering grains on the diffusing adhesive tape reflect back an incident beam of light to form a diffraction halo, similar to an Airy disk diffraction produced by a circular aperture [26]. The diameter of the diffraction halo at a distance l from the retro-reflective surface is

$$1.22\lambda l/s \ ,$$

where s is the diameter of the spheres and λ is the wavelength. In addition, the random spatial distribution of these densely packed spheres modulates the far-field diffraction pattern, i.e., it creates the speckled diffraction pattern.

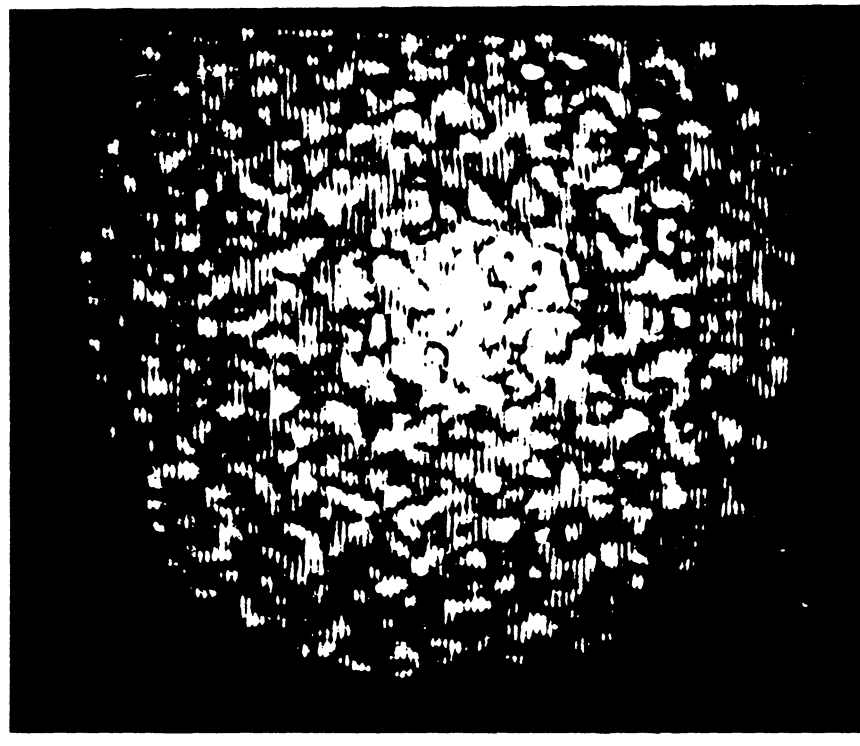

Figure 18. Laser speckle image of a small interrogating area of a retro-reflective diffusing surface.

4.4.2 System Configuration

In this optical configuration (Figure 19) the unexpanded laser beam converges by the action of a long focal-length condensing lens. A beam-splitter positioned close to the focusing lens divides the focusing beam into two components. Both focusing beams are directed onto the surface under study by deflecting mirrors located along their paths. The illuminated region of the test surface is covered with a diffusing retro-reflective tape. Due to retro-reflectivity of the illuminated area the speckle pattern formed by each of the beams is seen by the beamsplitter. The beamsplitter spatially superimposes these two identical speckles and forms the correlation speckle pattern. The speckle grains (spheres) are considered to be attached to the diffusing tape which in turn adheres to the object surface so that if the object surface is disturbed, the speckle patterns are disturbed too. Consequently, the motion of the points on the illuminated area causes a variation in the detailed distribution of the correlation speckle pattern. By detecting this speckle pattern deformation (twinkling of the combined speckle patterns), the information about the displacement amplitudes of the stress wave on the illuminated object surface can be obtained.

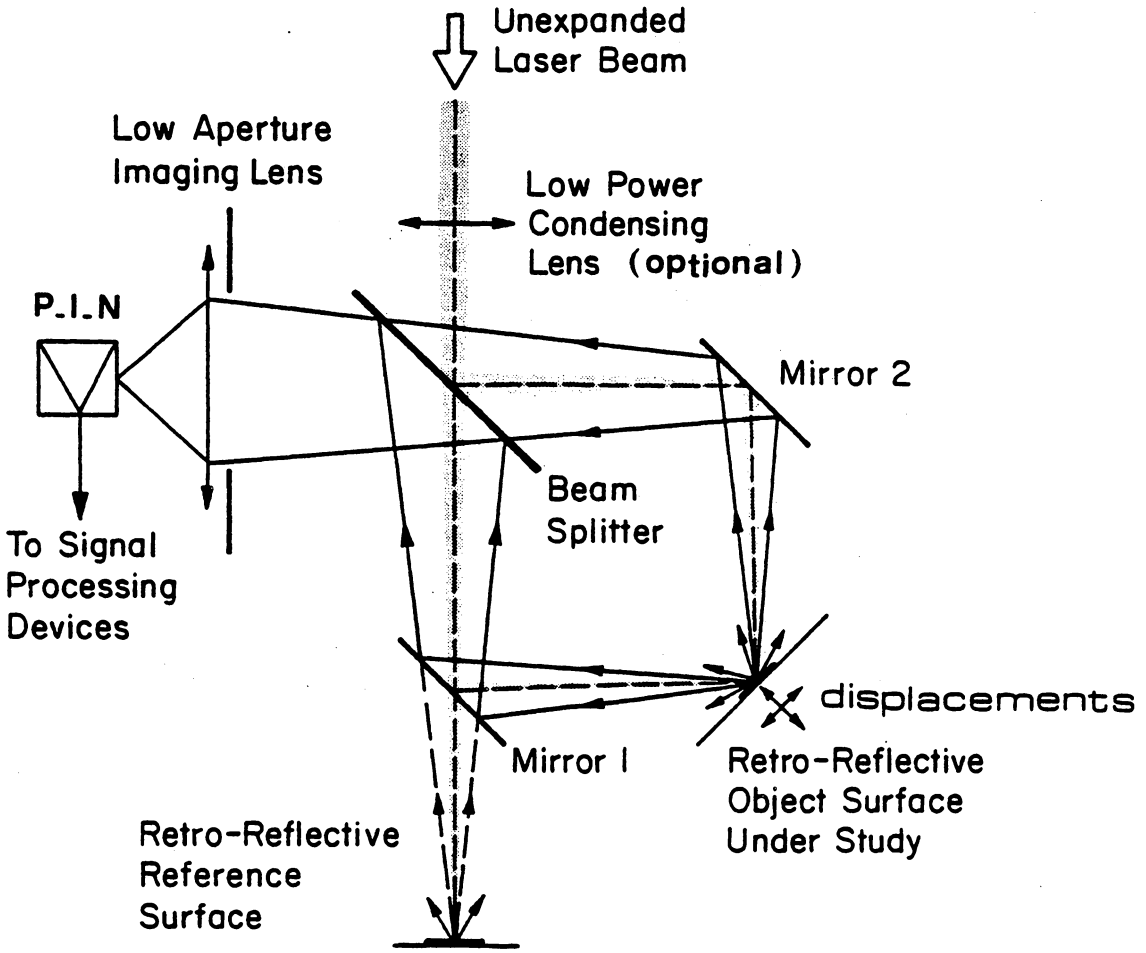

Figure 19. Schematic diagram of a laser speckle interferometric system for measuring small displacements of a retro-reflective diffusing surface; in-plane (with mirror 1) and out-of-plane (without mirror 1) displacement sensitive.

4.4.3 Resolution

The optional use of the focusing lens placed next to the beam-splitter facilitates the interrogation of a very small surface area (point-wise detection) and increases the sensitivity to the measured displacement amplitudes. The sensitivity to the acoustic amplitudes depends on the spatial resolution (size) of the focused laser beam. For ultrasonic wave detection, it is required that the diameter of the focused illumination beam be less than the wavelength of the acoustic wave. In other words, the smaller the focused laser beam diameter, the higher the detectable acoustic frequency or the broader the dynamic range. The aperture size of the image-forming lens influences the size of the speckle spots so that the speckle sizes are increased as the light-gathering diameter of the lens is decreased [27]. Since the absolute displacement amplitudes are obtained for object particle displacements of less than the speckle sizes, the production of relatively large speckle cells insures the linear response of the system.

4.4.4 Special Speckle Interferometric Arrangements

In the double illuminating arrangement of Figure 19, the in-plane displacement parallel to the direction of wave

propagation is obtained. The displacement is found to be a function of the resultant intensity of two coherently superimposed speckle pattern distributions. This intensity is a function of the phase difference (which in turn is a function of the optical path length difference) introduced by the motion of the speckle pattern [28]. The amplitude of the displacement can be obtained following proper analysis of the photodetector signal in the manner mentioned in reference [29]. Due to the angular symmetry of the double illumination beams with respect to the surface normal, only in-plane displacement of the illuminated area gives rise to twice the optical phase change for each beam. Although the normal (out-of-plane) displacement causes two optical phase changes of equal magnitude but opposite sense for the corresponding two beams, the net optical phase change contribution is always zero. By removing mirror 1 and directing the respective beam on a stationary retro-reflective tape, the superposition of two unidentical speckle patterns will be formed. This particular (single-illuminating) arrangement is primarily sensitive to the out-of-plane displacement of the test surface. Thus, both purely in-plane and mostly out-of-plane displacement sensitive measurements can be accomplished without disturbing the specimen---by simply removing one of the beam-deflecting mirrors. The above laser speckle interferometric system, in

addition to being sensitive to the in-plane/out-of-plane surface displacements, can also detect the direction of the wave propagation or identify the polarization direction of elastic modes of vibration. This is because in the double-beam illumination arrangement, the sensitivity to displacement in the interrogated surface area is only in the direction along the interface line between the plane of the two illuminating beams and the surface.

4.4.5 In-Plane/Out-Of-Plane Displacement Sensitivity

Figures 20-23 show the resultant optical path differences (OPD) for both the single-illumination / double-illumination beams on a specular and a retro-reflective surface. The arrangements of Figure 17 and Figure 19 are considered for the specularly diffusive and the retro-reflective diffusive surfaces, respectively. In these figures the optical path differences at a point of observation (on the interferometric speckle image) are calculated for the obliquely illuminated diffusing surfaces which undergo a displacement, D.

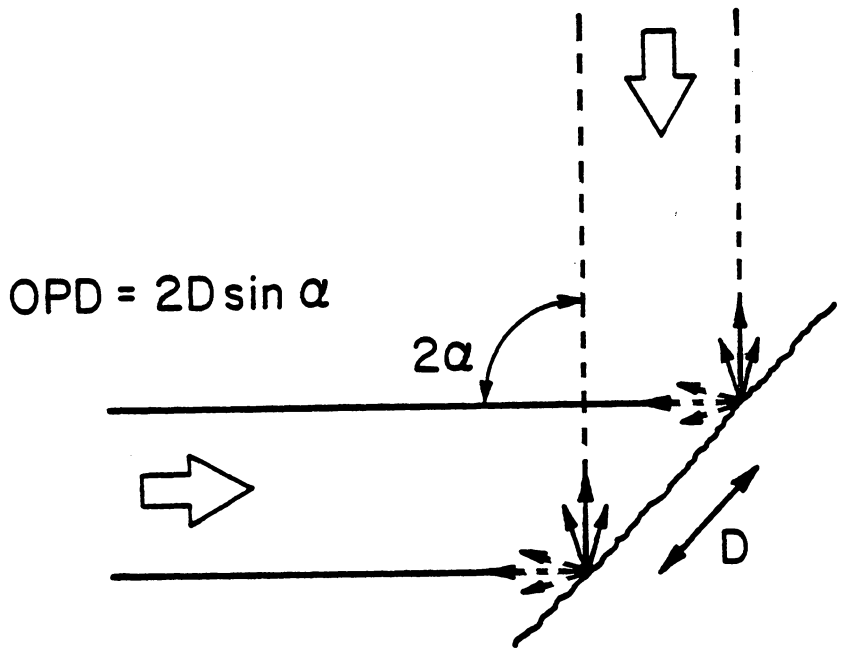

Figure 20. Double-beam illumination of a specularly diffusing surface and the corresponding optical path difference for in-plane surface displacement, D.

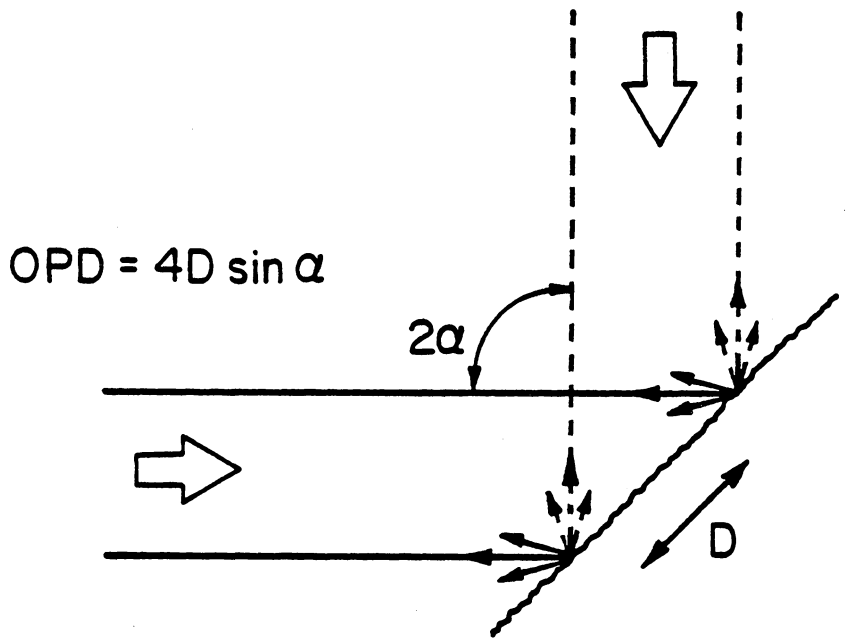

Figure 21. Double-beam illumination of a retro-reflective diffusing surface and the corresponding optical path difference for in-plane surface displacement, D.

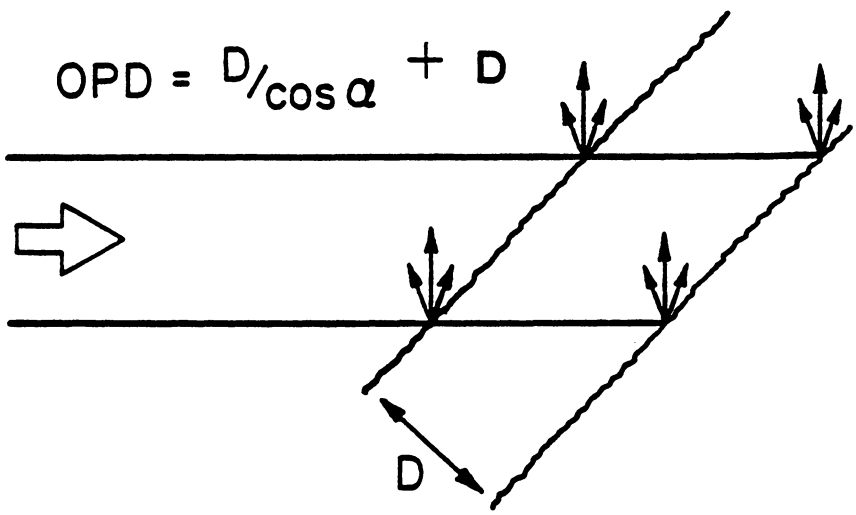

Figure 22. Single-beam illumination of a specularly diffusing surface and the corresponding optical path difference for out-of-plane surface displacement, D.

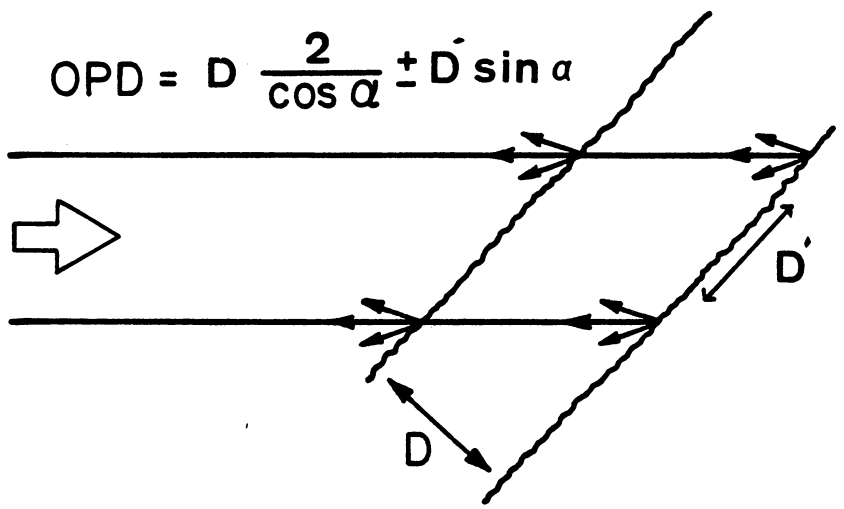

Figure 23. Single-beam illumination of a retro-reflective diffusing surface and the corresponding optical path difference for out-of-plane surface displacement, D.

For the single-beam illumination, the OPD (due to out-of-plane displacement) of a diffusing specular surface is

$D/\cos \alpha + D$ (see Figure 20).

And the OPD (due to the displacement) of a diffusing retro-reflective surface is

$2D/\cos \alpha \pm D' \sin \alpha$ (see Figure 21).

In this case, the second term (i.e., $D' \sin \alpha$) is the in-plane displacement contribution to the OPD. By rotating the specimen and positioning its surface perpendicular to the illumination beam, this term will disappear. Thus, the OPD becomes sensitive only to the out-of-plane surface displacement. For the double-beam illumination, the OPD (due to in-plane displacement) of a diffusing specular surface is

$2D \sin \alpha$ (see Figure 22).

And the OPD (due to in-plane displacement) of a diffusing retro-reflective surface is

$4D \sin \alpha$ (see Figure 23),

where α is the angle between the incident beam and the surface normal.

Due to the use of diffusing retro-reflective tape in this speckle interferometric arrangement (Figure 19), the sensitivity to the measured in-plane displacements is enhanced by a factor of two compared to the conventional speckle displacement interferometer (Figure 17). This arises from the fact that the optical path length difference caused by surface displacements is doubled as a result of retro-reflectivity (compare the OPD obtained in Figure 22 with Figure 23).

V. APPLICATIONS

Figure 24 is a schematic block diagram of a generalized ultrasonic nondestructive testing procedure. The specimen is excited ultrasonically either by internal mechanisms (e.g. acoustic emissions) or by external means. The external stimulation is done either by contacting excitation (e.g., the mechanical attachment of an ultrasonic transducer) or by noncontacting excitation (e.g., using capacitive, electromagnetic, or laser-induced ultrasonic generators). The output ultrasonic signal which will most likely be a transient mechanical disturbance needs to be monitored by a linear detector in a contacting or a noncontacting fashion. Finally, the detected analog signal is stored in an analog or digital form for subsequent physical interpretation. Figure 25 represents the schematic diagram of the instrument components setup used in the experiments that follow. These are: PZT transducer ceramics with gold polished surfaces; composite laminate specimens; small displacement-sensitive optical noncontacting ultrasonic detectors, e.g., laser and laser speckle interferometers; a broad-band ultrasonic amplifier (PANAMETRICS, serial 5660B/475); a filter; a high-speed (20 MHz ADC) data acquisition system (IBM PC plug-in transient waveform recording board with 8-bit resolution); a display monitor.

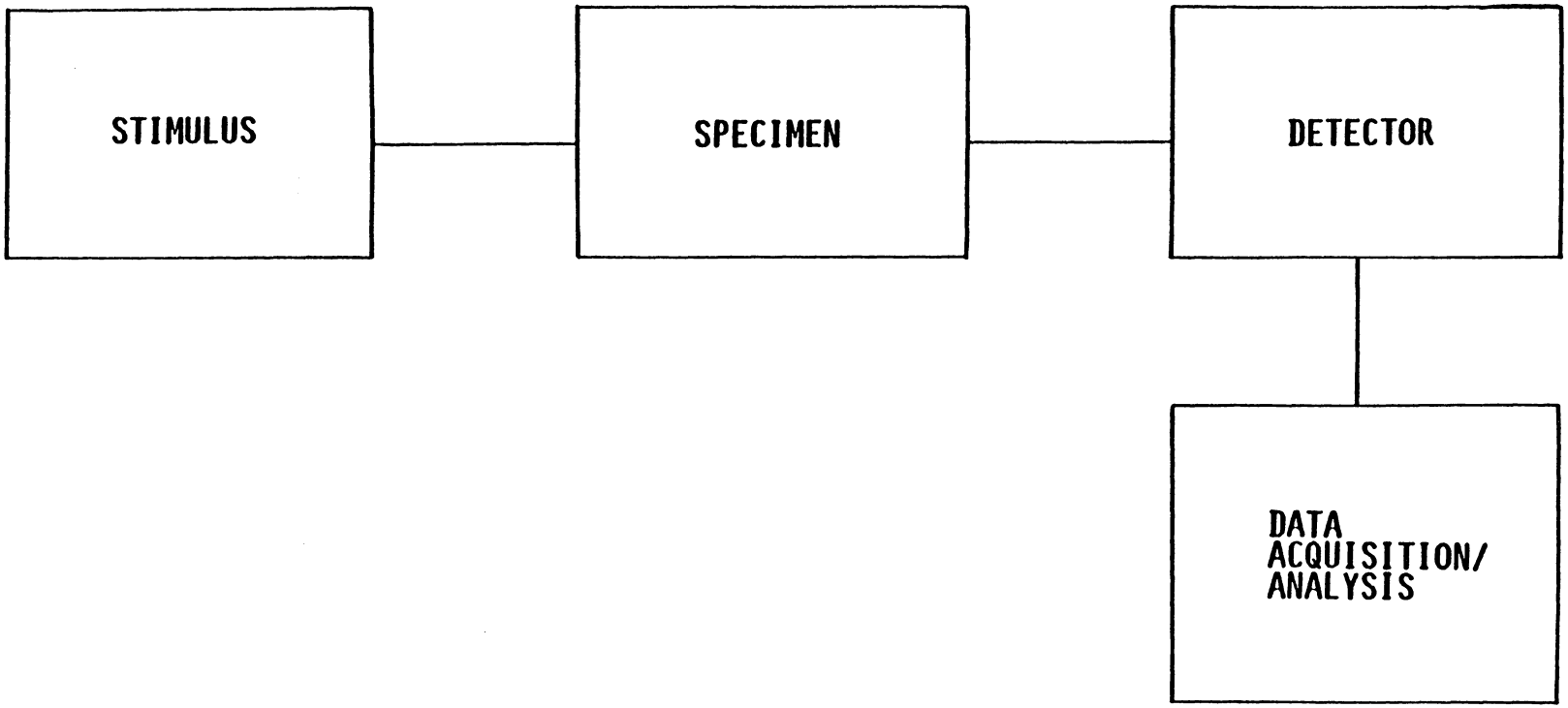

Figure 24. Block diagram of a generalized ultrasonic NDT system.

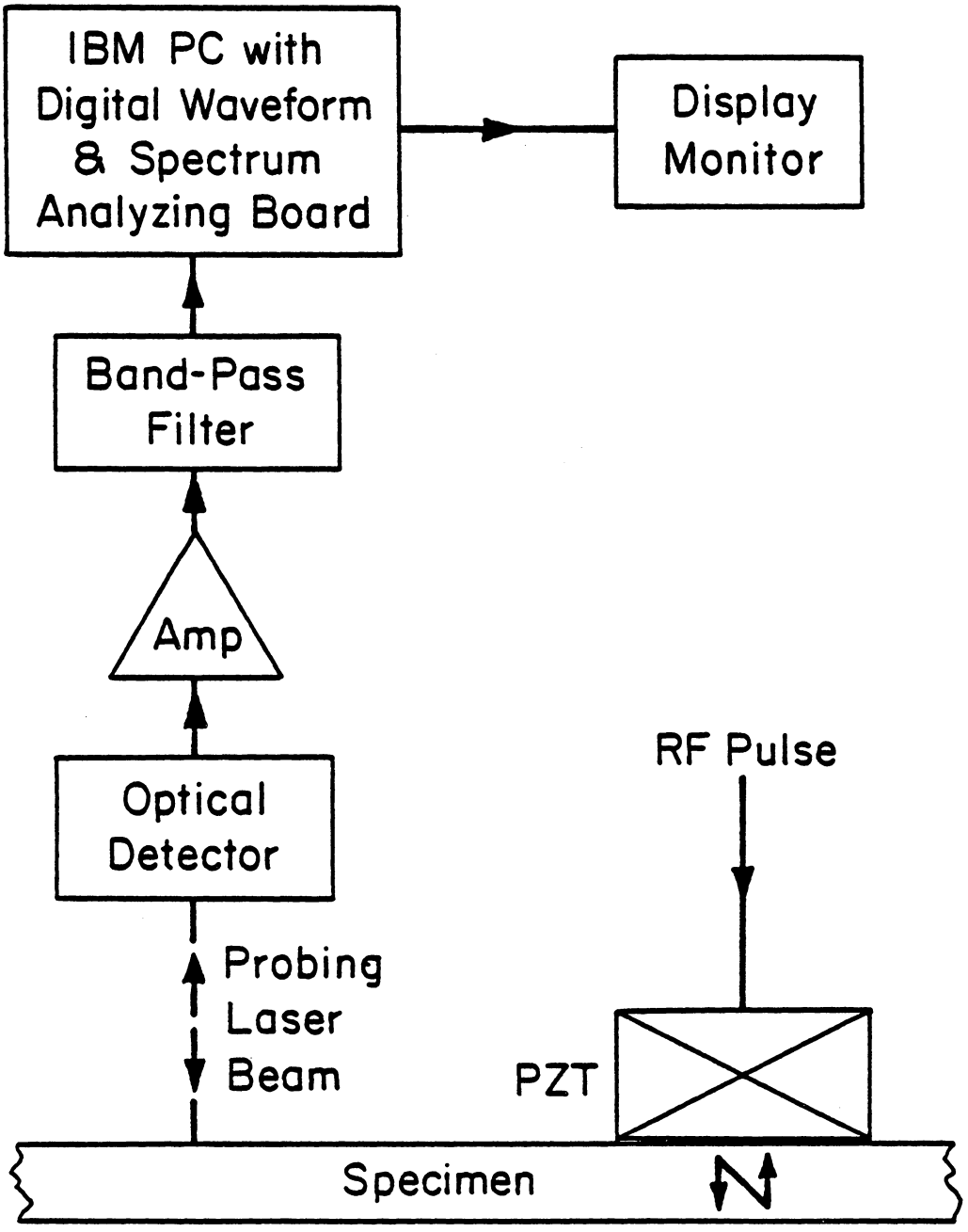

Figure 25. Schematic diagram of an optical sensor viz. the ultrasonic signal analysis system.

The additional electrical/optical components used in the system are: ultrasonic signal generators (PANAMETRICS Model 5052 UA and MATEC Model 6000) which induce the RF-pulsed and burst excitations, respectively; a low-power (10 mW) He-Ne laser (EALING); a high-speed photodetector (PHOTOP™ UDT-455HS).

5.1 Light Scattering Surface Preparation

The use of thin retro-reflective diffusing tape not only negated the need for diffusive surface preparation which is usually done through etching and white painting of the specimen surface, but also led to a new laser speckle arrangement which utilizes most of the scattered laser light and contains an improved (e.g., double for in-plane) sensitivity to displacement. However, some thought was given to the influence of this finite-thickness stick-on tape on the detected ultrasonic waves. In looking at the possible variation (e.g. damping) of surface ultrasonic displacement amplitudes, the following observations were made.

First, the surface displacement amplitude of a circular transducer element (PZT-5A, 0.5" diameter, 0.5 MHz compressional mode) driven by a MATEC ultrasonic generator was observed using the laser speckle interferometric system. Both the double-beam illumination and the single-beam illumination arrangements were used. For both arrangements,

the transient mechanical excitations of the transducer surface were recorded when the interrogation point was at the center of the surface, covered with one and subsequently two layers of diffusing retro-reflective tape. Figures 26 and 27 represent the detected in-plane (radial) displacement signals using the double-beam illumination when the interrogated area is covered with one and two layers of tape, respectively. The error in reading the displacement off the grid scale is ± 1/32 of full scale (i.e. peak-to-peak). Figures 28 and 29 represent the detected out-of-plane (normal) displacement signals using the single-beam illumination when the interrogated area is covered with one and two layers of tape, respectively. Secondly, the double-beam illumination procedure was also applied for a rectangular transducer element (PZT-5A, 1" X 1/2", 0.25 MHz shear mode). Figures 30 and 31 represent the detected in-plane displacement signals along the transducer's width when the interrogated area is covered with one and two layers of tape, respectively. And Figures 32 and 33 represent the detected in-plane displacement signals along the transducer's length when the interrogated area is covered with one and two layers of tape, respectively. Finally, the above transducer (i.e., the rectangular element) along with the double-beam illumination technique was applied both on a plexiglas coupon and on a thin composite plate covered with one and also two layers of tape at the point of interrogation.

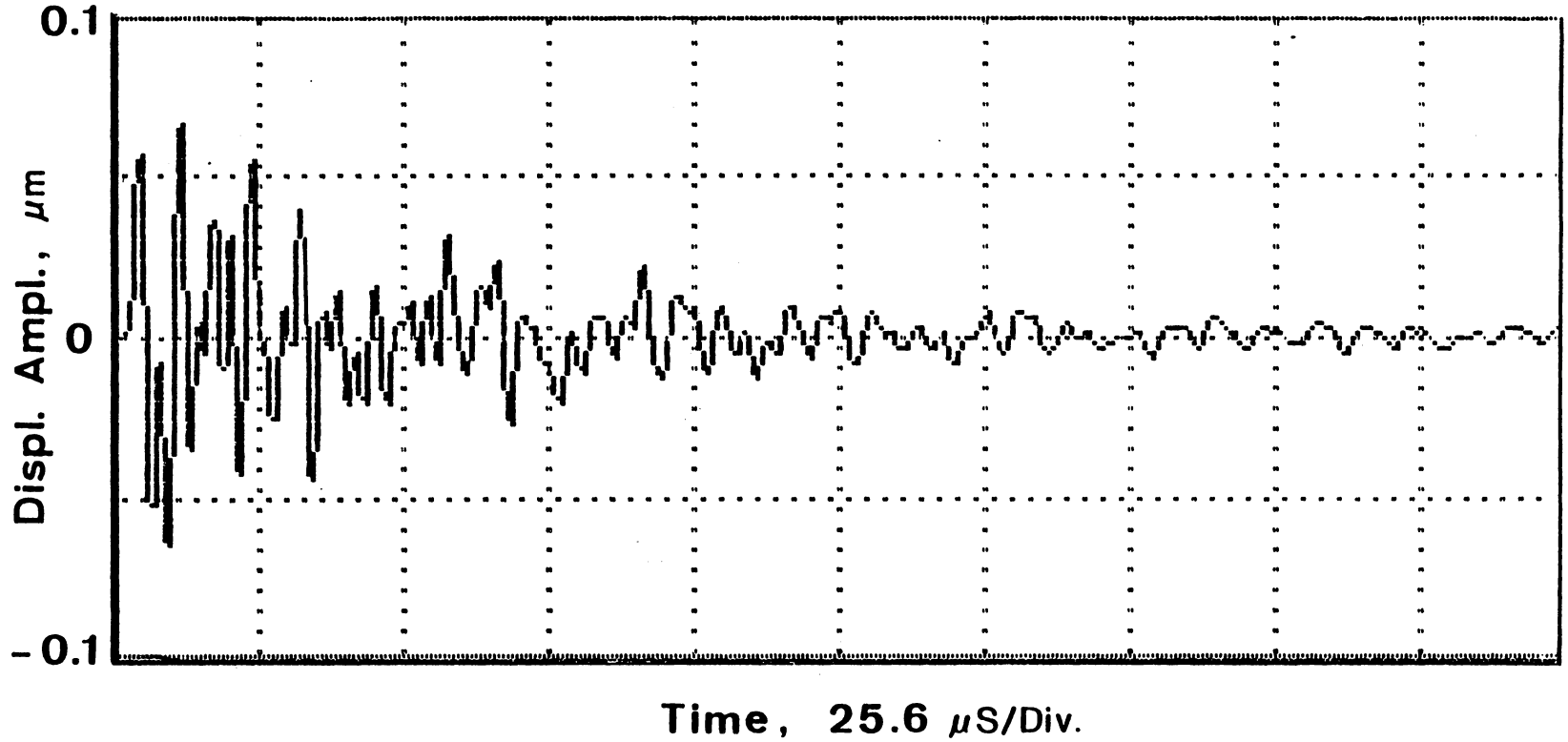

Figure 26. An optical response to the transverse surface displacement of a PZT ceramic covered with one layer of diffusing retro-reflective tape at the interrogated area.

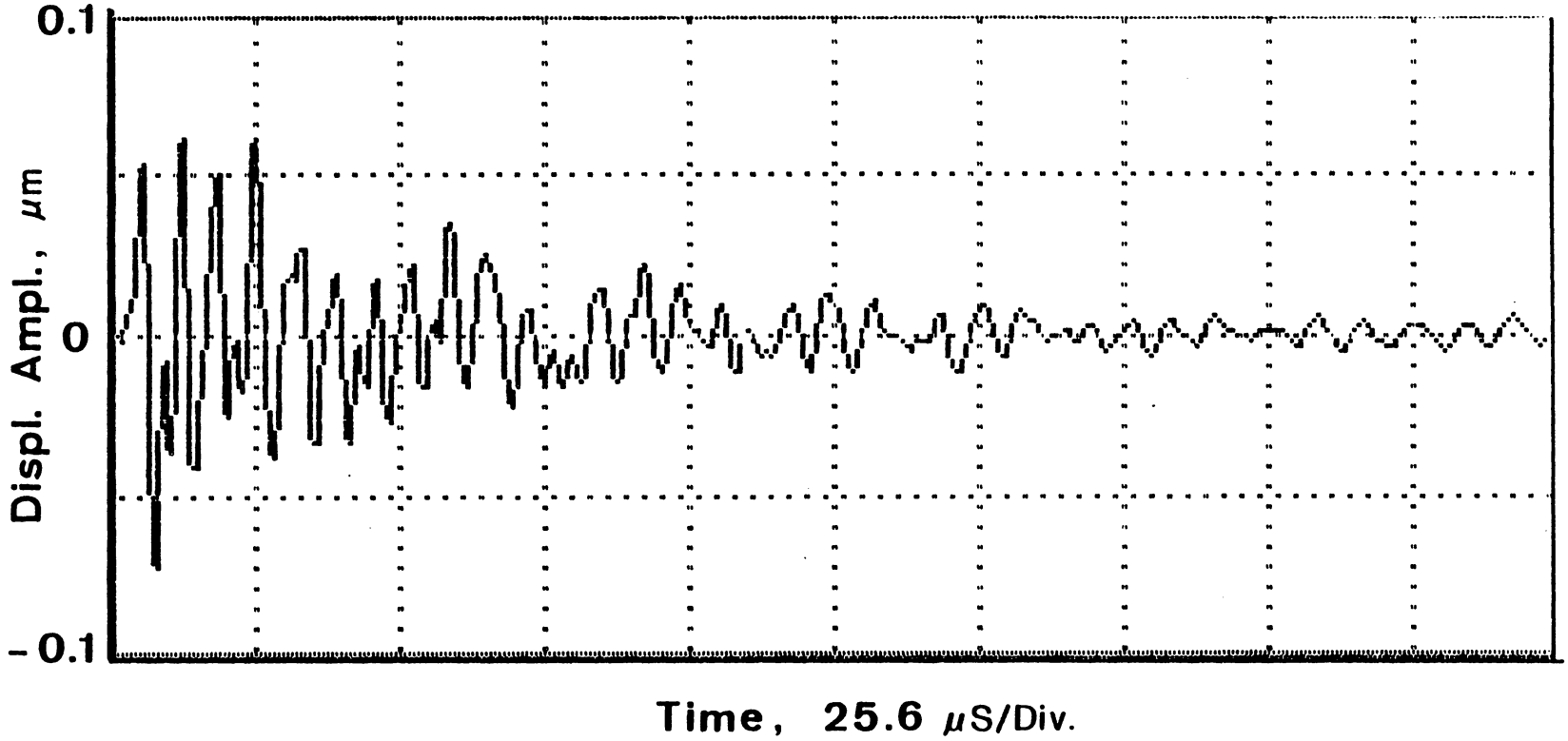

Figure 27. An optical response to the transverse surface displacement of a PZT ceramic covered with two layers of diffusing retro-reflective tape at the interrogated area.

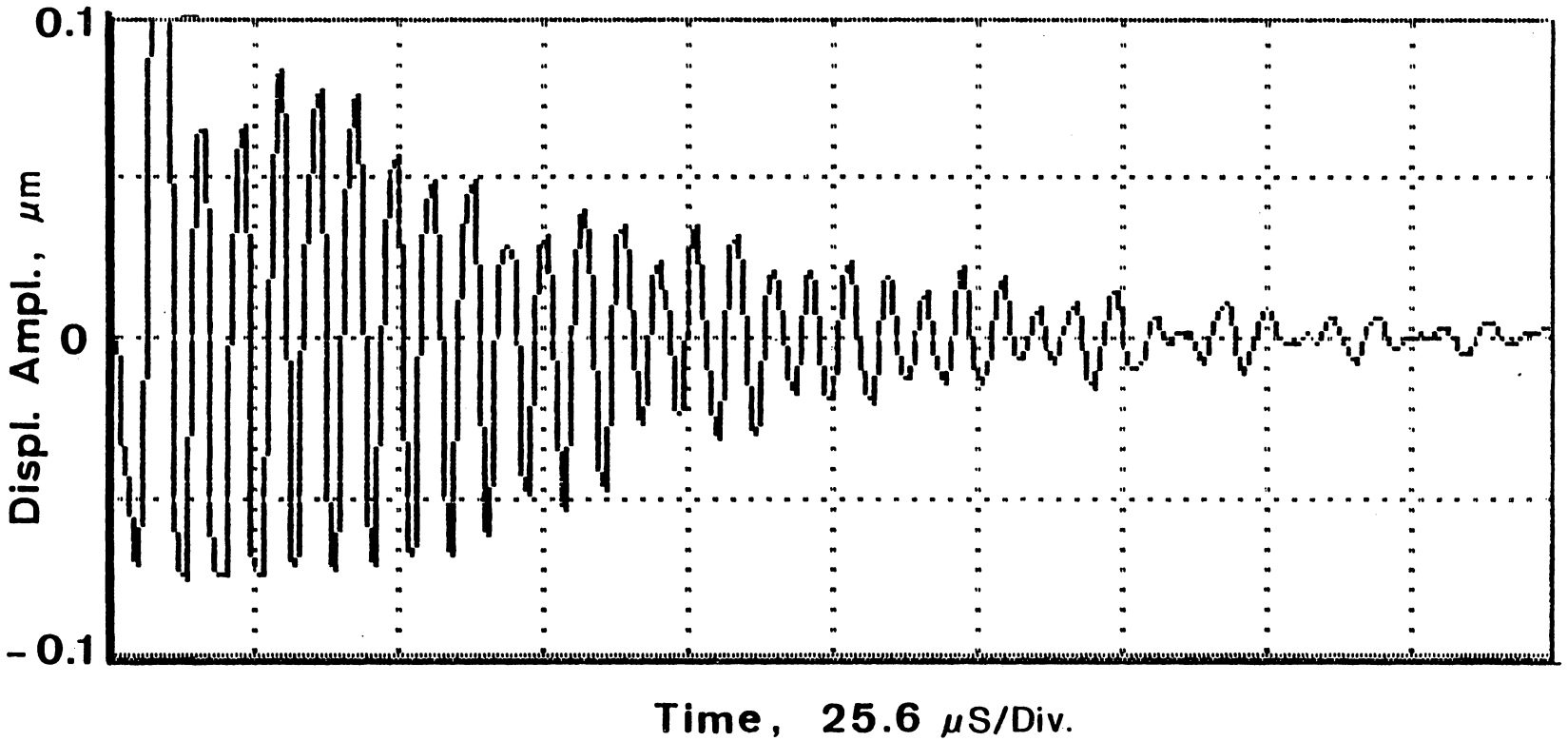

Figure 28. An optical response to the normal surface displacement of a PZT ceramic covered with one layer of diffusing retro-reflective tape at the interrogated area.

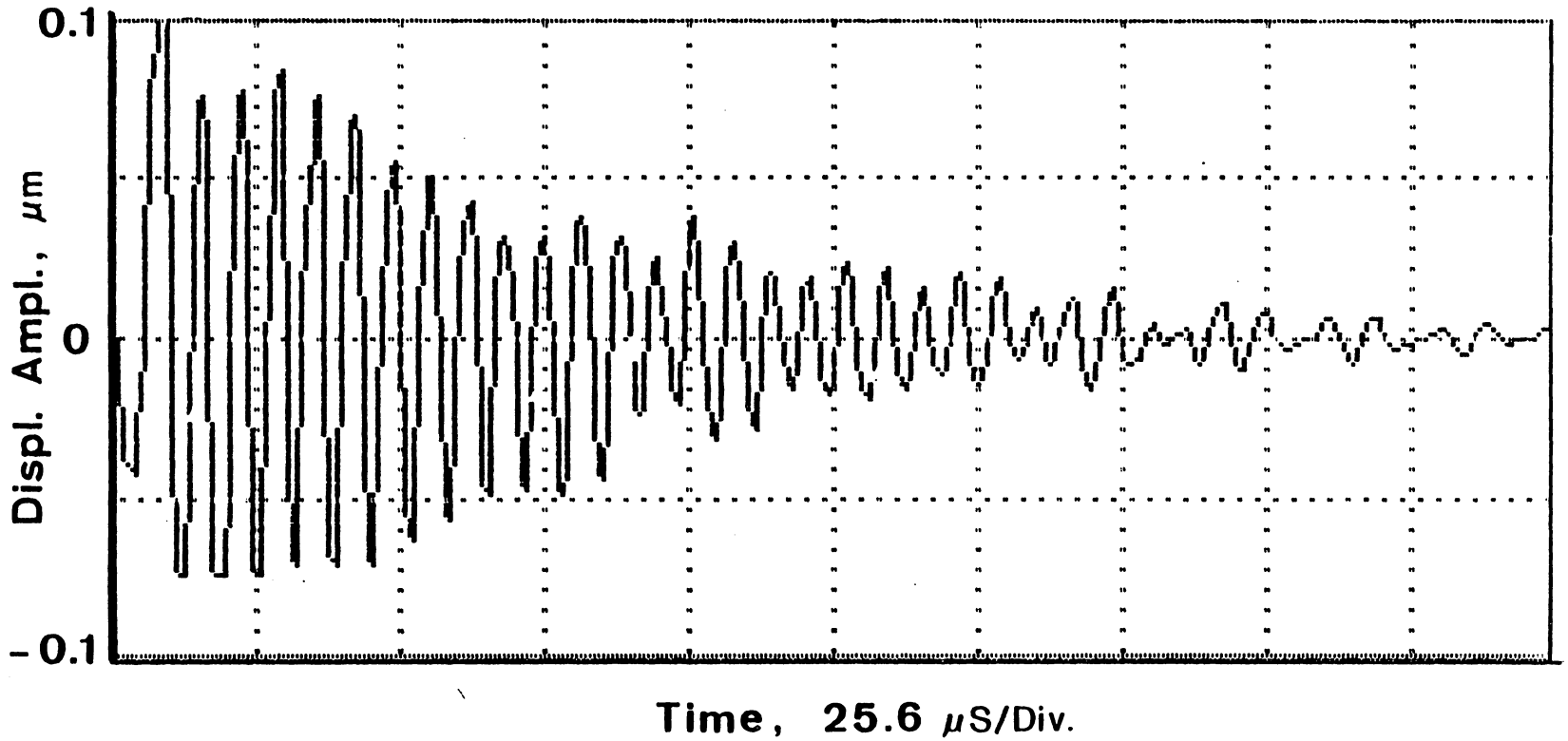

Figure 29. An optical response to the normal surface displacement of a PZT ceramic covered with two layers of diffusing retro-reflective tape at the interrogated area.

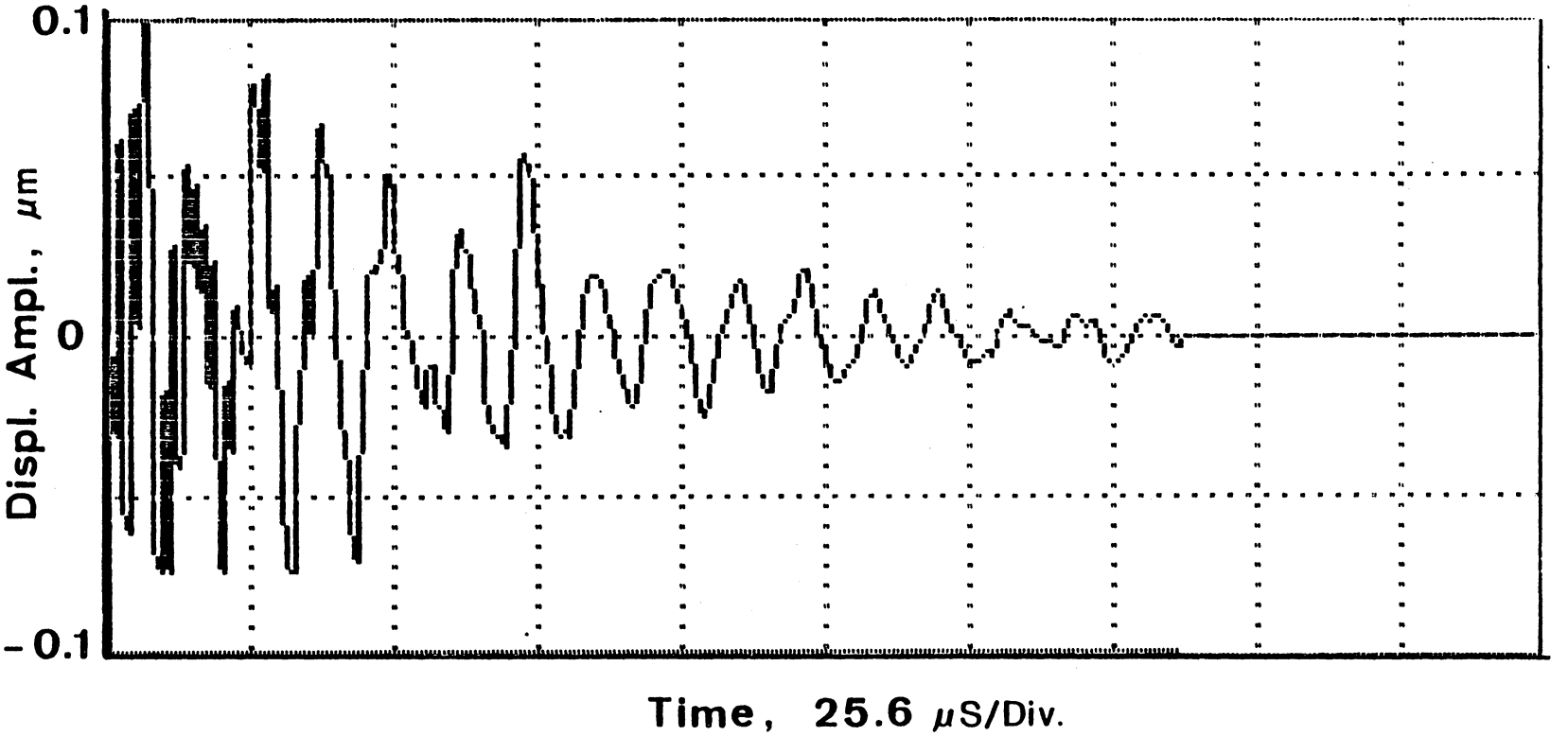

Figure 30. An optical response to the transverse surface displacement along the width of a PZT ceramic covered with one layer of diffusing retro-reflective tape at the interrogated area.

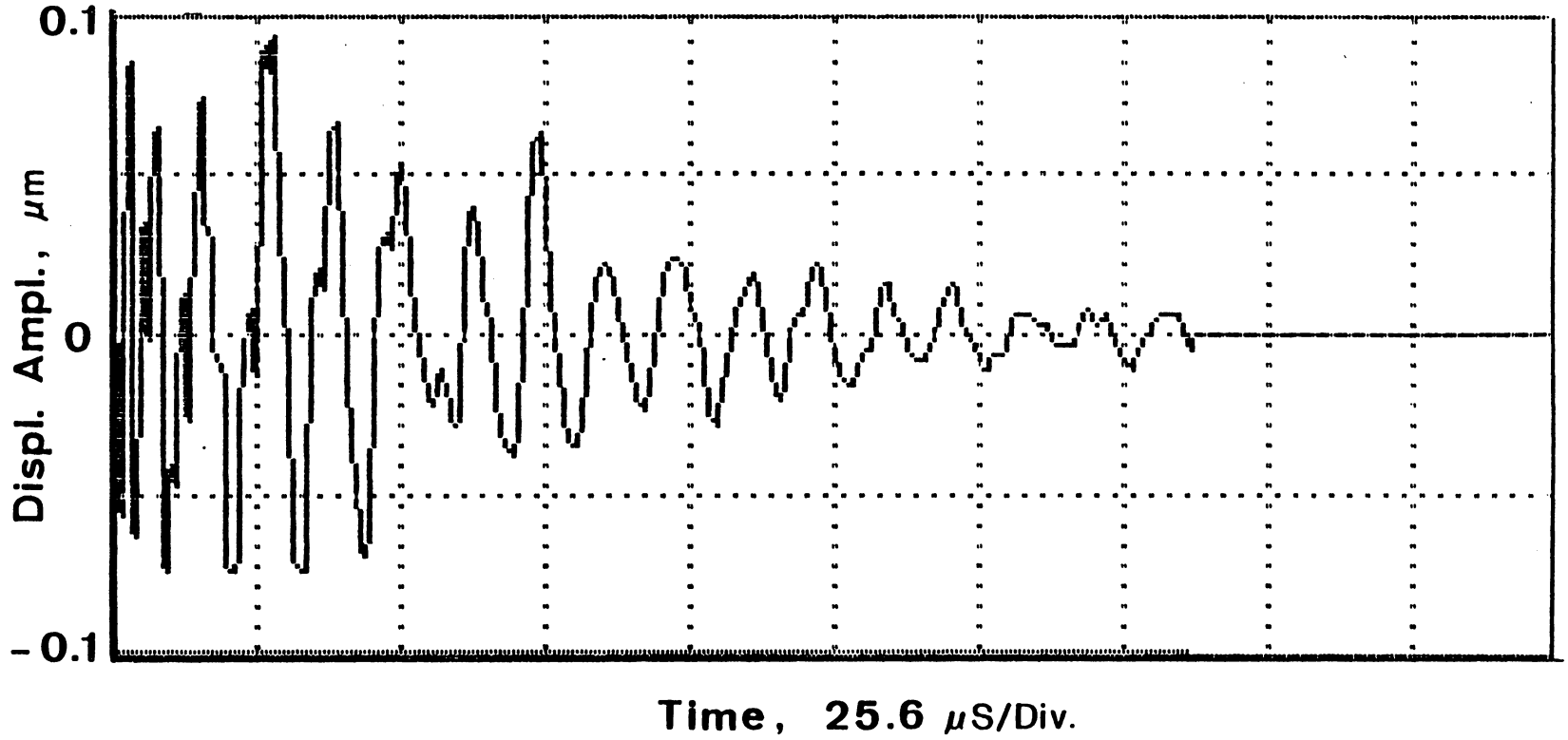

Figure 31. An optical response to the transverse surface displacement along the width of a PZT ceramic covered with two layers of diffusing retro-reflective tape at the interrogated area.

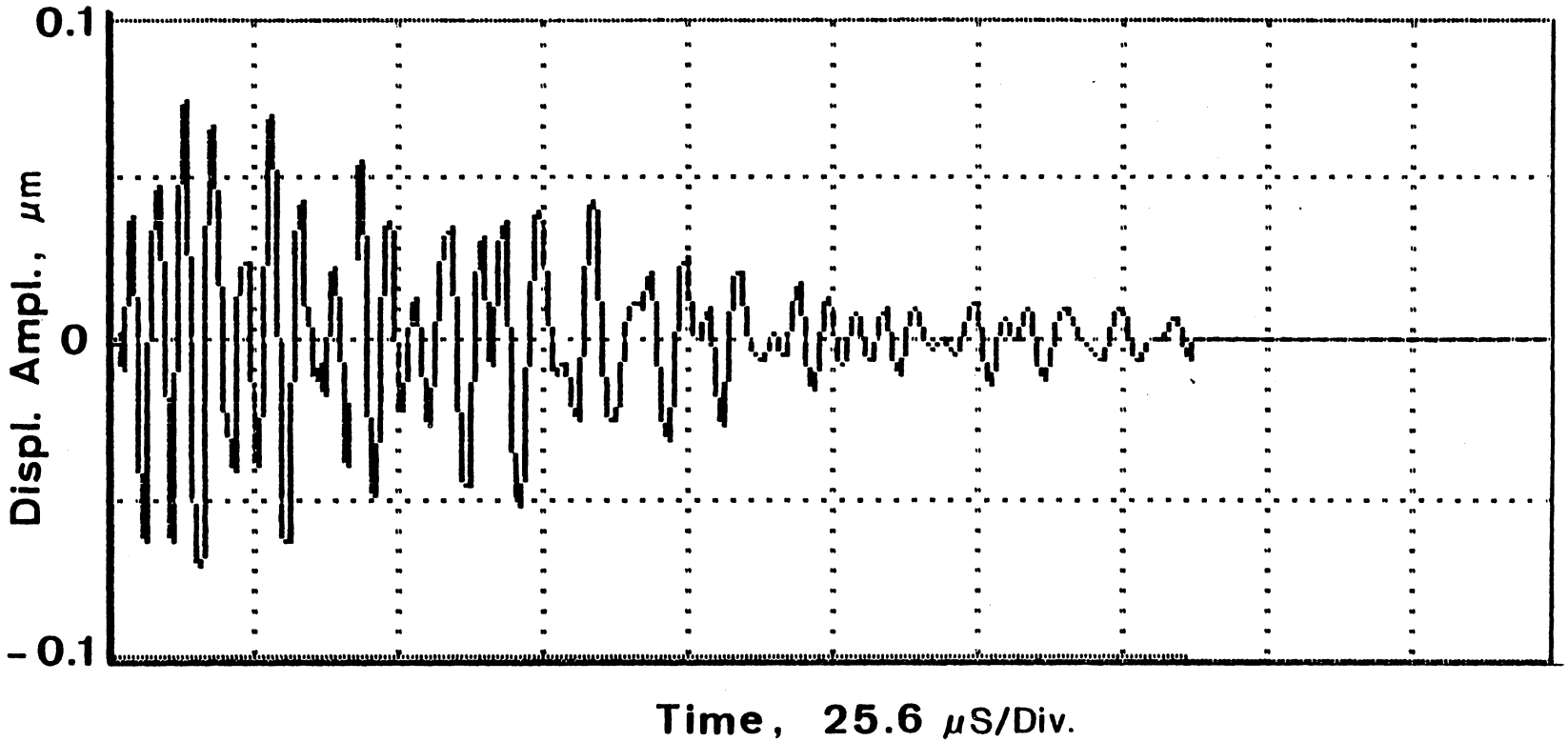

Figure 32. An optical response to the transverse surface displacement along the length of a PZT ceramic covered with one layer of diffusing retro-reflective tape at the interrogated area.

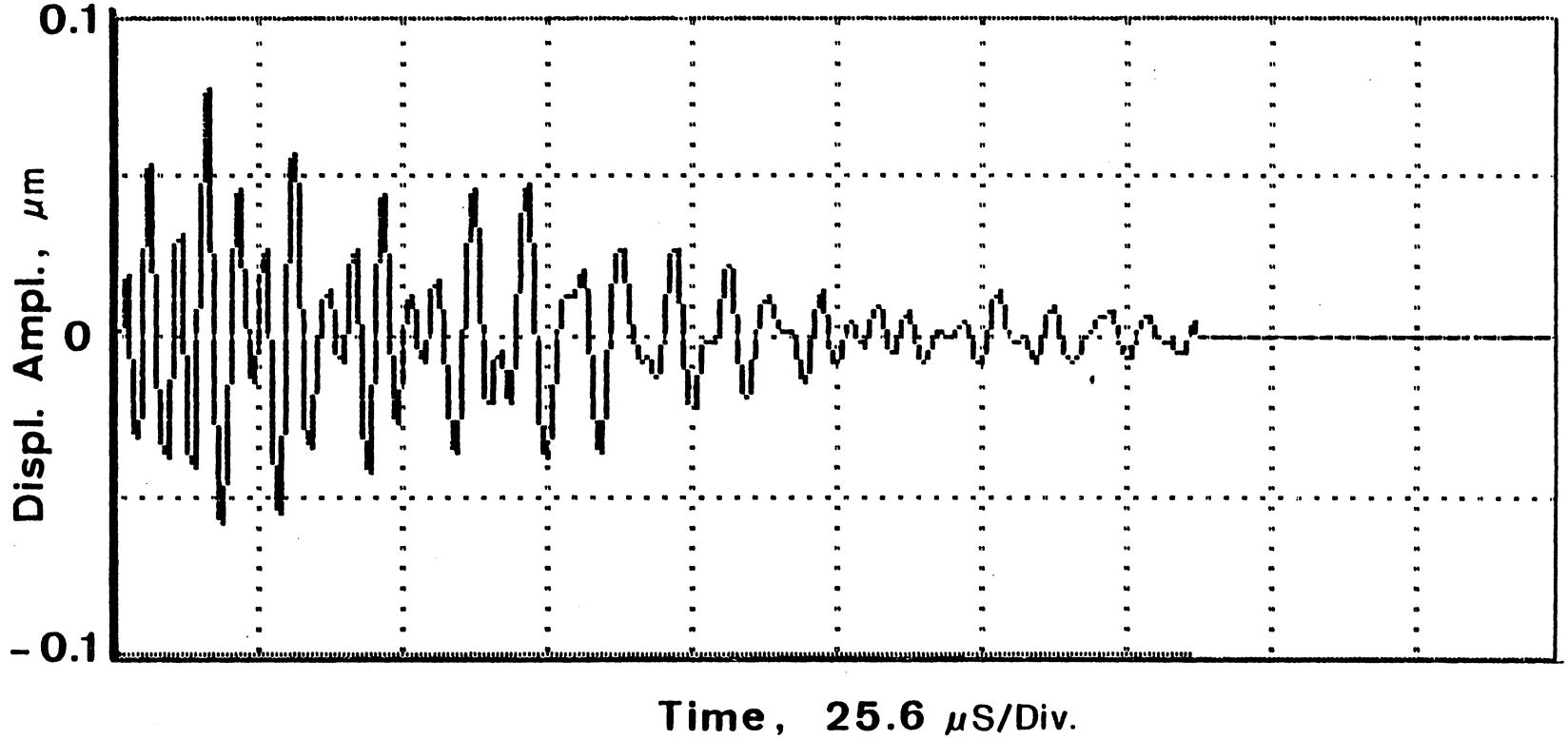

Figure 33. An optical response to the transverse surface displacement along the length of a PZT ceramic covered with two layers of diffusing retro-reflective tape at the interrogated area.

The transducer (mounted about one inch from the observation point) was electrically excited to generate an ultrasonic wave in the specimens. Figures 34 and 35 represent the detected in-plane displacement signals on the interrogated area of plexiglas covered with one and two layers of tape, respectively. Figures 36 and 37 represent the detected in-plane displacement signals on the interrogated area of the composite plate covered with one and two layers of tape, respectively.

The observations made from these test results indicate that, fortunately, the presence of this thin film of retro-reflective material does not perturb the output ultrasonic signal. Although one might expect to observe a slight reduction in signal amplitude of the detected ultrasonic wave caused by two layers of stacked tapes compared to one layer of tape, the distortion was considered insignificant. So, the overall performance of such a quantitative laser speckle displacement interferometer remains intact.

5.2 Lateral Resolution

The ability to focus the interrogating laser beam on a small region makes the optical detector highly sensitive to the identification of small-size flaws, and to shape and boundary determination of delaminations in composites. To

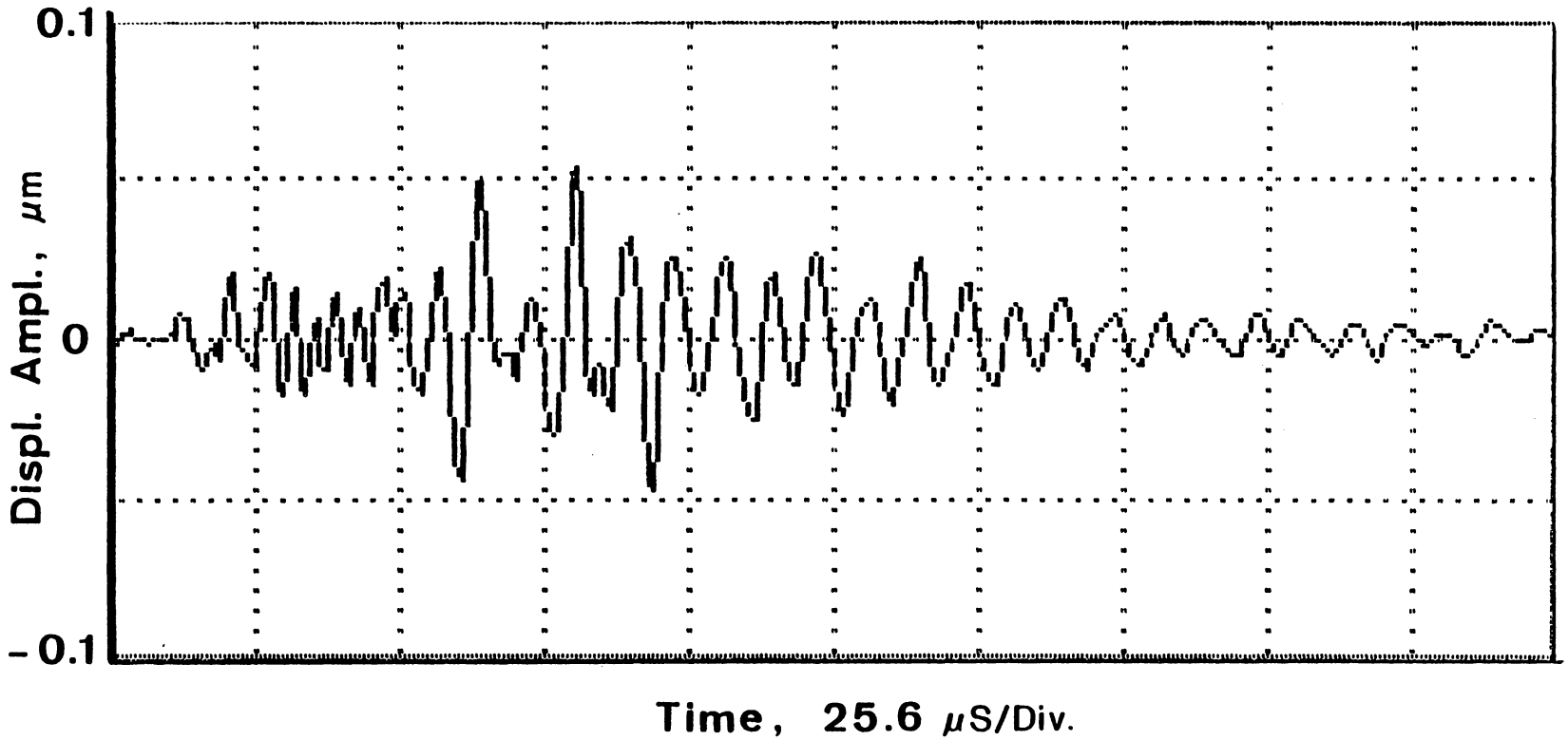

Figure 34. An optical response to the transverse surface displacement of a PZT driven plexiglass covered with one layer of diffusing retro-reflective tape at the interrogated area.

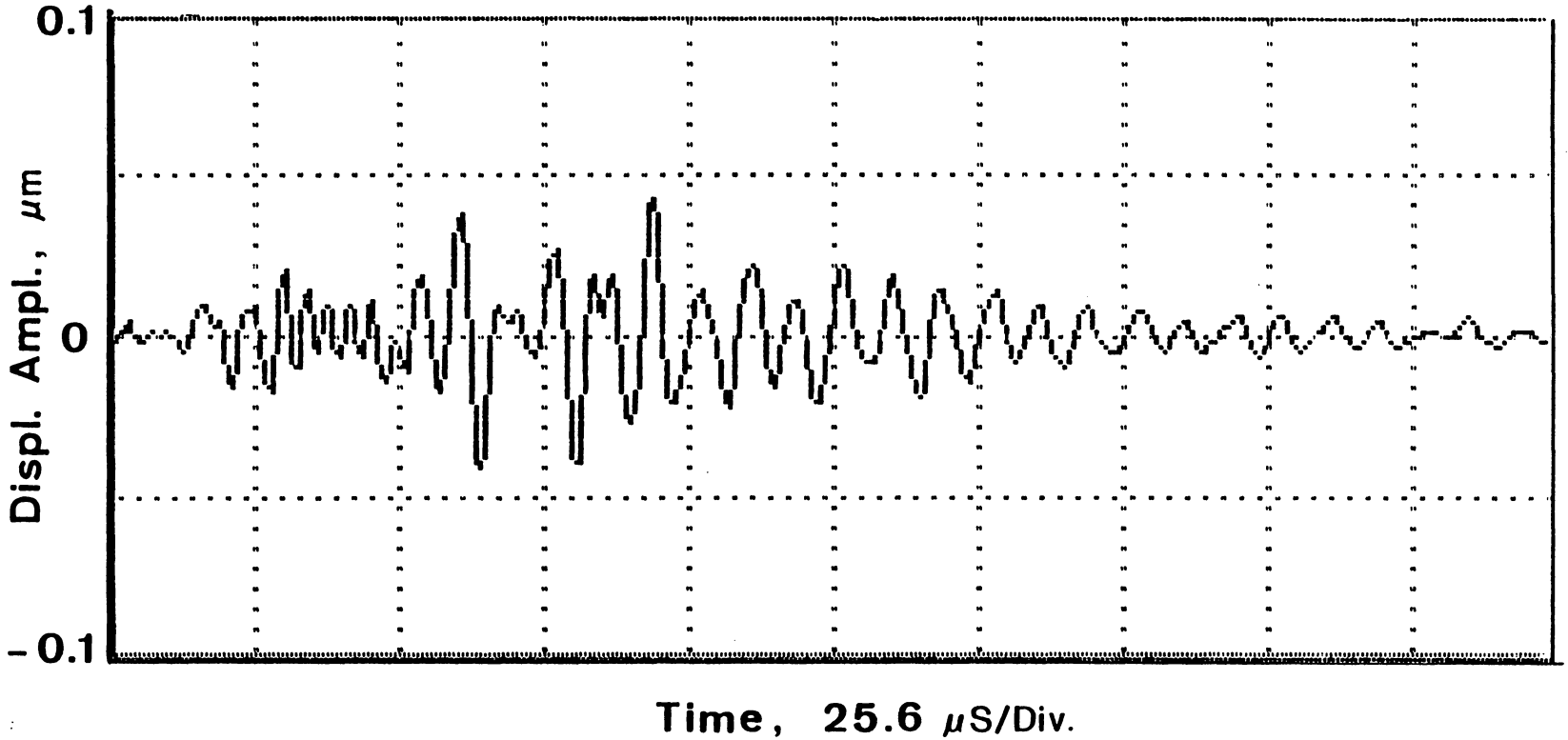

Figure 35. An optical response to the transverse surface displacement of a PZT driven plexiglass covered with two layers of diffusing retro-reflective tape at the interrogated area.

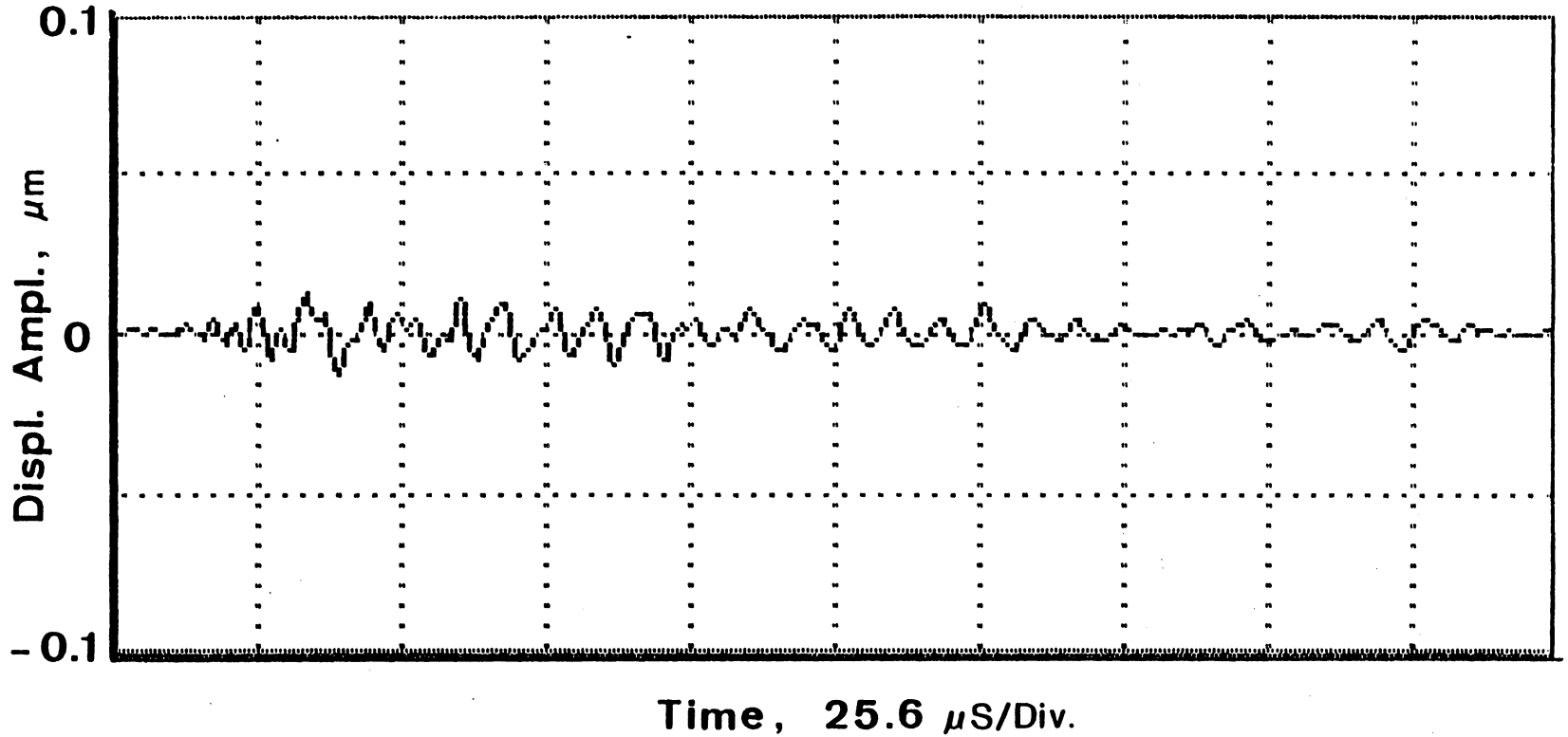

Figure 36. An optical response to the transverse surface displacement of a PZT driven composite plate covered with one layer of diffusing retro-reflective tape at the interrogated area.

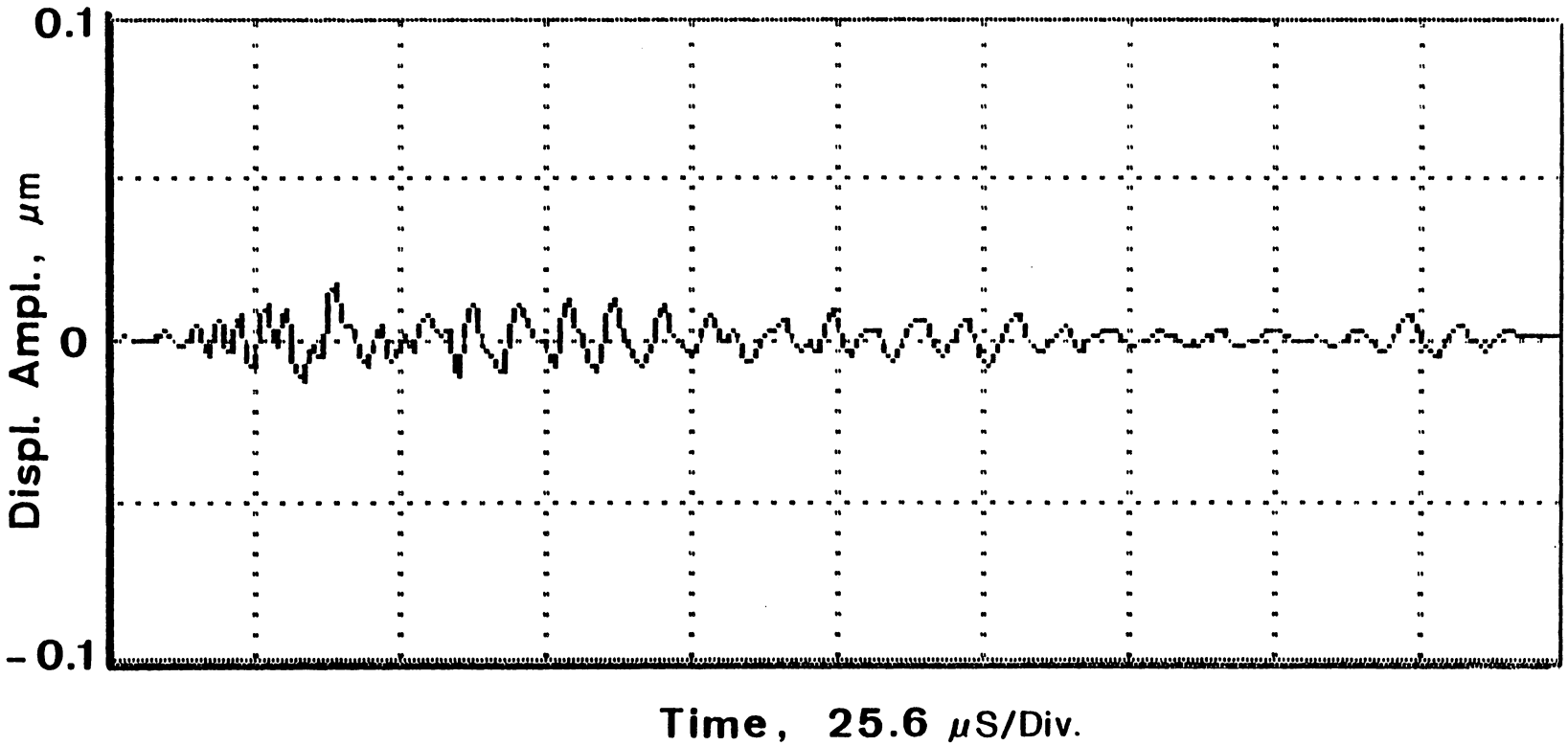

Figure 37. An optical response to the transverse surface displacement of a PZT driven composite plate covered with two layers of diffusing retro-reflective tape at the interrogated area.

demonstrate that capability, two composite laminates were tightly sandwiched together. In only a small region between the two plates was a couplant applied to simulate a "good region", where delamination had not occured. The sandwiched plates were excited ultrasonically by a 1 MHz piezoelectric transducer on one side and the output signal was optically detected (using the fiber optic interferometric sensor) at the epicenter on the other side. Figure 38 shows the specimen/transducer assembly and the associated fiber optic probing beam which scanned along a straight line but always remained at the epicenter of the transmitting ultrasonic transducer. In this figure, the gap between the two sandwiched plates is somewhat exaggerated. For the interferometric beam probing the center face of the good region (see Figure 39a), a relatively large signal amplitude was observed (Figure 40). For the probing beam located around the edge of the "delamination" (see Figure 39b), a significant decrease in the amplitude of the detected signal was noticed (Figure 41). Finally, for the interrogated location over the "delamination" (see Figure 39c), the signal amplitude was negligible (Figure 42).

The above experiment was a crude observation in which only three data points were considered. In general, the sensor is able to perform a more detailed identification of the discontinuities in materials due to its small beam-diameter focusing capability.

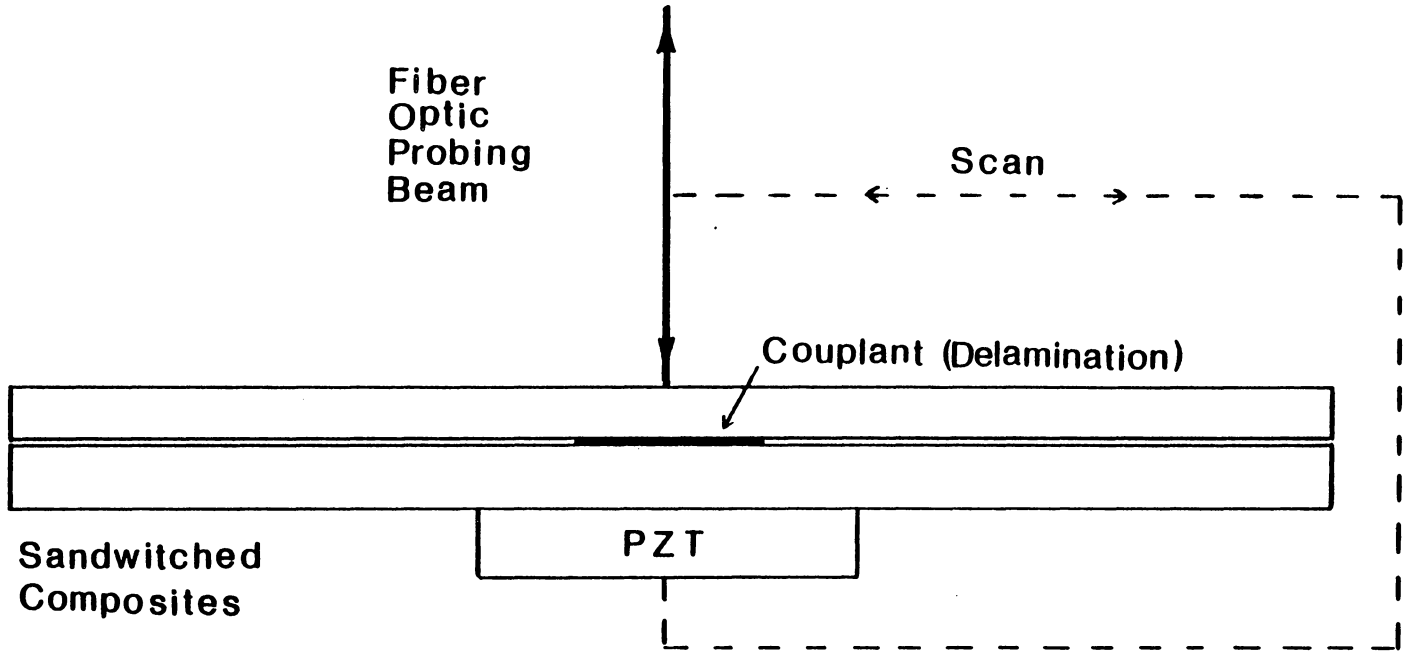

Figure 38. Two sandwiched plates containing a couplant area to simulate "delamination".

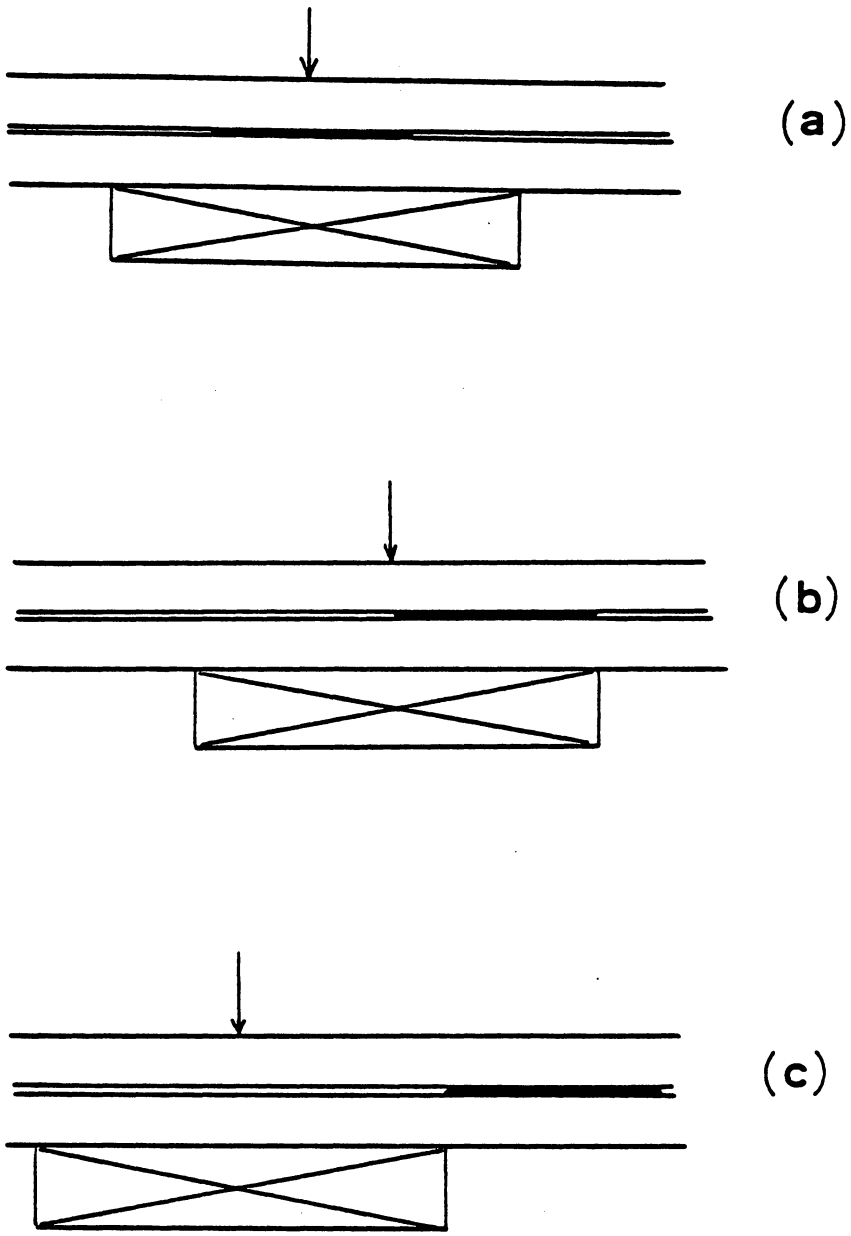

Figure 39. Positions of an epicentered fiber optic probing beam with respect to the couplant.

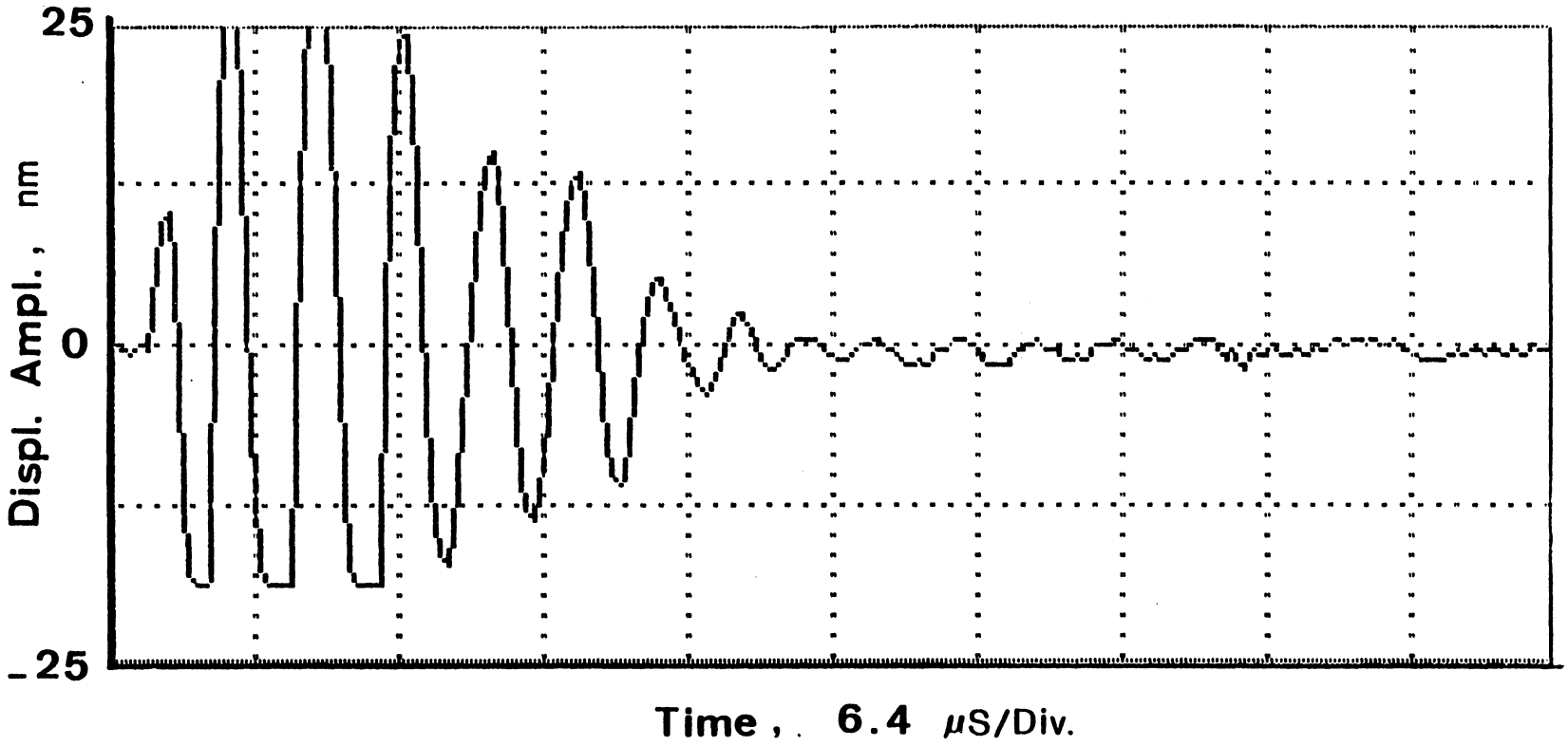

Figure 40. An optically detected ultrasonic signal amplitude for the position (a) in Fig. 39.

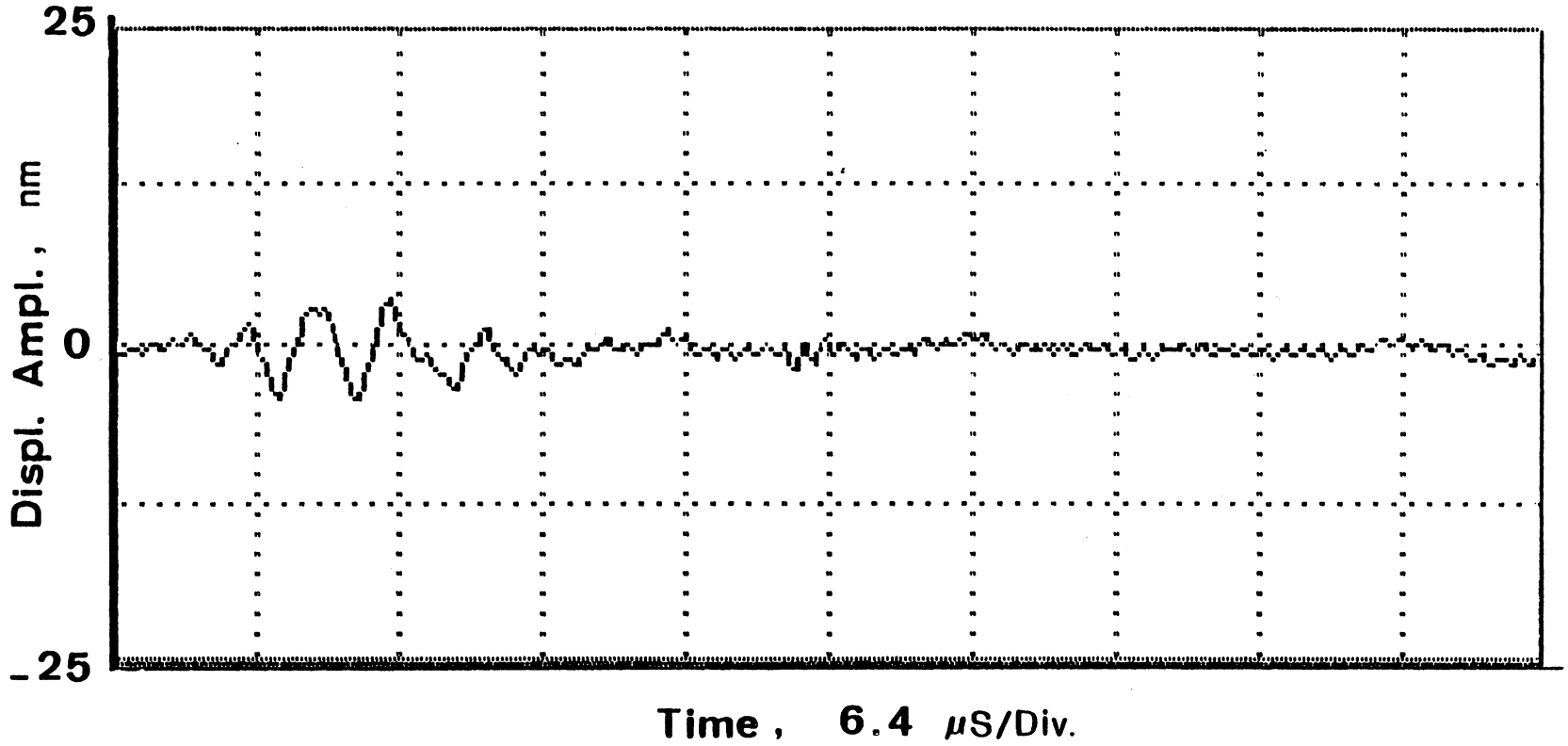

Figure 41. An optically detected ultrasonic signal amplitude for the position (b) in Fig. 39.

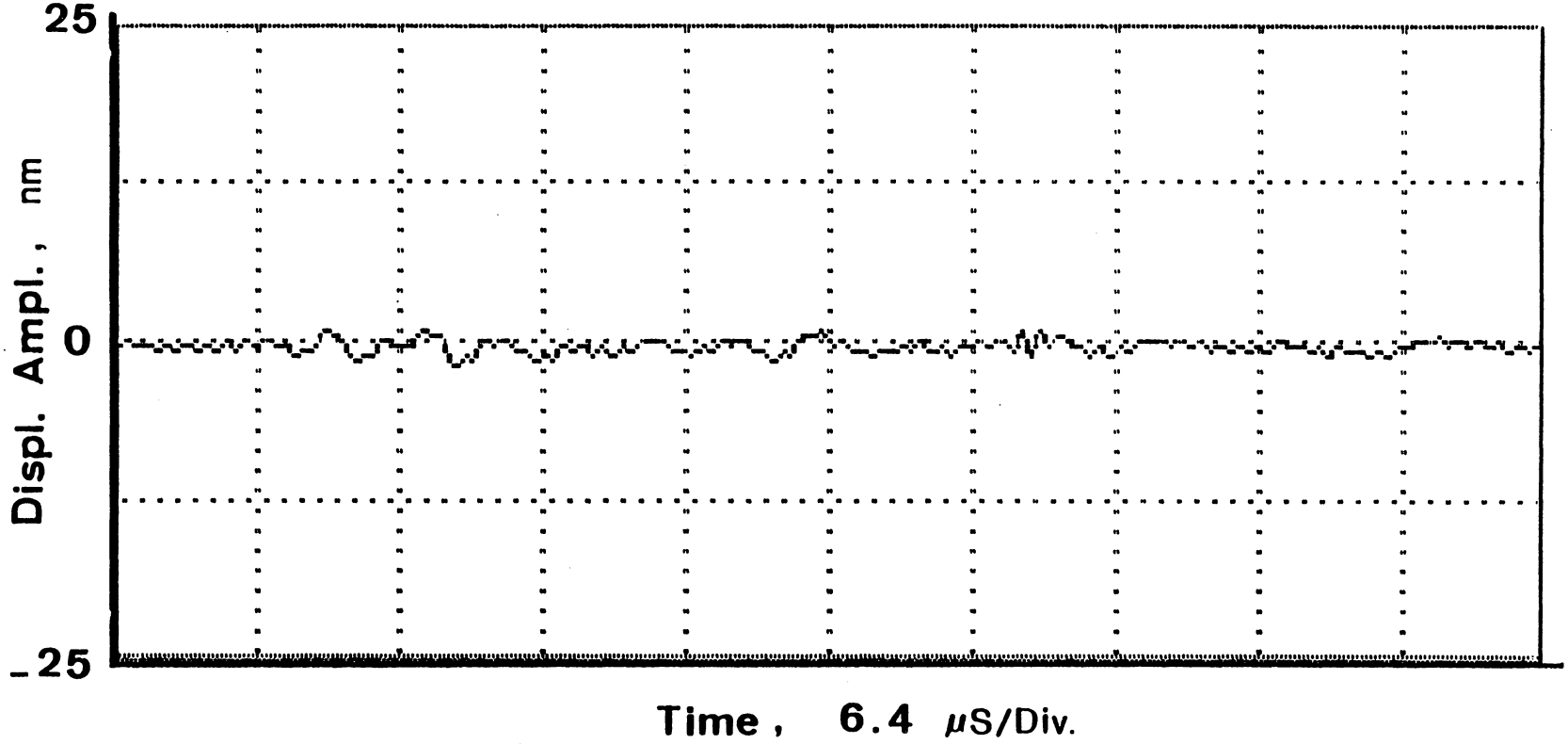

Figure 42. An optically detected ultrasonic signal amplitude for the position (c) in Fig. 39.

The small diameter of the laser probing beam facilitates the ultrasonic beam profile characterization and the calibration of the piezoelectric transducer's waveform in the medium of solids or fluids. From both the analytical calculation and the experimental observation of the diffraction phenomenon owing to the wave characteristics of optics and ultrasonics, it is well understood that collimated wave packets emitted from the front surface of a transducer (e.g., circular piezoelectric disk in the thickness-expander vibrational mode) diverge some distance away from the transducer. Figure 43 shows the conceptually visualized wave divergence of a transducer. The collimated near-field (Fresnel) region is defined over the range of

$$D^2/4\Lambda,$$

in which D and Λ are the transducer's diameter and resonating frequency, respectively. The expanding far-field (Fraunhofer) region immediately follows the near-field zone. Clearly, the larger the ratio of D/Λ, the longer the collimated region.

However, in order to sustain a narrow beam of collimated ultrasonic wave, a small diameter transducer of high resonating frequency is required. The particle displacement of an ultrasonically excited medium in the near-field region is more difficult to obtain mathematically. But in the

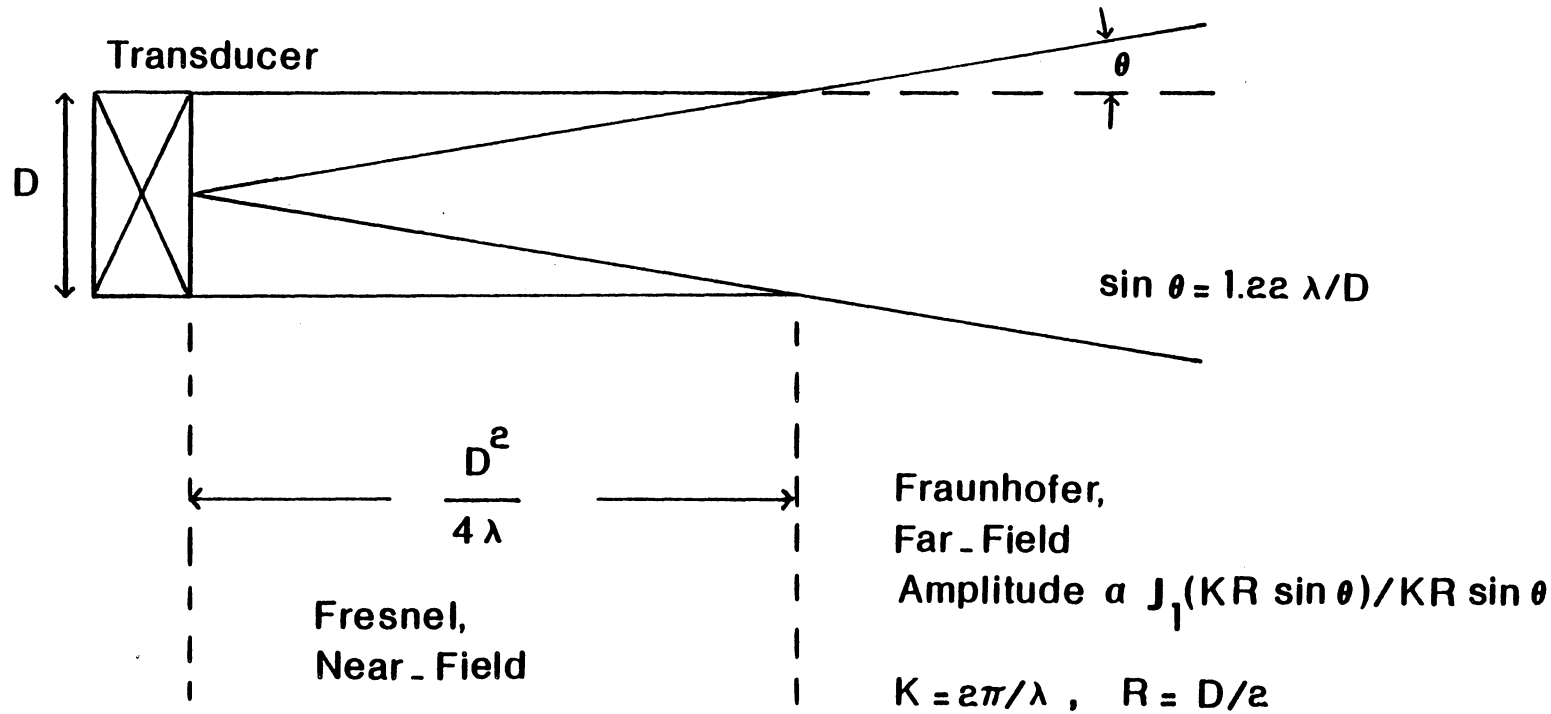

Figure 43. The near-field (Fresnel) and the far-field (Fraunhofer) beam profiles for a circular ultrasonic transducer.

far-field region, the displacement amplitude of a circular ultrasonic beam, the amplitude diffraction pattern, is found to be proportional to

$$2J_1(KR \sin \theta)/(KR \sin \theta),$$

where $J_1()$ is the Bessel function of the first kind, $R = D/2$ is the circular transducer's radius, and θ is the angle between the transducer axis and the point (located in a plane perpendicular to the axis at the far-field region) at which all the contributing points of excitation on the transducer surface are added together. The contours of equal displacement amplitudes in the far-field of the diffraction pattern are concentric circular fringes in which the Airy disk radius, defined by Rayleigh criterion, the first dark fringe, is obtained when

$$J_1(KR \sin \theta) = 0.$$

That is, the value of the Bessel function of the first kind is zero for

$$KR \sin \theta = 3.83 ,$$

i.e.,

$$\sin \theta = 1.22\lambda/D.$$

The above expression for the angular beam divergence is the diffraction-limited point resolution of a finite-size circular imaging aperture. This implies that the image of a point is not a point but has a finite dimension. Moreover, for a transducer of finite aperture size resonating at an unknown range of frequencies, the far-field beam profile should be experimentally determined.

In the experiment represented in Figure 44, a three-inch-thick aluminum block of 10.6" X 6" was used to observe the far-field amplitude diffraction pattern of an ultrasonic wave in its medium. A circular PZT element one-inch in diameter and of a 0.5 MHz resonant frequency was acoustically coupled to one side of the block. The small-diameter probing laser beam (≈ 30 μm) of the laser speckle interferometer (here, the single-beam illumination arrangement) was used to scan the surface on the opposite side in a straight line direction. The aluminum block was translated on an optical rail in 3/16-inch (≈ 5 mm) intervals. In general, the point-scanning interval could be much smaller (but larger than the focused beam diameter) for a more refined interrogation. Figure 45 represents a transient record of mechanical excitation at a point on the face of a three-inch-thick aluminum block.

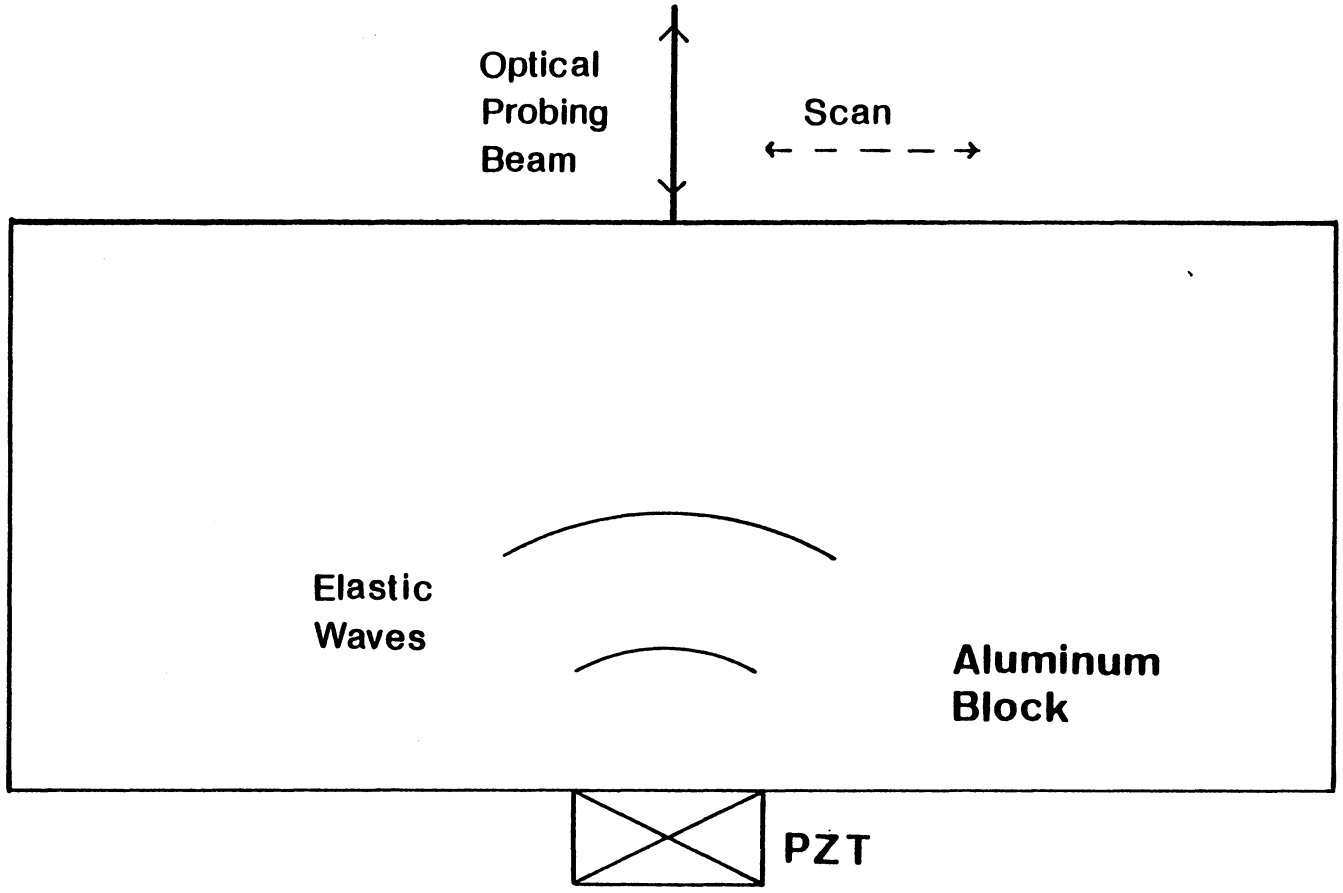

Figure 44. Schematic diagram of a transducer/aluminum block assembly used for the observation of the far-field amplitude diffraction pattern using a small-diameter interferometric probing beam.

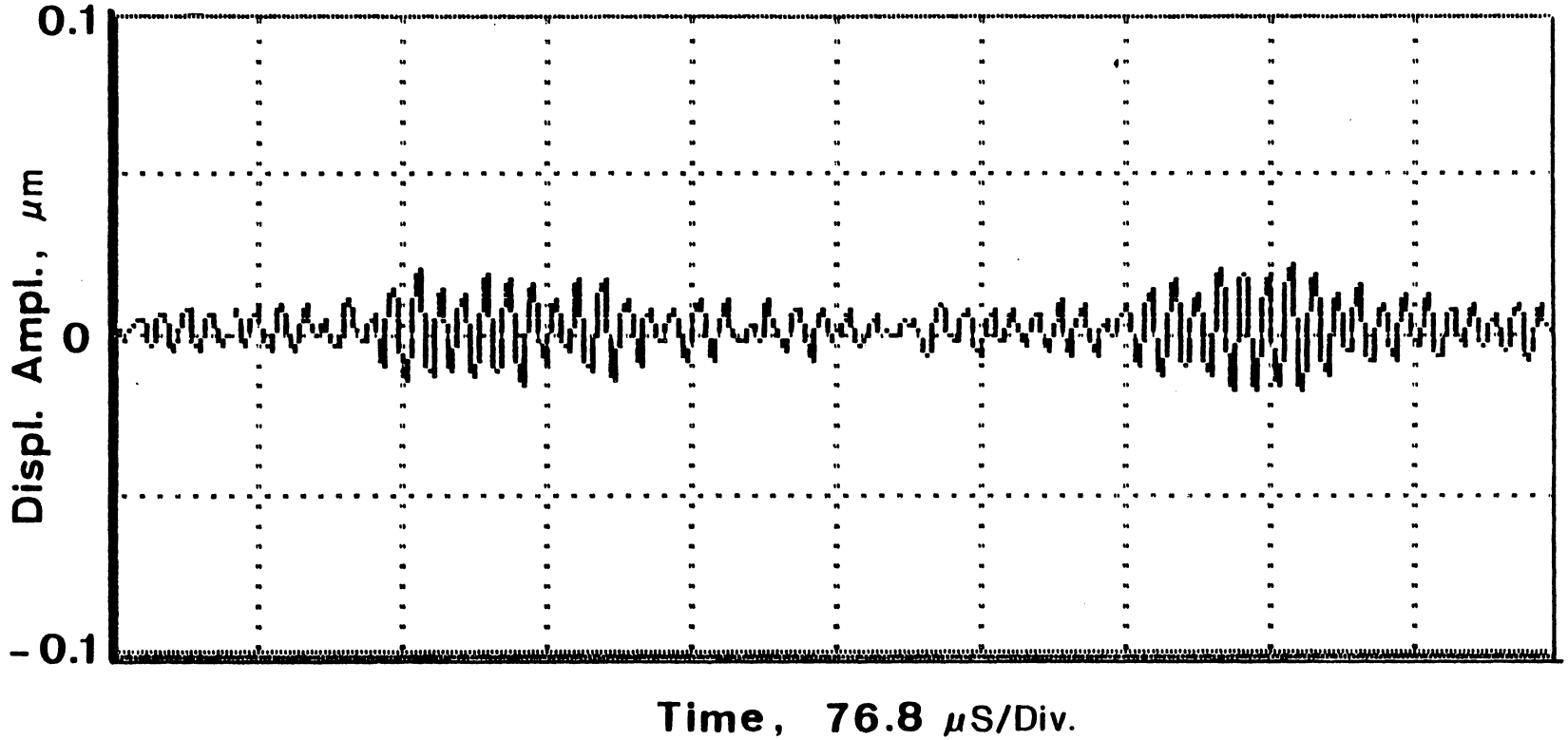

Figure 45. Optically recorded transient signal of an undamped transducer element in a 3-inch-thick aluminum block.

The undamped (acoustically unbacked) transducer element was driven by a MATEC ultrasonic generator. The first (far left) disturbance is the compressional wave followed by the second disturbance (shear wave). It should be realized that the laser speckle interferometer is sensitive to both longitudinal and transverse waves. To construct the far-field amplitude diffraction curve (Figure 46), the peak amplitude of the detected signal was observed at each interrogated point. There is a considerably large discrepancy between the data and the solid line due to measurement error caused by output signal instability, which is inherent in the system. Even so, the experimentally obtained data more or less follow the predicted curve.

5.3 Directivity Measurement

In an experiment a repetitive electronic short pulse was transmitted to drive a 1 MHz piezoelectric transducer of the thickness-expander type which was coupled acoustically to one side of a unidirectional fiber-reinforced composite laminate. The interrogation point on the same side of the specimen was mirrorized for light reflectivity. Then three different transducer positions about 1 inch from the point were chosen such that the transducer could propagate elastic waves parallel to, off-axis to, and perpendicular to the fiber axis. The resultant surface displacement excitations were

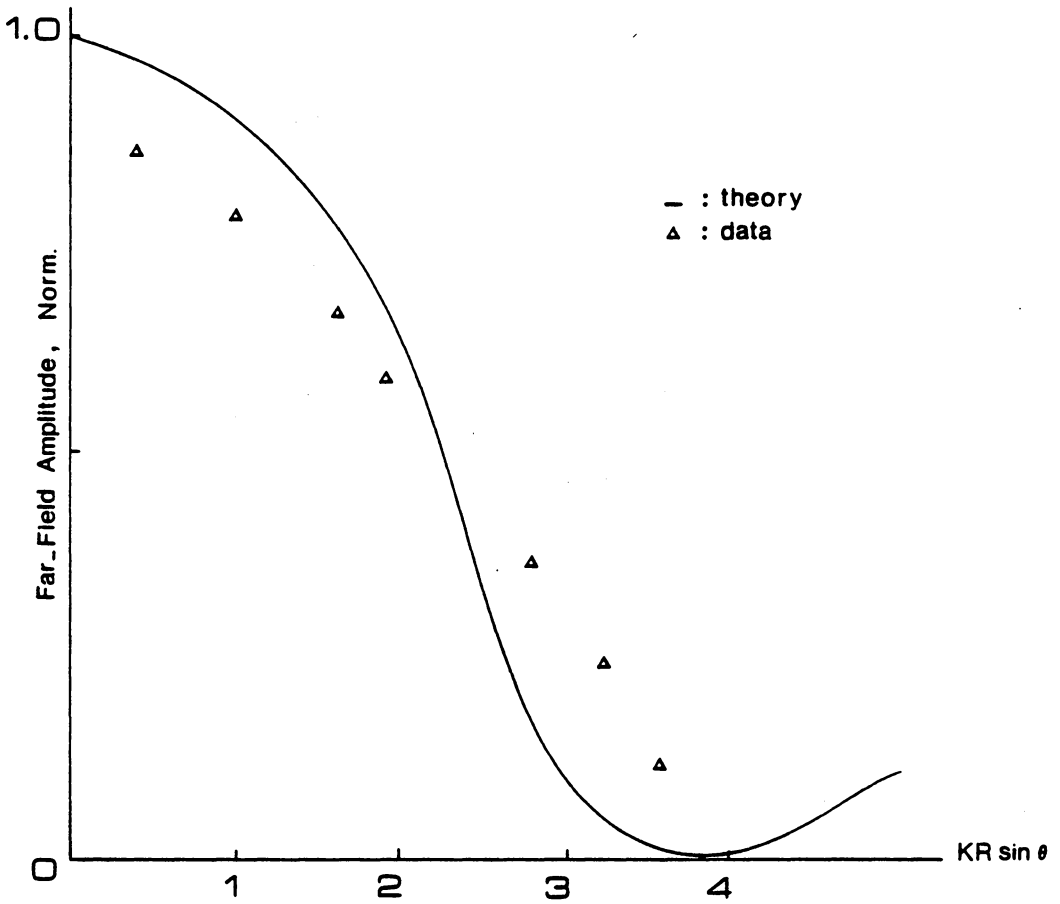

Figure 46. Far-field amplitude diffraction curves.

detected by the linear optical sensor (the fiber optic interferometric probe discussed in Chapter IV). After signal amplification and suitable filtering, the information pertaining to the amplitude of acoustic disturbances was obtained. The time-domain amplitudes of the detected stress waves for the aforementioned transducer positions are shown in Figures 47-49, respectively. Note that the magnitude of surface displacement is larger in Figure 48 than in Figure 47 and is drastically reduced in Figure 49. Figure 50 shows the three positions of the sending ultrasonic transducer around the optically interrogated point. The three maximum amplitudes obtained in Figures 47-49 are drawn in Figure 51. In this figure, the experimentally observed amplitudes (ADA) are normalized with respect to the maximum value obtained in Figure 48. The amplitude of the dotted curve containing the three points is increased to the maximum at an off-axis direction with respect to the fiber's orientation (0-degree angle). Then, the amplitude is drastically decreased toward the normal to the fiber direction (90-degree angle). This acoustic displacement directivity behavior was rather unexpected; an elliptically shaped acoustic displacement amplitude variation had been expected.

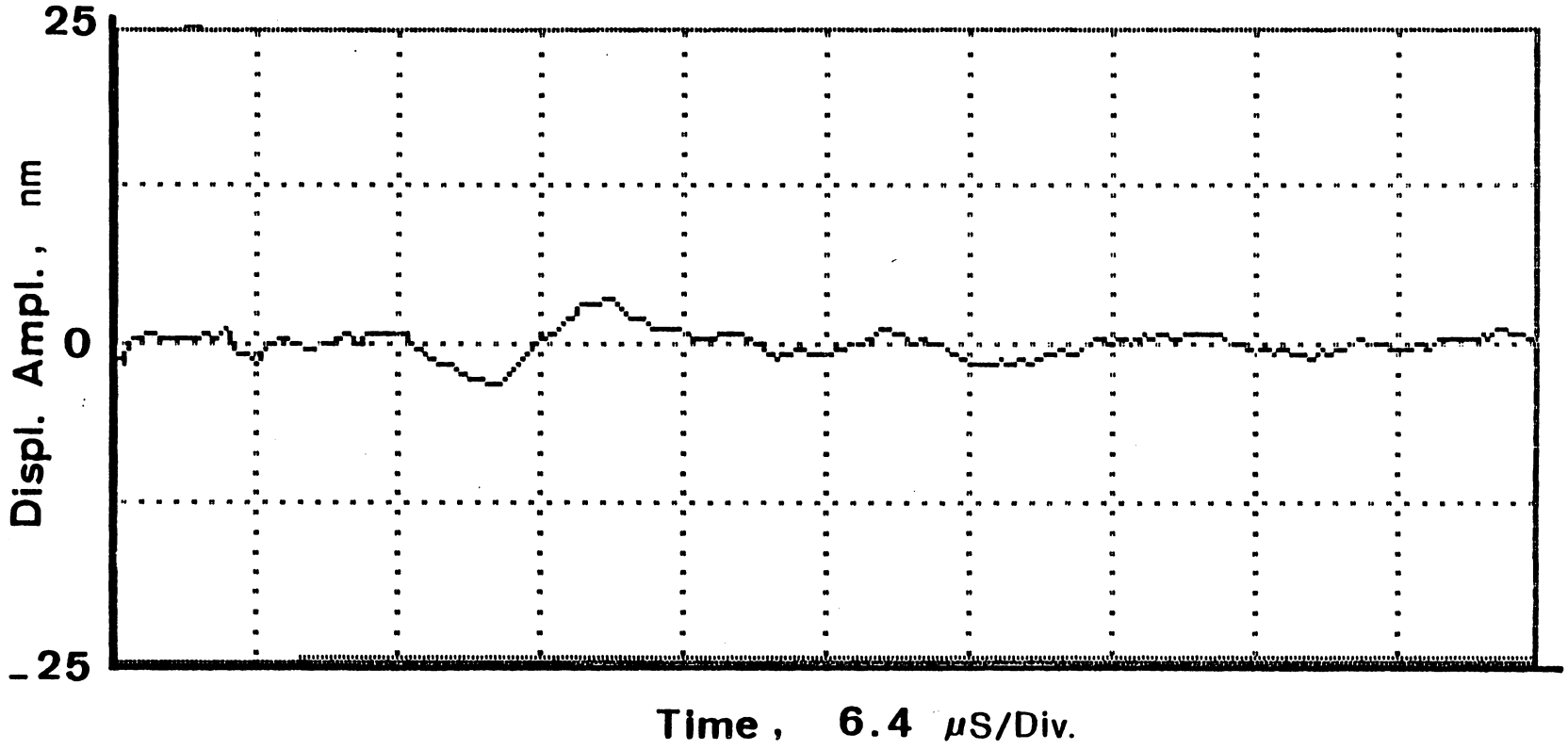

Figure 47. Optically recorded signal for the transducer axis along the fiber orientation.

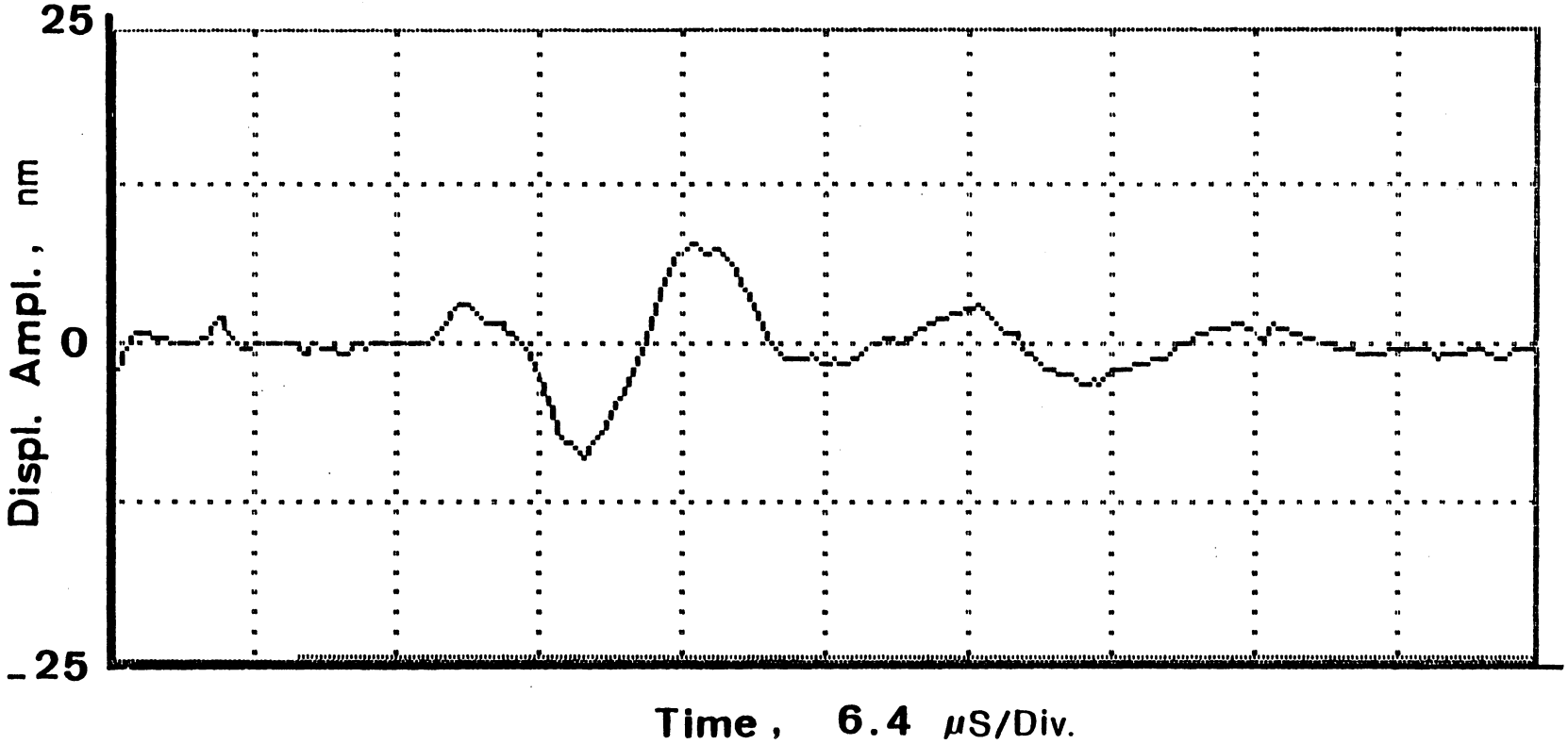

Figure 48. Optically recorded signal for the transducer axis along the off-axis to fiber orientation.

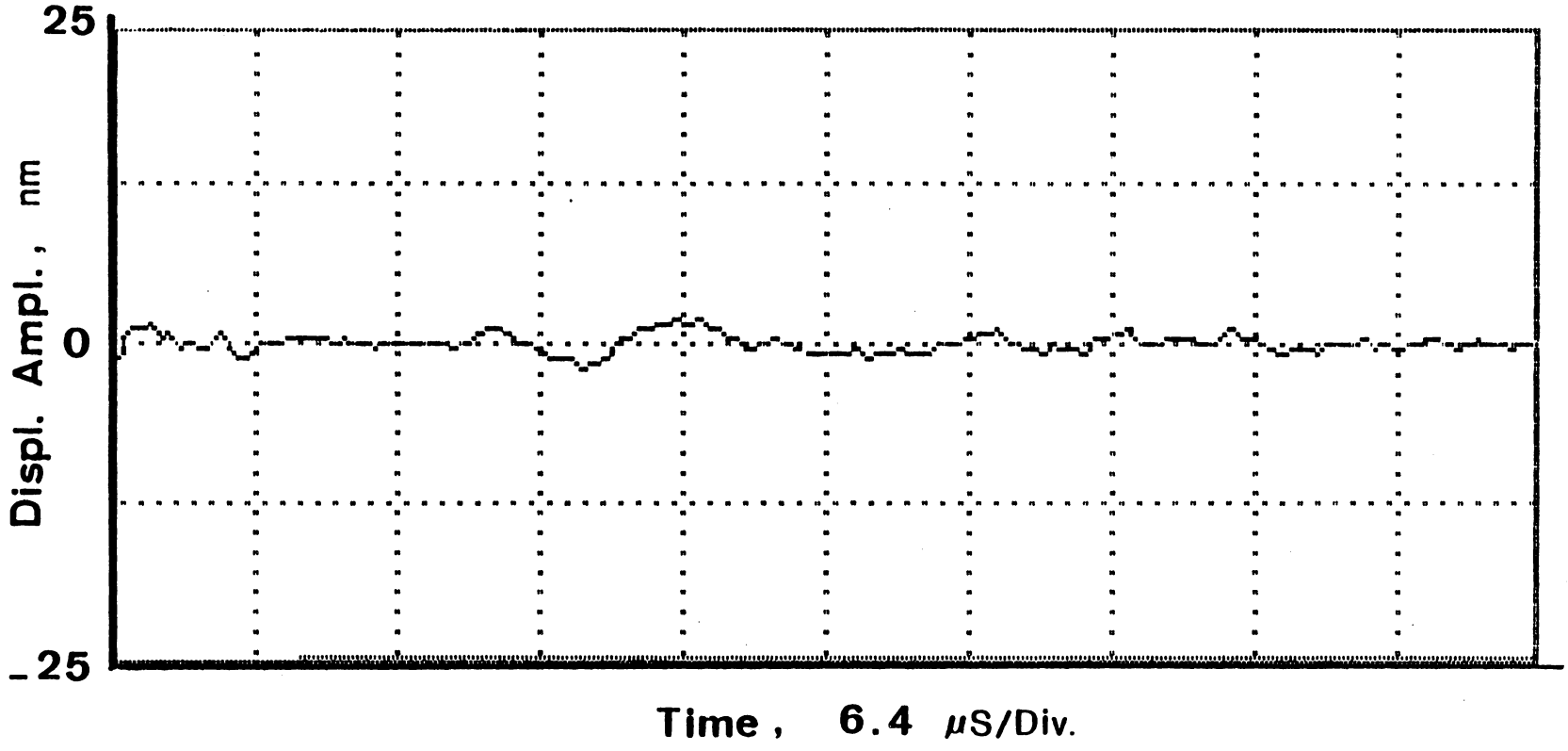

Figure 49. Optically recorded signal for the transducer axis perpendicular to fiber orientation.

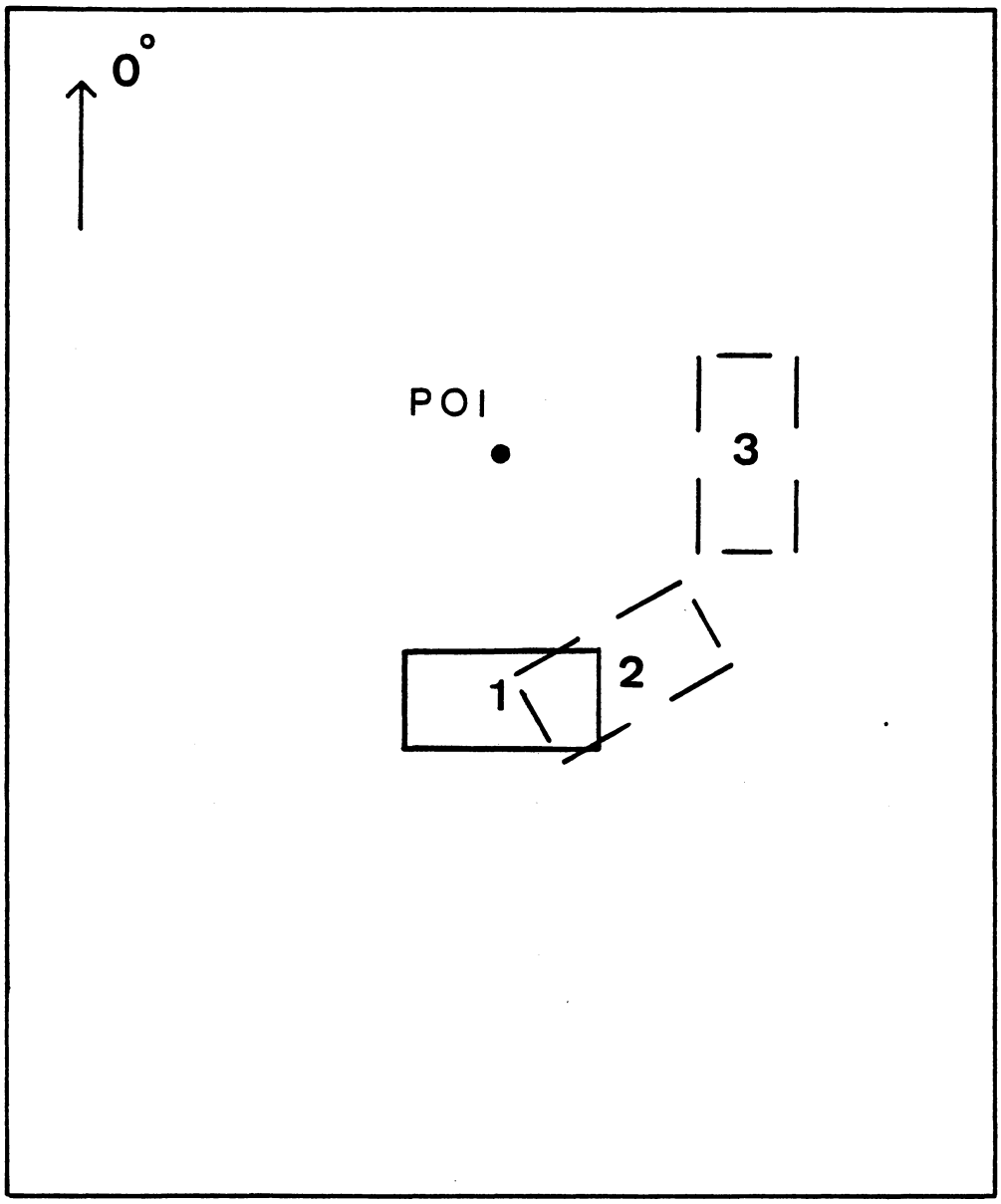

Figure 50. The three positions of the sending ultrasonic transducer around the point of interrogation.

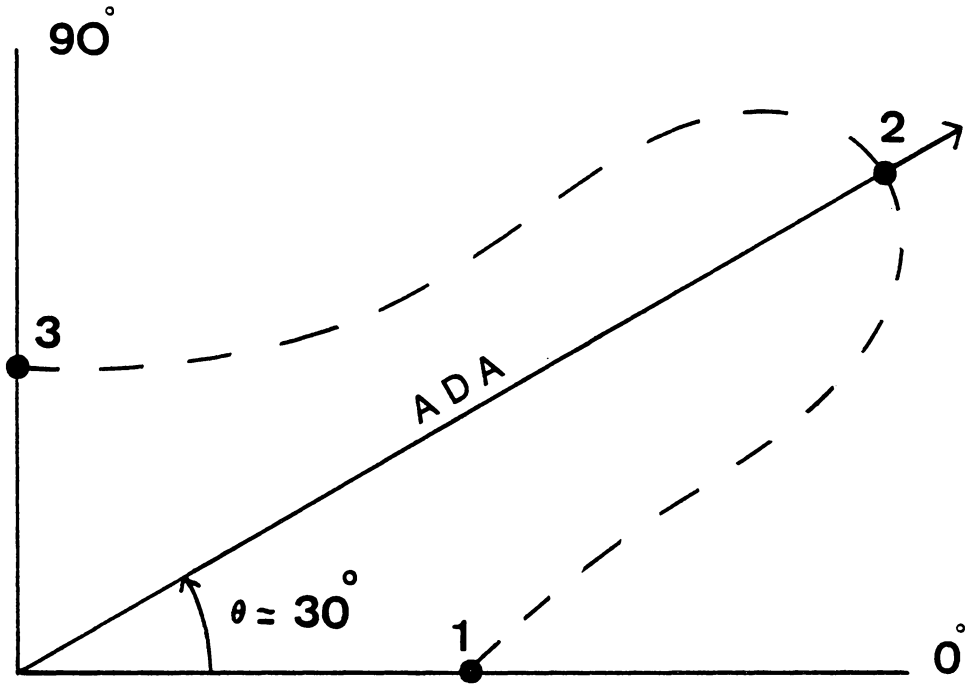

Figure 51. Experimentally observed acoustic displacement amplitudes around an ultrasonic source for a unidirectional composites.

5.4 Excitation Characteristics of Piezoelectric Transducers

In a series of recordings, a couple of PZT ceramics with different resonating frequencies were analyzed for their surface acoustic excitation. In one experiment, the transducer element was driven by an RF pulsed excitation (MATEC Model 6000). For a disk element (PZT-5A, 0.5" diameter, 0.5 MHz) designed to resonate in the thickness-expander mode, an unwanted radial mode of vibration was observed, in addition to a compressional excitation. Figures 52 and 53 represent the optically detected transient excitation at the center face of the element using the double-beam and the single-beam illumination arrangements of the laser speckle displacement interferometer, respectively. In another experiment, when the same transducer element was excited by an RF pulsed signal (PANAMETRICS Model 5052 UA), an optically-detected signal (Figure 54) representing the out-of-plane surface displacement using the two-beam unequal-path interferometric setup (the fiber optics probe) was recorded.

For a rectangular element in the thickness-shear mode (PZT-5A, 1" X 1/2", 0.25 MHz), the transient surface displacements in the plane normal direction and the plane tangential direction of the ceramic driven with an RF pulsed ultrasonic generator (PANAMETRICS Model 5052 UA) were observed. Figures 55 and 56 represent the detected signals

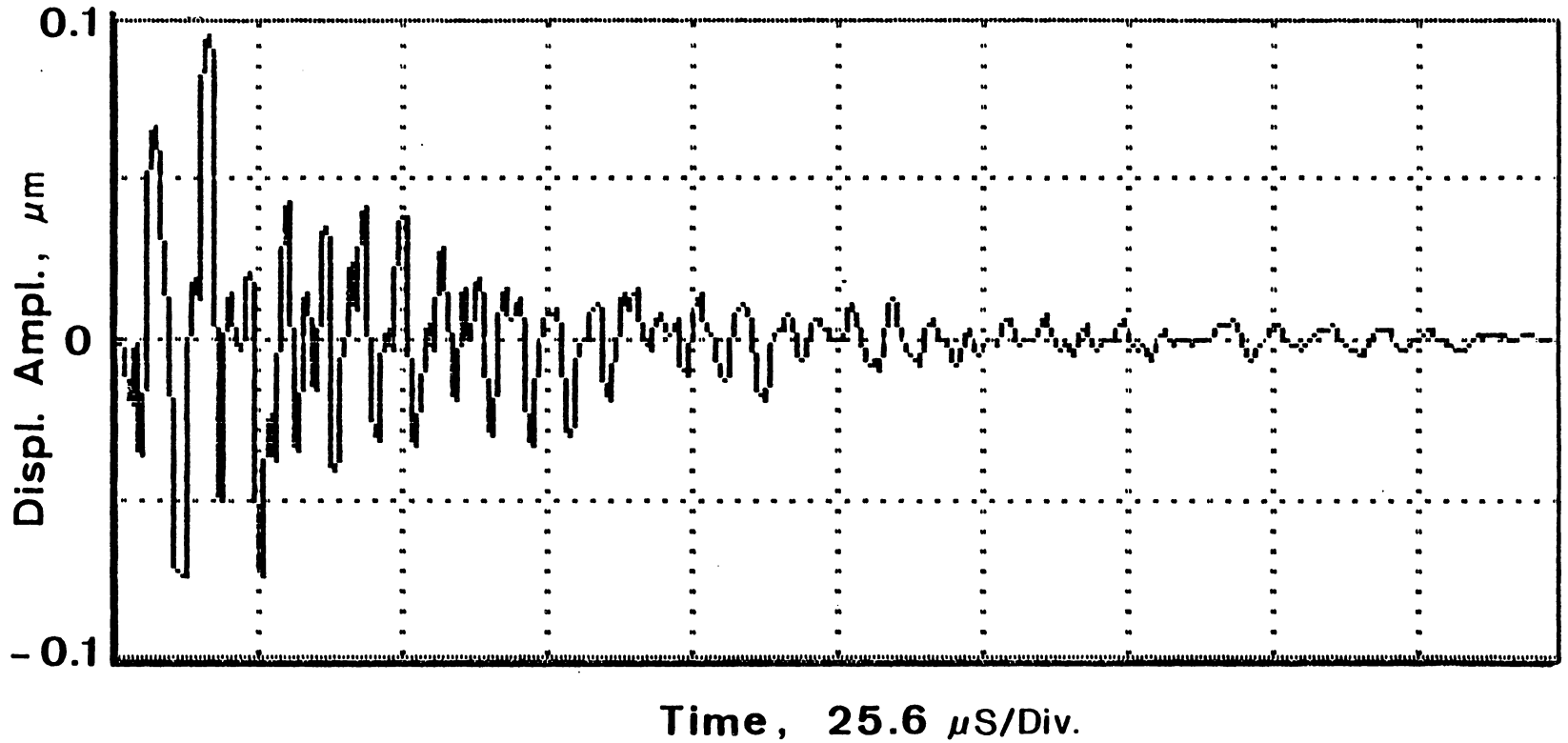

Figure 52. Optical response of an unwanted radial excitation for a thickness-expander piezoelectric ceramic disk.

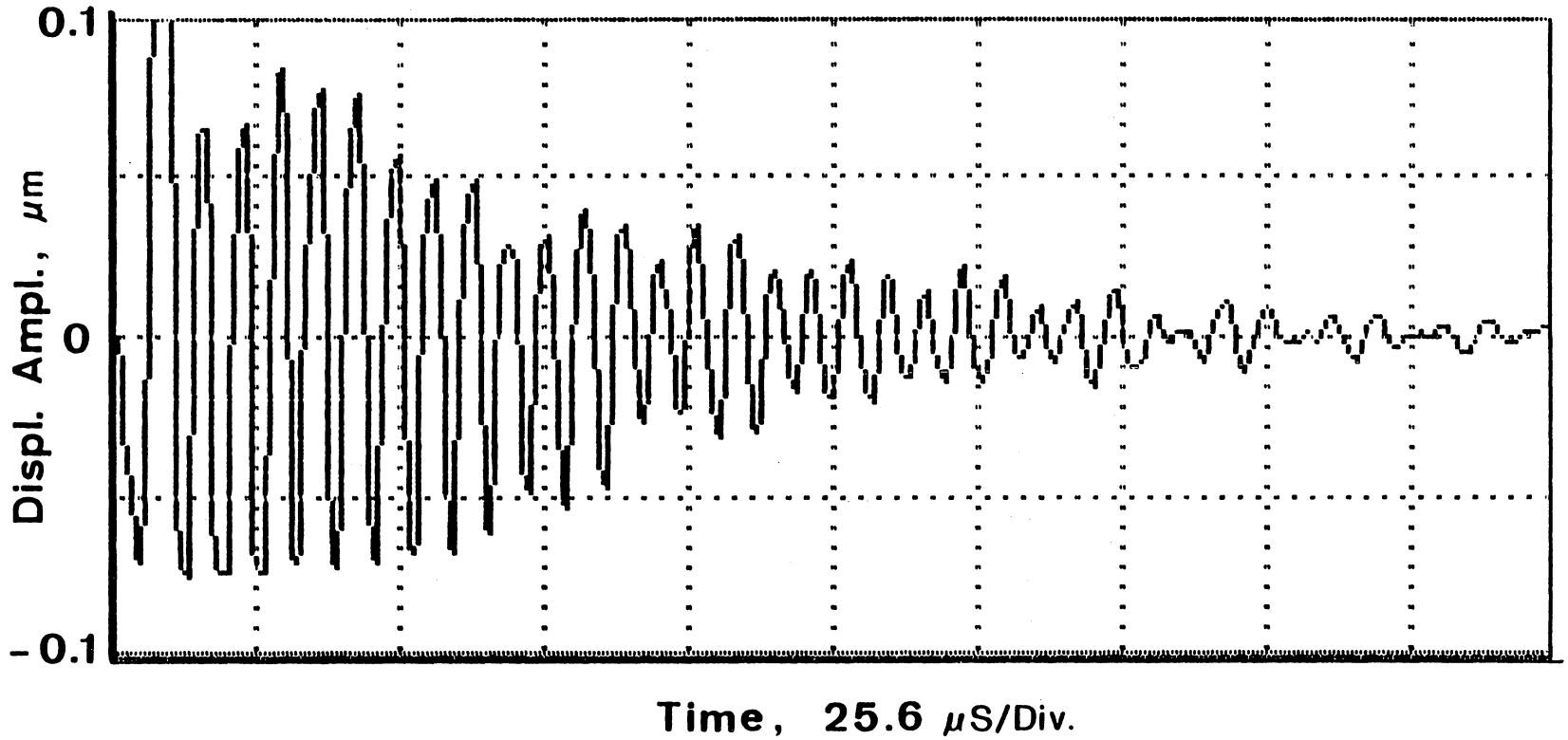

Figure 53. Optical response of a normal excitation for a thickness-expander piezoelectric ceramic disk.

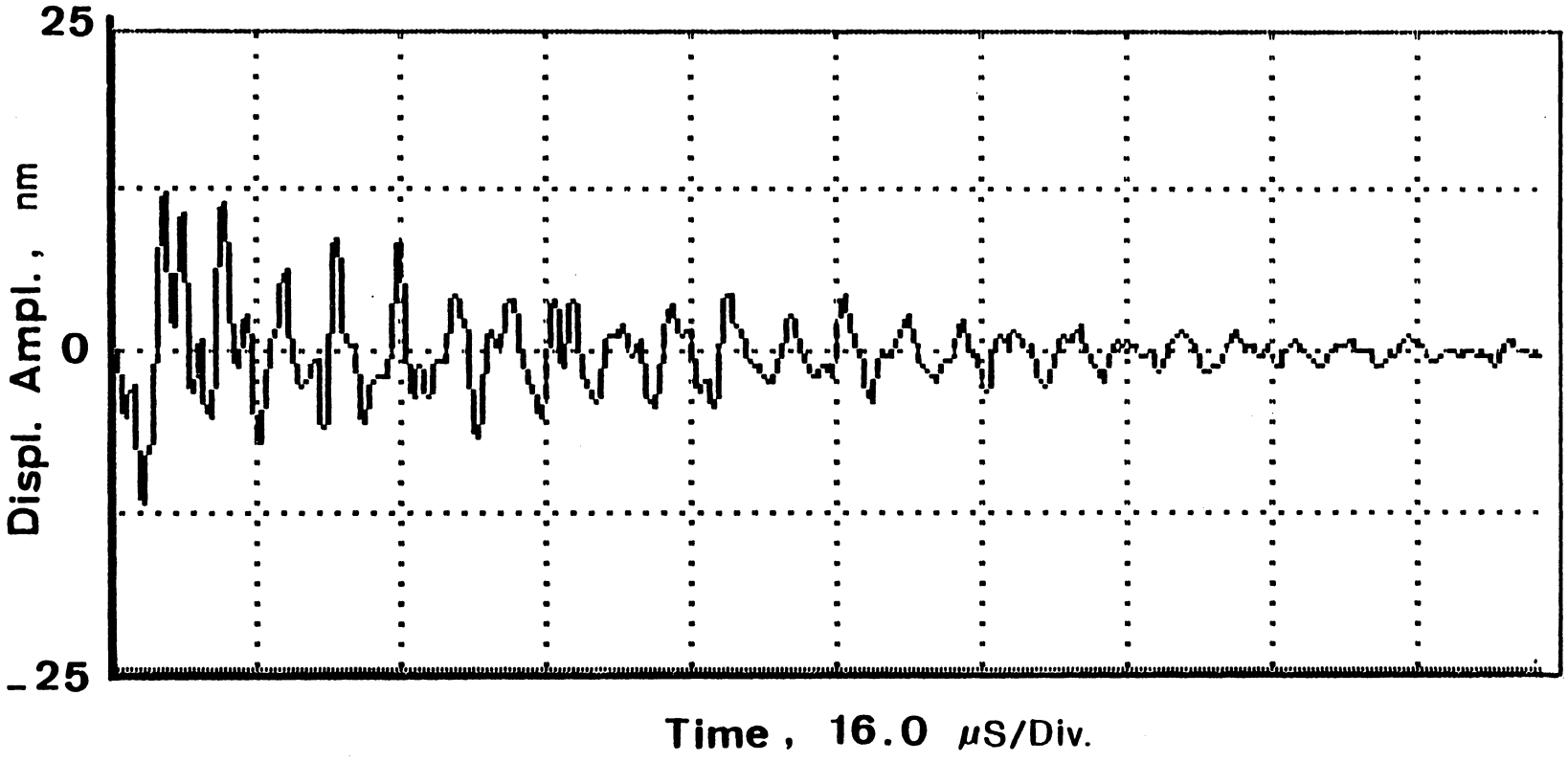

Figure 54. The same as Fig. 53, using the fiber optic interferometer.

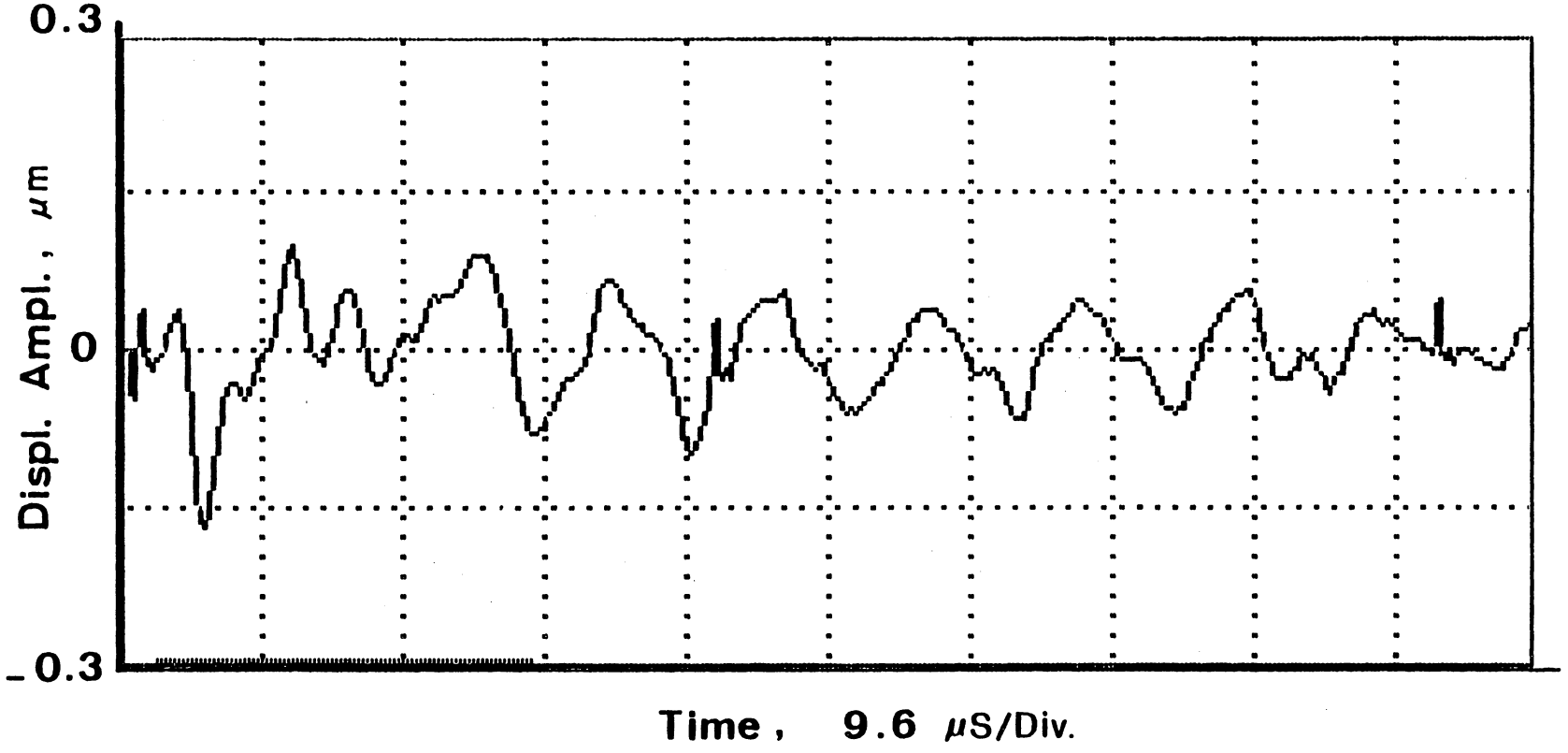

Figure 55. Optical response of a normal excitation for a thickness-shear piezoelectric plate.

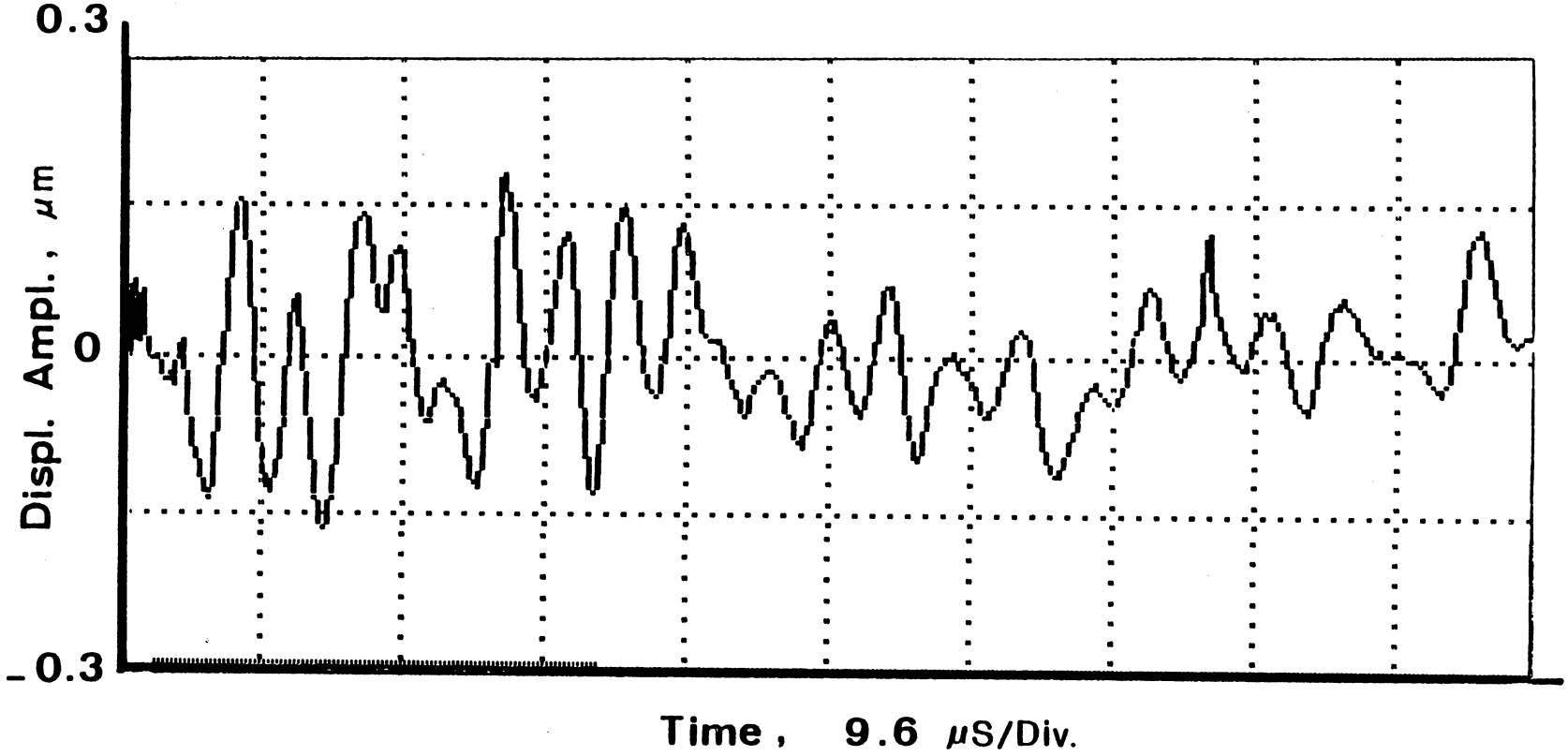

Figure 56. Optical response of a transverse excitation for a thickness-shear piezoelectric plate.

using the out-of-plane displacement-sensitive and the in-plane displacement-sensitive laser speckle interferometers, respectively. Finally, for another rectangular ceramic element (PZT-5A, 1"x1/2", 0.1 MHz) driven by the above ultrasonic pulser, the two principal in-plane as well as out-of-plane surface displacements were obtained. Using the double-beam illumination arrangement, the two surface responses representing the transverse (shear) displacement vibration in two orthogonal directions (along the major and the minor axes of the PZT plate) were recorded. The two optically-detected signals, Figures 57 and 58, were obtained by simply rotating the transducer ceramic $\pi/2$ radians around its surface normal direction. Using the single-beam illumination arrangement, the optically-detected vertical (normal) surface displacement was also recorded (see Figure 59). From these observations, it becomes clear that the amplitude, mode, and frequency of the transient ultrasonic signal is quite different for each axis of the PZT ceramic and, in general, is a function of the element's geometry. Therefore, the optical sensors of this kind can reveal details more readily than the commonly used off-the-shelf mechanical transducers.

In another experiment, the optically-detected ultrasonic wave was compared with the piezoelectrically-detected signal. A quasi-isotropic laminate of thin composite was ultrasonically excited by a 1

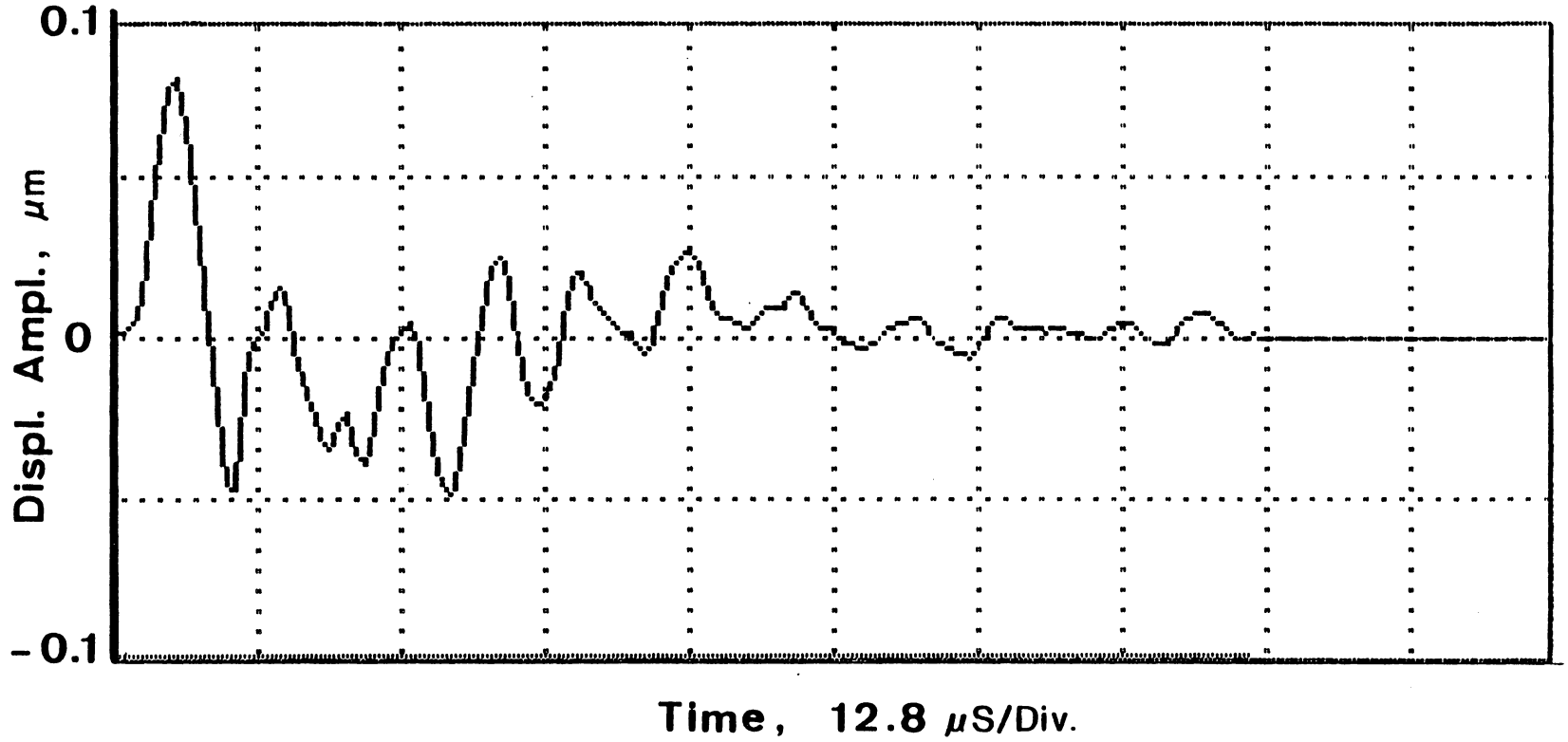

Figure 57. Optical response of a transverse excitation along the length of a thickness-shear piezoelectric plate.

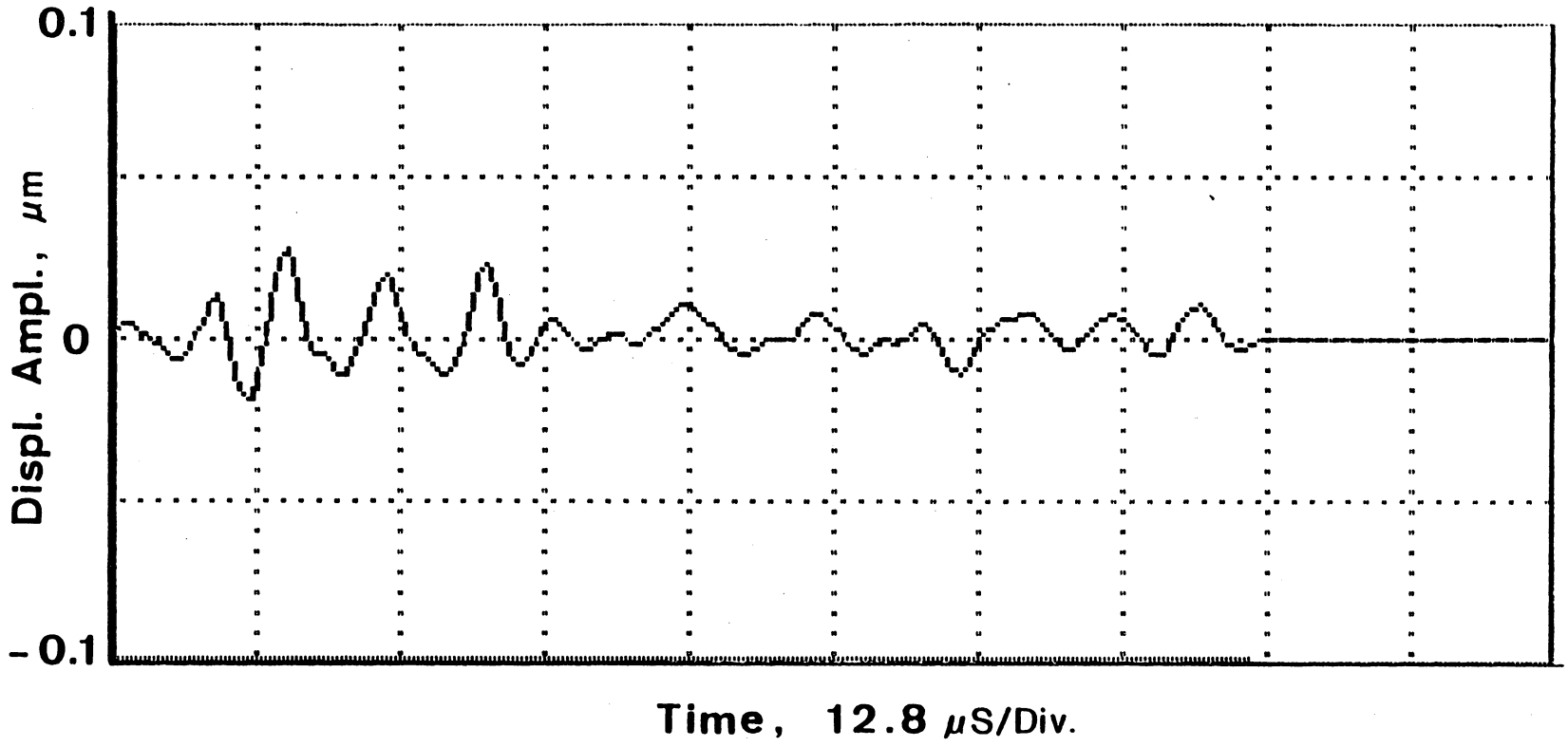

Figure 58. Optical response of a transverse excitation along the width of a thickness-shear piezoelectric plate.

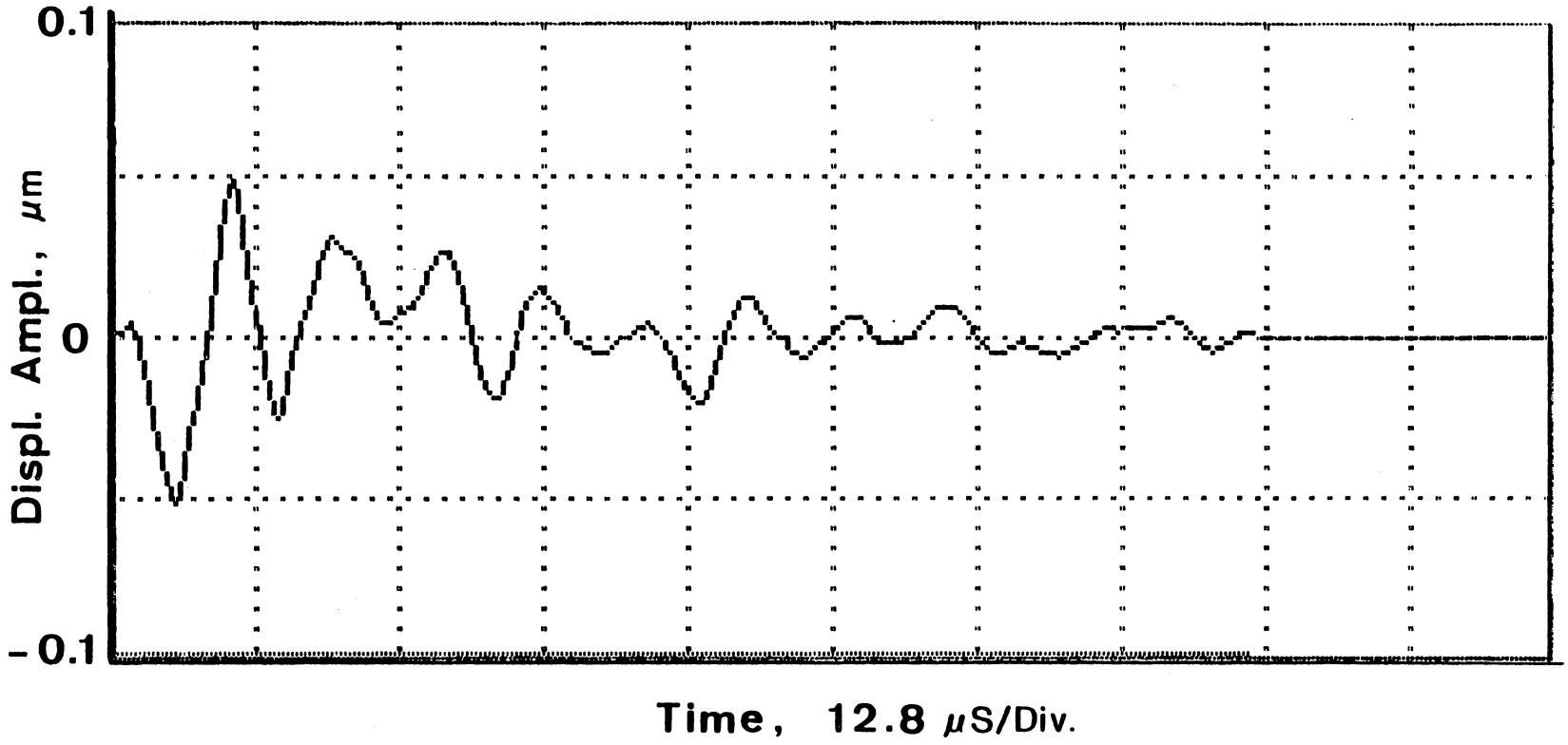

Figure 59. Optical response of a normal excitation for a thickness-shear piezoelectric plate.

MHz transducer. The interrogation point was along the transducer's transmitting axis, on the same side of the specimen as the transducer and about one inch away from it. Figure 60 represents the response of the fiber optic sensor to the RF pulsed transducer driven by a MATEC ultrasonic generator. Figure 61 represents the response of a broad-band (5 MHz) 0.5-inch diameter, circular transducer for the same excitation. Surprisingly, the optical and the piezoelectric responses were quite similar.

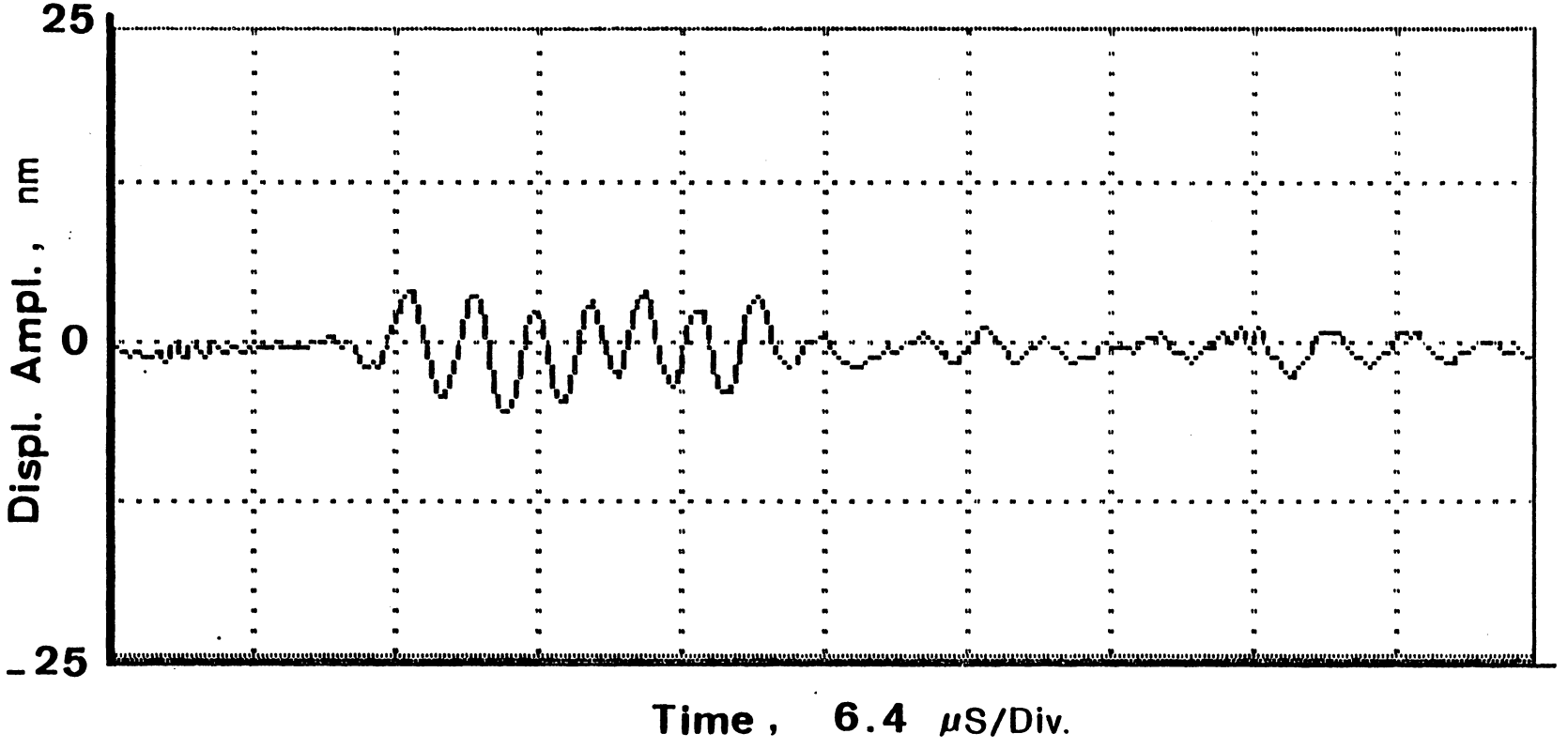

Figure 60. Optical sensor response of an ultrasonically excited specimen.

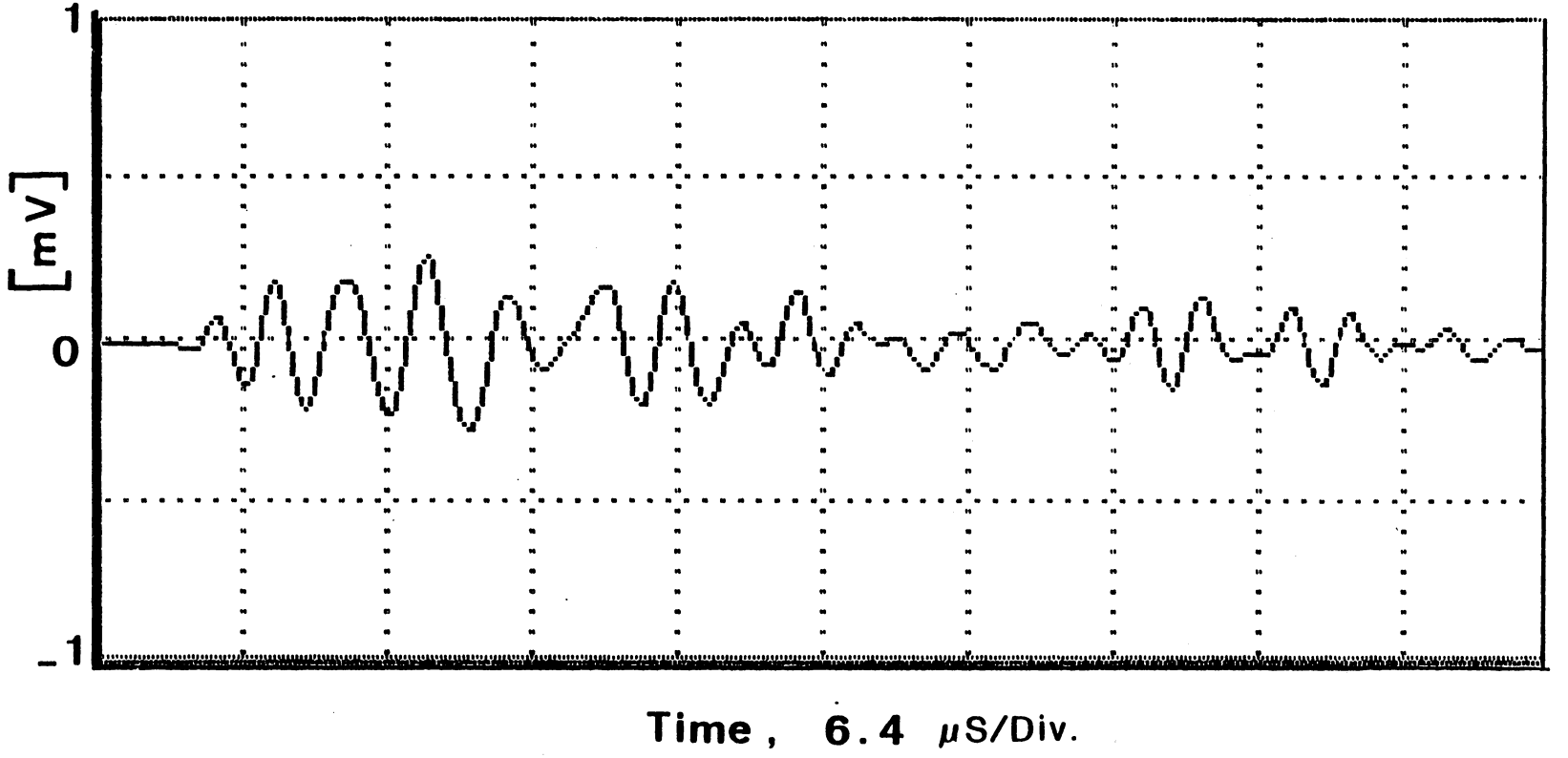

Figure 61. Piezoelectric transducer response of an ultrasonically excited specimen.

VI. SUMMARY AND REMARKS

Laser interferometric displacement measurement techniques for the detection and analysis of surface/transient acoustic waves, acoustic sensing, are useful due to the noninvasive characteristics of optical noncontacting sensors in ultrasonic nondestructive evaluation. Different optical set-ups can be constructed and optimized for looking at a particular particle disturbance (out-of-plane/in-plane displacement) of the material under study. The analysis of this optical system shows that the stress wave causes a change in interferometric light intensity due to surface disturbance. The deviation in light intensity is detected photoelectrically and the output signal is found to be proportional to the instantaneous surface displacements. Through suitable calibration of the system, the absolute measurement of surface displacements is obtained. The ultimate sensitivity of these interferometric optical transducers is limited in part due to the photodetector shot-noise current and in part due to optical path length differences. The small optical wavelength gives rise to much smaller optical path length differences which may be less than the atomic dimension. There are major advantages in these optical sensors. They are non-contacting so that no alteration of actual surface displacement occurs.

They can be used in hostile environments, in particular for high temperature materials characterization (under proper conditions). They are sensitive --- e.g., displacements of sub-angstrom magnitudes can be measured. Because of the ability to focus the laser beam on a spot size region, point-by-point interrogation of the surface and complete characterization of the displacement field is readily accomplished.

Several distinct optical systems were presented for the measurement of acoustic surface displacements produced by ultrasonic waves. One example of this kind of system was a simple optical arrangement based on the principles of "diffraction image" for a linear grating. Although this sensor was not fully implemented, its system design makes it a potentially useful candidate for detecting the surface acoustic (Rayleigh) waves. Another optical system was developed following the suggestion made in [29] by using a blazed reflection diffraction grating as the beamsplitter/recombiner and the reference mirror in a Michelson-type interferometer. The addition of an optical fiber to the test arm of the interferometer as a light guiding medium has been shown to be a great advantage in optical probing flexibility. For this reason, an attempt to utilize single-mode fiber optic interferometry for remote sensing was justified. Finally, an optical displacement sensor was designed using laser speckle interferometry for a

retro-reflective diffusing surface under study. This new speckle interferometer can detect the complete disturbances (in-plane as well as out-of-plane) of the object surface, having twice the sensitivity (to in-plane disturbances) of conventional laser speckle interferometers. The scattered light-gathering capability of this system is also greatly improved as compared to its counterparts where a lens of finite size aperture is used in forming the two image speckle patterns needed for superposition analysis. This system like the two-beam interferometer using the blazed grating can also be modified so that the test-piece under study can be isolated from the optical table where the rest of the optical components are located. This flexibility can be achieved by replacing the two interrogating beams of the laser speckle interferometer with a flexible optical fiber bundle (with associated optical coupling lens at each fiber end) for each arm. The advantages of adding optical fibers to the sensor for the noncontacting remote detection of acoustic emission and ultrasonic stress waves in a service environment are yet to be realized.

As was mentioned in Chapter III, sensitivity to the detected displacements was derived to be a function of system parameters. For example, the observed noise displacement (the measured minimum detectable displacement) for the laser speckle interferometer of retro-reflective diffusing illumination was about 50 A^0 . This is much greater than the

calculated minimum detectable displacement of $3x10^{-4}$ A^0. The large discrepancy is believed to be mainly due to the noisy output power of the laser source used in the system. The use of a highly-stabilized single-frequency laser is practically essential for controlling the optical power fluctuation and subsequently minimizing the noise signal amplitude.

Since the main use of quantitative optical noncontacting sensors is in ultrasonic material characterization, NDE, the knowledge of the exact input ultrasonic wave characteristics and consequent monitoring of the material-induced variations in input signal are highly desired. In line with that, to characterize the signal output characterization of different sources of ultrasonic regimes, the front surface displacement, or input signal, analysis of the ultrasonic transducers was demonstrated. As a closing remark it should be added that in order to quantitatively characterize materials using ultrasonic methods, a well characterized quantitative detection method in conjunction with a well characterized source of ultrasonic excitation must be used. The applications of noncontacting optical sensors along with optical generation of ultrasound are conducive to a more refined analysis in NDE.

APPENDIX A. FIBER-END PREPARATION

The ends of the single-mode optical fiber must be properly prepared for the efficient coupling of light into the fiber. The idea is to cut the fiber of such a small core diameter size mirror flat and perpendicular to the fiber axis. If the coupling entrance and exit ends of the fiber are not optically flat, the spherical optical wavefronts entering one end of the fiber will no longer exit with a uniformly diverging spherical wavefront. The front end surfaces of the fiber can be made optically smooth by a diamond-tip cutting tool or by fine polishing. One simple procedure for cutting the stripped end of the optical fiber is the "scribe-and-break" method. That is, while the fiber is held in tension, scribing is done (e.g., using a silicon carbide blade) perpendicular to the fiber axis.

Figure 62 shows the typical resulting fiber end cuts for this not completely reliable method. In Figure 62a, a highly inefficient rough fiber end is shown. A flat but inclined fiber (with respect to the fiber axis) cross section, shown in Figure 62b, will also not produce an efficient coupling of the fiber light with the microscope objectives. Figure 62c represents a properly cut fiber end, the condition of which can be checked with an optical microscope. Figure 63 shows a couple of stripped fiber ends photographed from the

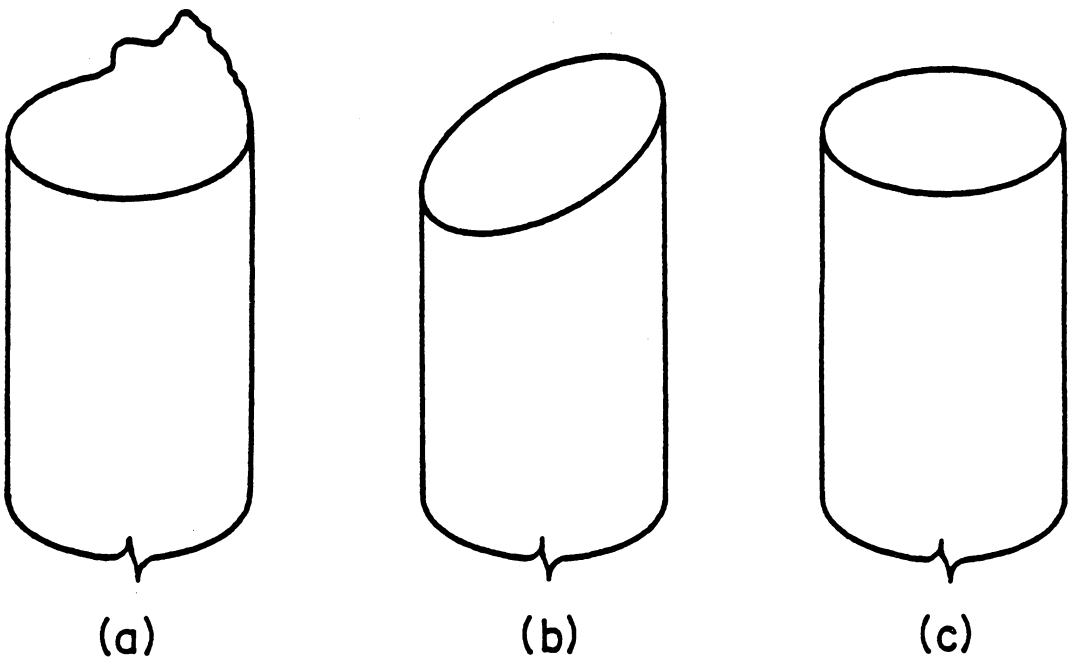

Figure 62. Optical fiber end conditions (a)rough; (b)tilted; (c)good.

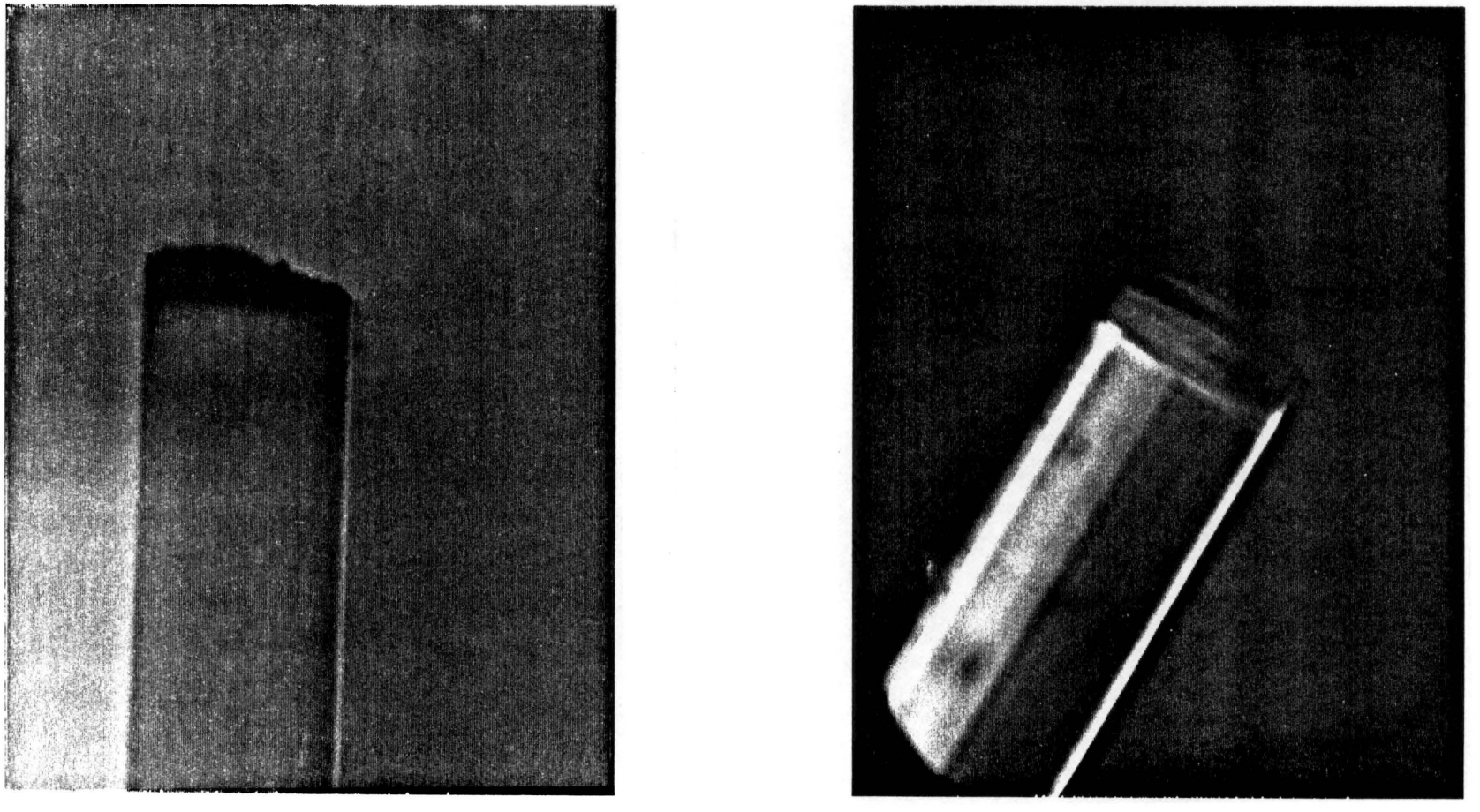

Figure 63. Typical examples of fiber end preparations.

side at 200X. The one on the left has a rough fractured end but the one on the right has a plane end.

APPENDIX B. DIFFUSIVE RETRO-REFLECTION

The thin reflective tape applied in the laser speckle interferometric system (described in Chapter IV), in addition to being diffusive, is also retro-reflective. A cat's eye is a simple example of a retro-reflector as are special prisms which have the property of total internal reflection. Figure 64 shows a schematic ray diagram of a cube corner retro-reflector, 64(a), and a glass bead (spherical) retro-reflector, 64(b). In the laser speckle system, the commercial product (3M Retro-reflective Material Type 7610 Scotch®) used for the diffusive preparation of the specimen surface, contains densely packed (several hundreds per millimeter squared) small ($\simeq$ 40 μm in diameter) spheres of titanium dioxide on a thin stick-on plastic sheet. The photograph shown in Figure 65 is the top view of such a retro-reflective tape taken at 100X.

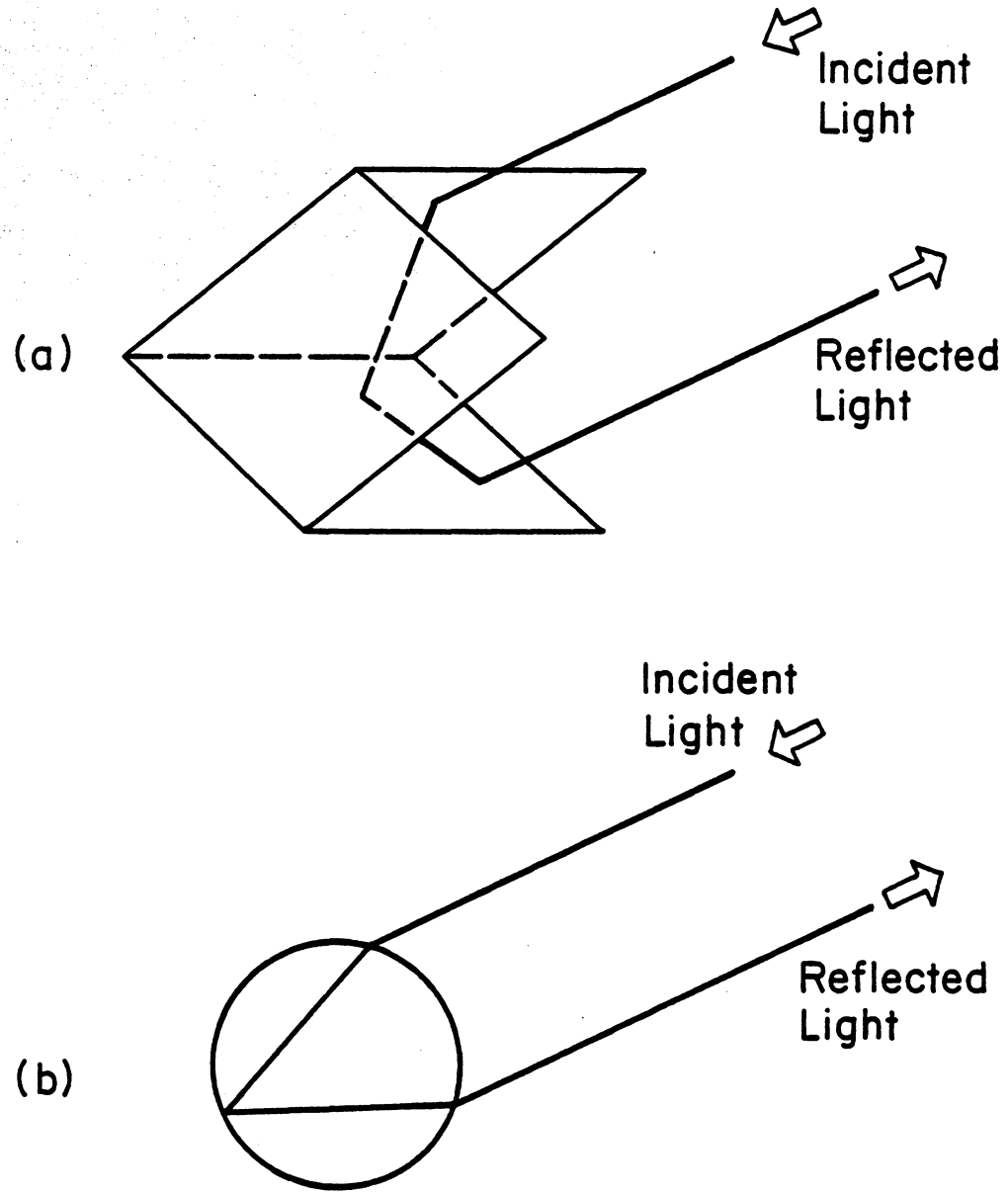

Figure 64. Schematic ray diagram of retro-reflector material: (a)cube corner; (b)glass bead (sphere).

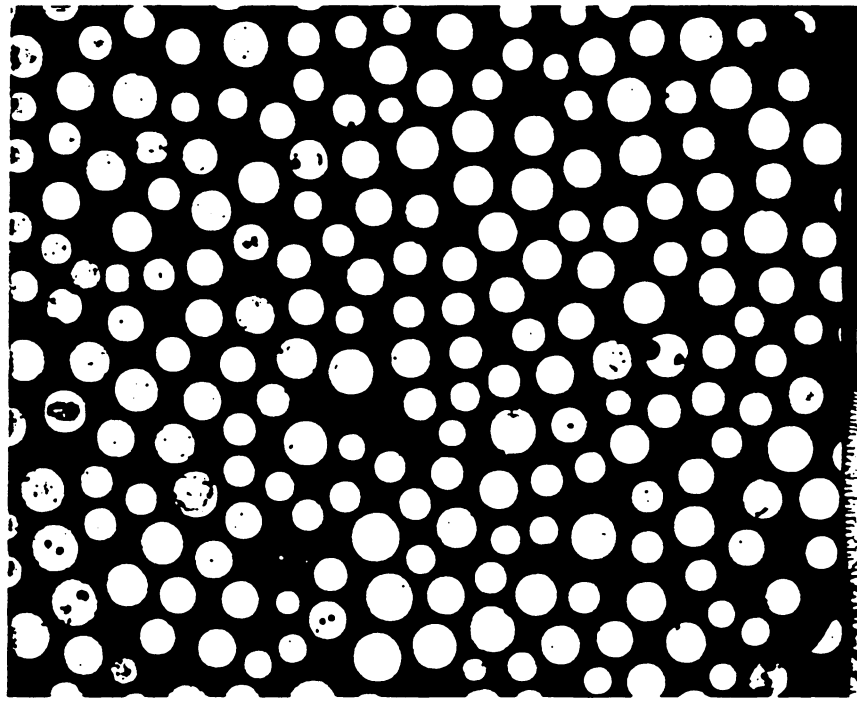

Figure 65. Magnified (100X) top view of retro-reflective spheres on tape surface.

REFERENCES

1. Stegeman,G.I., "III. Optical Probing of Surface Waves and Surface Waves Devices," IEEE Trans. Sonics Ultrason., Vol. SU-23, No. 1, January 1976, pp. 33-63.

2. Mayer, W.G., Lambers, G.B., Auth, D.C., "Interaction of Light and Ultrasonic Surface Waves," J. Acous. Soc. Amer., Vol. 42, No. 6, 1967, pp. 1255-1257.

3. Whitman, R.L., Korpel, A., "Probing of Acoustic Surface Perturbations by Coherent Light," Appl. Opt., Vol. 8, No. 8, August 1969, pp. 1567-1576.

4. Haskell, R.E., "Fourier Analysis Using Coherent Light," IEEE Trans. Educ., Vol. E-14, No. 3, August 1971, pp. 110-115.

5. Jablonowski, D.P., "Simple Interferometer for Monitoring Rayleigh Waves," Applied Optics, Vol. 17, No. 13, July 1978, pp. 2064-2070.

6. Mezrich, R., Etzold, K.F., and Vilkomerson, D., "System for Visualizing and Measuring Ultrasonic Wavefronts," RCA Review, Vol. 35, December 1974, pp. 483-519.

7. Mezrich, R., Vilkomerson, D., and Etzold, K., "Ultrasonic Waves: their interferometric measurement and display," Appl. Opt., Vol. 15, No. 6, June 1976, pp. 1499-1505.

8. Palmer, C.H., and Green, R.E., Jr., "Materials Evaluation by Optical Detection of Acoustic Emission Signals," Materials Evaluation, October 1977, pp. 107-112.

9. Kline, R.A., Green, R.E., Jr., "A Comparison of Optically and Piezoelectrically Sensed Acoustic Emission Signals," J. Acous. Soci. Amer., Vol. 64, No. 6, December 1978, pp. 1633-1639.

10. Palmer, C.H. "Ultrasonic Surface Wave Detection by Optical Interferometry," J. Acous. Soc. Amer., Vol. 53, No. 3, 1973, pp. 948-949.

11. Palmer, C.H., Claus, R.O., and Fick, S.E., "Ultrasonic Wave Measurement by Differential Interferometry," Appl. Opt., Vol. 16, No. 7, July 1977, pp. 1849-1856.

12. Claus, R.O., and Cantrell, J.H., Jr., "Optical Probing of Pulsed Acoustic Surface Waves Using Wideband Differential Interferometry," Acous. Lett., Vol. 5, No. 1, 1981, pp. 92-95.

13. Leendertz, J.A., "Interferometric Displacement Measurement on Scattering Surfaces Utilizing Speckle Effects," J. Phys. E(Sci. Instrum.), Vol. 3, 1970, p. 214+.

14. Joyeux, D., and Lowenthal, S., "Real time measurement of angstrum order transverse displacement or vibrations, by use of laser speckle," Opt. Commun., Vol. 4, No. 2, Oct. 1971, pp. 108-112.

15. Ueha, S., Shiota, K., Okada, T., and Tsujiuchi, J., "Optical Heterodyne Measurement of In-Plane Vibrations," Opt. Commun., Vol. 10, No. 1, January 1974, pp. 88-90.

16. Iijima, K., Tsuzuki, Y., Hirose, Y., and Akiyama, M., Proc. IEEE, Vol. 64, 1976, p. 386+.

17. Dandliker, R., and Willemin, J.-F., "Measuring micro-vibrations by heterodyne speckle interferometry," Optics Letters, Vol. 6, No. 4, April 1981, pp. 165-167.

18. Post, D., "Optical interference for deformation measurements--classical, holographic, and Moire' interferometry," Mechanics of Nondestructive Testing, W.W. Stinchcomb, (ed.), Plenum Press, 1980.

19. Palmer, C. H., Claus, R. O., and Fick, S. E., "Ultrasonic Wave Measurement by Differencial Interferometry," Applied Optics, Vol. 16, 1977, pp 1849+.

20. Hecht, E., "Theory and Problems of Optics, "Schaum's Outline Series, McGraw-Hill, Inc., 1975.

21. Loewen, E. G., "Diffraction Gratings, Ruled and Holographic," Applied Optics and Optical Engineering, Vol. IX, Academic Press, 1983.

22. Kroll, M. and Djordjevic, B. Boro, "A Laser Stress-Wave Probe with Sub-angstrom Sensitivity and Large Bandwidth," 1982 Ultrasonic Symposium, pp. 864-866.

23. Dakin, J.P., "Optical Fibre Sensors-Principles and Applications," Proc. No. 53, (International Conference on) FIBRE OPTICS, pp. 39-47, London, 1982.

24. Johnson, Mark, "Fiber displacement sensors for metrology and control," Opt. Engr., Vol. 24, No. 6, pp. 961-965, Nov./Dec. 1985.

25. Wyant, J.C., Speckle, in "McGraw-Hill Encyclopedia of Science and Technology," Vol. 12, pp. 852-853, 1982.

26. Palmer, D.A., "Retro-reflective materials and optical imaging," Appl. Opt., Vol. 24, No. 10, pp. 413-414, May 1985.

27. Froely, C., "Speckle Phenomenon and some of its applications," Proc. IUTAM Symposium in Optical Methods in Mechanics of Solids, Poitiers, France, pp. 279-313, 1979.

28. Joyeux, D. and Lowenthal, S., "Real time measurement of angstrom order transverse displacement or vibrations, by use of laser speckle," Opt. Commun, Vol. 4, No. 2, pp. 108-112, October 1971.

29. Bahadur, H., and Parshad, R., in "Physical Acoustics--Principles and Methods," (W.P. Mason and R.N. Thurston, eds.), Vol. XVI, p. 119, Academic Press.

30. Munnerlyn, C. R., "A Simple Laser Interferometer," Applied Optics, 8(4), 1969, pp. 827-829.

The vita has been removed from the scanned document